Joint Monitoring Programme for Ambient Noise North Sea

2018 – 2021

Guidelines for modelling ocean ambient noise

Deliverable/Task: WP 3&4

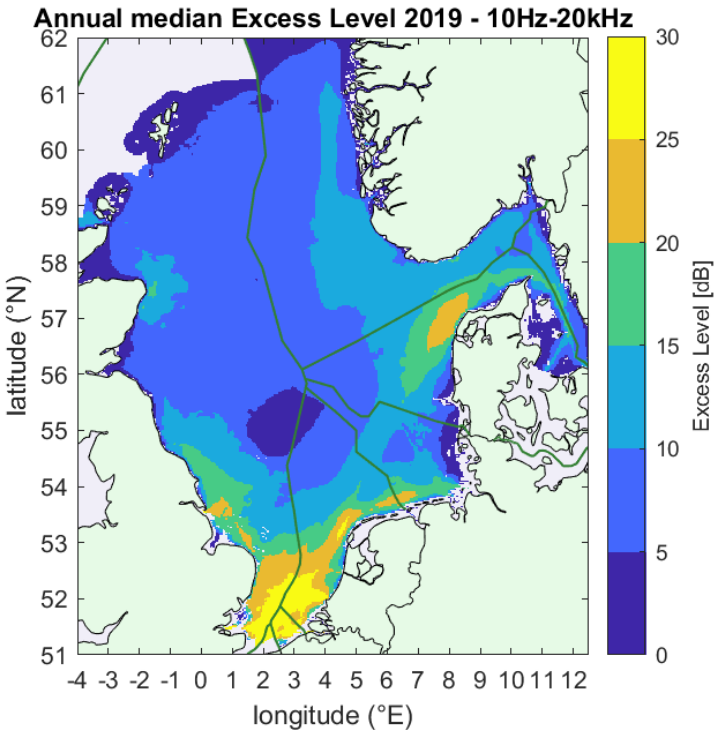

Authors: Christ de Jong, Bas Binnerts, Stephen Robinson, Lian Wang

Affiliations: TNO (NL) and NPL (UK)

Date: June 2021

Project Full Title	Joint Monitoring Programme for Ambient Noise North Sea
Project Acronym	Jomopans
Programme	Interreg North Region Programme
Programme Priority	Priority 3 Sustainable North Sea Region

Colophon	
Author	Christ de Jong (WP4)
Organization Name	TNO
Email	christ.dejong@tno.nl

This report should be cited:
de Jong, CAF, Binnerts, B, Robinson, S, Wang, L (2021) *Guidelines for modelling ocean ambient noise*. Report of the EU INTERREG Joint Monitoring Programme for Ambient Noise North Sea (Jomopans)

Cover picture: Annual average map of median excess level (ship noise over wind noise)

Table of contents

Summary

The aim of the Jomopans project was to develop a framework for a fully operational joint monitoring programme for ambient noise in the North Sea. Output will be the tools necessary for managers, planners and other stakeholders to incorporate the effects of ambient noise in their assessment of the environmental status of the North Sea, and to evaluate measures to improve the environment.

The proposed framework applies numerical modelling for creating sound maps of the North Sea area, supported by local measurements for evaluation of the uncertainties in the numerical modelling.

This report provides a description of the sound map modelling that has been applied to produce the Jomopans soundscape maps of the underwater sound of shipping and wind in the North Sea in the twelve months of 2019. It provides examples of these maps.

The lessons learned in the Jomopans project on the various choices and considerations for producing these large scale maps are converted into guidelines and recommendations for future sound mapping efforts.

1 Introduction

The Jomopans project has developed a framework for a joint monitoring programme for ambient noise in the North Sea. The proposed framework applies numerical modelling for creating soundscape maps of the North Sea area, supported by local measurements for evaluation of the uncertainties in the numerical modelling. Output will be the tools necessary for managers, planners and other stakeholders to incorporate the effects of ambient noise in their assessment of the environmental status of the North Sea, and to evaluate measures to improve the environment.

1.1 Underwater ambient noise modelling

Numerical modelling of ocean ambient sound has the advantage that it can enable a much wider spatial and temporal coverage than achievable with measurements from offshore monitoring stations, with much technical difficulties (reliability and robustness of the stations and self-noise at the sensors) and at much lower cost. Moreover, numerical models provide insight in the contributions of individual source types to the ambient sound and enable studies of various past or future offshore scenarios and for noise mitigation strategies.

On the other hand, numerical modelling is limited to the sources and propagation effects for which models and the required input data for these models are available. The reliability of the model output can be limited by model simplifications, that can be necessary to keep computations manageable. The reliability also depends on the completeness and quality of the input data.

1.2 Jomopans North Sea soundscape map modelling

The Jomopans modelling framework is currently limited to the sound from shipping and from wind - generated surface wave breaking. These two were expected to be the dominant sources of the 'continuous low frequency sound (ambient noise)' that is addressed by Indicator 11.1.1 of the European Marine Strategy Framework Directive.

Summarized, the Jomopans sound map modelling focussed on the following aspects:

- Sources:
  - Ship traffic monitored by AIS/VMS,
    - characterized by 'type', length and speed
    - sampled at 10-minute intervals
  - Wind generated surface waves
    - characterized by 10 min-average wind speed amplitude at 10 m above the water surface, from satellite observations
    - available at 1-hour intervals, linearly interpolated to 10-minute intervals
- Environment
  - Bathymetry
    - Characterized by local water depth at lowest astronomical tide
  - Sea water
    - Characterized by sound speed, density and absorption: assumed to be uniform in space and constant in time
  - Sea floor
    - Characterized by the local median grain size of the upper sediment layer at the source locations, converted to sound speed, density and absorption

The Jomopans measurements (WP5) are applied for model uncertainty assessment (WP6).

The modelled soundscape maps are applied to quantify to what extent the shipping noise exceeds the 'natural' ambient sound, represented by the modelled wind noise. The effect of this exceedance (quantified as 'excess level', see section 2.4) on marine life remains to be quantified, but Jomopans proposes to apply statistical soundscape modelling to quantify the proportion of the time (per calendar month) and the proportion of the area (per assessment region) over which this excess level is higher than a specified cut-off value.

The Jomopans North Sea sound maps for 2019 can be downloaded from and displayed in the Jomopans GES Tool[1] (WP7).

[1] Hosted at https://jomopans.michaelcarder.co.uk/en/ until the end of 2022.

1.3 Jomopans modelling guidelines

Various previous efforts have demonstrated that modelling shipping noise based on distribution of ship traffic is feasible, see e.g. [Erbe et al, 2012; MacGillivray et al, 2014; Porter & Henderson, 2014; Folegot et al, 2015; Gervaise et al, 2015; Folegot et al, 2016; Prins et al, 2016; Sertlek, 2016; Aulanier et al, 2017; Redfern et al, 2017; Joy et al, 2019; Farcas et al, 2020; Erbe et al, 2021]. However, there has been limited work producing modelled sounds maps with a large geographic coverage using input data from different institutions as in the Jomopans project. A direct comparison of the various sound maps produced in these publications is complicated by differences in modelling approach and the presented acoustic metrics in terms of parameters such as frequency range, averaging time and receiver depth.

An important goal of the Jomopans modelling work package (WP4) was to be as clear as possible about the selection of metrics, models, model setting and input parameters, so that the reported approach can be used as guideline for future ambient noise modelling projects.

1.4 Outline

- Chapter 2 of this guide provides a general overview of approaches to modelling ocean ambient noise.
- Chapter 3 describes the specific implementation for the modelling of the ambient noise in the North Sea that was developed in Jomopans.
- Model verification and experimental validation are described in Chapter 4.
- Uncertainties are discussed in Chapter 5.
- Chapter 6 gives examples of the Jomopans North Sea sound maps.
- Chapter 7 provides guidelines for modelling ocean ambient noise, based on the lessons learned in Jomopans.

2 Modelling ocean ambient noise

Modelled ocean ambient noise provides means to study and assess the effects of the noise on marine life over large scale. The modelling work consists of using all noise sources that propagate from the sources to areas of interest. Although, in situ measurements present ground truth that includes all sources of sounds in underwater environments, it is impossible to carry out large scale measurements over a large area to have a complete map due to constrains of time and cost. In comparison, modelled ocean ambient noise can cover the full area of regional seas over long time periods. This capability allows users to acquire information in time and make decisions accordingly.

This guide presents procedures to model ocean ambient noise. All underwater sources are listed with shipping and wind noises as contributors in the modelling. Environmental parameters affecting underwater sound propagation are considered. Various propagation models were evaluated for suitability on the application. Validations of selected propagation models with measurements were carried out.

However, there are many issues in modelling ocean ambient noise accurately. The main issues are the knowledge gaps on many noise sources, lack of complete information on the underwater channel for sound propagation, and limitations of propagation models currently available. Most relevant issues were discussed, and the effects were examined.

2.1 Propagation model types

Ocean acoustic propagation models have been widely used for several decades, to support a broad range of applications including anti-submarine warfare [Bucker, 1976], global scale underwater sound propagation [Heaney et al., 1991; Collins et al., 1995] characterisation of acoustic communications channels [Simons et al., 2001], passive acoustic monitoring of marine biota [e.g. Potter et al., 1994; Stafford et al., 1998; McDonald et al., 1999; Thode et al., 2004; Helble et al., 2013], ocean acoustic tomography [Munk and Wunsch, 1979; Cornuelle et al., 1989; Worcester et al., 1999]), ambient noise forecasting [Wenz, 1962; Heitmeyer, 2006; Merchant et al., 2012] and other oceanographic applications [Harrison 1989; Buckingham, 1992; Jensen et al., 1997]. Since the first underwater sound experiment, conducted by Colladon and Sturm in 1826 on Lake Geneva, it has been known that sound travels extremely well underwater [Lichte, 1919]. With the advent of large-scale submarine warfare during the Second World War and the subsequent Cold War, there was intense effort to understand and predict the propagation of sound in the ocean, accruing a wealth of knowledge about underwater sound propagation, and its environmental dependencies [Ainslie, 2010].

In general, propagation modelling solutions can be divided into three large classes based upon i) the frequency characteristics of the source; ii) the range dependence of the propagation region; and iii) the water depth (in combination with seabed parameters, i.e. critical angle). Models within class ii) are generally categorised as *range independent* (the environmental parameters are kept fixed with range), and *range dependent* (environmental input parameters, such as water depth and sound speed, are allowed to vary with distance from the source), the latter being the preferred choice when the bathymetry or water column conditions change along the propagation path.

Ocean acoustic propagation models solve usually the Helmholtz equation in frequency domain, or wave equation with time dependency. This is generally done for a given frequency, and broadband signals, for example, a pulse, may have to be modelled at all the frequencies within the pulse first, and then converted to time domain signal, or using a time-domain model [Fumiaki, 2000]. Alternatively, a solution is calculated for each frequency or frequency band across the required frequency range, with the use of a suitable inverse transform. It is also worth noting that not every propagation model will consider all of the environmental factors which may influence the propagating wave.

Figure 2.1 summarizes the general applicability of various propagation models in two dominant parameters: frequency and water depth. Given a particular frequency band and environment, the choice of a suitable propagation model can be made (see also section 2.1.7). There are a wide variety of models available, some of which are available for download free of charge, but these complex models require some expertise to run successfully. The available propagation models are commonly categorised based on their underlying method into the following groups [Jensen et al., 2011; Etter, 2013], which captures the most commonly used methods:

- Ray theory
- Normal mode
- Parabolic equation
- Wavenumber integration
- Energy flux

Shallow water - low frequency	Shallow water - high frequency	Deep water - low frequency	Deep water - high frequency
Ray theory	*Ray theory*	*Ray theory*	*Ray theory*
Normal mode	*Normal mode*	*Normal mode*	*Normal mode*
Wave number integration	*Wave number integration*	*Wave number integration*	*Wave number integration*
Parabolic equation	*Parabolic equation*	*Parabolic equation*	*Parabolic equation*
Energy flux	*Energy flux*	*Energy flux*	*Energy flux*

Green – suitable; Amber – suitable with limitations;
Red – not suitable or applicable

Figure 2.1 Applicability of propagation models

2.1.1 Ray method

Following the analogy of optics, the wave equation can be solved in the high-frequency limit by integrating Snell's law and the associated eikonal equation. This ray tracing solution is highly intuitive because the sound paths can be traced and show the path of each ray. Ray tracing is very efficient (fast). Once the rays are computed, the acoustic field levels are calculated by summing the rays near the receiver. The rays are often extended in size by using the Gaussian beam approximation. Ray interaction with the seafloor is achieved using a reflection coefficient without penetration into the seafloor. Ray theory is limited in accuracy at low frequencies (typically below around 200 Hz) where diffraction is significant (plane wave incident reflection assumptions no longer applicable) and where seabed penetration occurs. The ray theory approach performs poorly when there are surface ducts and other sound speed fields with discontinuities and rough surfaces. It is the same for other propagation models with the rough surface with entrapped air bubbles below due to the temporal variations of the acoustic properties. Ray theory handles arbitrary range-dependent environments, is best in deep water and is suitable at higher frequencies. Ray theory is computationally intensive with long running time and requires large memory.

2.1.2 Normal mode method

A full-field solution to the wave equation involves using separation of variables to solve the local vertical part of the wave equation and then apply various solutions to the horizontal component. The vertical wave equation solutions are standard normal modes, charactered by eigenvalues. The modes are then summed up in varying fashion, depending upon the horizontal propagation, at the source and receiver to generate the full acoustic field. These modes encompass the solution to the wave equation including sound speed and density discontinuities and sound field in the seabed. The horizontal component of the solution can be (i) carried out trivially for range-independent environments, (ii) solved easily using adiabatic mode theory [Tindle and Zhang, 1997] for mildly range-dependent environments, and (iii) solved explicitly using coupled mode [Collins 1993a; Preisig and Duda, 1997; Holland 2010; or by parabolic equation models for complex 3D range-dependent environments [Heaney et al., 2012]. Normal mode solutions are best suited to mildly range-dependent environments and at lower frequencies as the number of modes goes up linearly with frequency. They are used extensively in both shallow and deep water. It is easy to find the proper modes which have real eigenvalues. It becomes challenging to find all the im-proper modes (or leaky modes). The im-proper modes contribute substantially at close range. Normal mode method should be applied at range not too close to source since the contribution from branch cut is typically ignored [Stickler, 1975]. Recently, Sertlek proposed an efficient analytical solution for depth dependent propagation in a Pekeris waveguide, by converting an analytical normal mode sum into an integral based on a hypothetical continuum of modes, and effective depth theory for obtaining the modal eigenvalues analytically [Sertlek, 2014, 2016, 2018]. Normal mode method is fast especially if only real modes are used, and it does not require large memory.

2.1.3 Wave number integration method

The wave equation can be solved exactly at close range using the numerical approach of spectral wavenumber integration. Such solutions are often called Fast-Field Programs (FFP). For range-independent environments they compute the exact field and are often used as benchmark solutions. The method has been extended to range-dependent environments, but this extension is not freely available, and is thus less widely used. The run time and memory requirement of Wave number integration method are between Ray method and normal mode method.

2.1.4 Parabolic equation method

Almost all acoustic modelling involves the computation of the field propagation from a source to a distant receiver. In this problem the propagation is one-way. Separating the wave equation into incoming and outgoing solutions leads to the Parabolic Equation. Neglecting incoming (back-scattered energy), the acoustic field can be computed using a marching algorithm referred to as the Parabolic Equation (PE) model. There are two mostly used classes of PE models available – the split-step Fast Fourier Transform solution developed by Tappert [1977] and the Padé expansion solution developed by Collins [1993b]. The PE is an efficient marching solution that is suitable for range-dependent environments, discontinuous sound speed profiles and is commonly used in shallow and deep water. The PE computational requirements increase with frequency squared (or $f \cdot \log(f)$ for the Fourier PE) and therefore the PE is generally used at frequencies less than 1 kHz. The split-step Fast Fourier Transform approach does not handle density discontinuities easily and therefore it is not the model of choice in shallow water. The memory requirement is high.

2.1.5 Energy flux method

A hybrid solution first developed by Weston [Weston 1959; 1968], between rays and modes is the energy flux model, based upon the Hamiltonian action [Holland, 2010]. Analytic solutions exist for simple environments (iso-velocity water, flat bottom) and extensions to depth dependent sound speeds and range dependence have been made [Harrison, 2012]. These flux-based solutions are extremely fast, handle diffraction but are not used to compute the coherent acoustic field and often neglect high spatial frequency interference. For accuracy and speed, they lie somewhere between ray theory and mode theory, as the solution suggests.

2.1.6 Finite difference / finite element method

A common computational physics approach to solving 3D problems is to grid the entire environment, and solve the wave equation in space and time. These Finite Difference (FD) and Finite Element (FE) models are rarely used in ocean acoustics. The computational expense of gridding each, sub-wavelength spaced, grid-point for the scale of most ocean acoustic problems is prohibitive. These solutions are generally applied to scattering or very near source propagation. They have been applied to pile-driving excitation problems and the seismic generation of low frequency modes in the oceans sound speed minimum channel. Both methods are computationally intensive, and require large memory to run.

2.1.7 Selection of propagation models based on number of real modes in shallow water

It is helpful to estimate the number of standard real normal modes in shallow water channels to decide what are the appropriate propagation models to use for a given scenario. For example, wavenumber integration and PE should be used where there is no standard normal mode, but only leaky modes which have only imaginary eigenvalue as in channels with muddy seabed, and shallow water and low frequency. It is more efficient to use normal mode and PE where there are a few modes in shallow water channels, Flux and Ray methods where there are many real modes. Agreement should be achieved between different models applicable in the same scenario (see e.g. Ozkan Sertlek benchmarking work).

2.1.8 3D modelling

Most propagation models are two-dimensional solutions, calculating the propagation loss along a transect, which does not include horizontal refraction, reflection or diffraction (i.e. each transect modelled is independent of the neighbouring transect). In many cases, such models provide sufficient accuracy and can provide three-dimensional maps by combining, often through interpolation, a number of two-dimensional (distance and depth) transects.

However, in some instances the use of two-dimensional models may not be sufficient to accurately model the sound propagation. A possible example includes a scenario where an island or land mass is

situated between the source and receiver. A two-dimensional model will result in a shadow behind the land mass where the modelled transects intersect the land mass. In reality, diffraction will occur causing bending of the sound around the land mass. In such cases, it may be necessary to use a three-dimensional model, which accounts for horizontal diffraction to accurately represent the sound field. Other scenarios where two-dimensional models may not provide sufficient accuracy may be environments characterised by sub-surface obstacles such as sand banks, or where there is a strong up-sloping or down-sloping seabed, such as propagation around continental shelves.

In general, three-dimensional implementations can be computationally intensive, and it may be appropriate to utilise a two-dimensional solution, which will be sufficient in most cases.

2.2 Input parameters

Underwater sound propagation is influenced by the local propagation environment, which may vary spatially and temporally. As such the accuracy of a propagation model output relies on representative environmental input data to the model. Environmental variables such as *bathymetry*, *seabed properties* and *sound speed profile*, surface loss are the primary factors, all influence the propagating sound and changes in these parameters may lead to considerable differences in the characteristics of the propagated sound. Other more specific model input parameters, such as wind speed, used as a proxy input when surface scattering requires consideration, for example, may also represent a source of uncertainty, and should be considered carefully.

2.2.1 Bathymetry

Bathymetry is particularly important for shallower water propagation. It is not just the water depth, which influences the propagation, but also the shape of the seabed. Near continental shelves or in regional seas, the sloping seabed can have a significant influence on the propagating sound.

Whilst higher resolution bathymetry data may provide a fine scale representation capable of capturing small scale seabed features, such as sand waves and ripples, which can influence the propagating sound, these seabed features are dynamic and might be expected to change with time.

Besides the resolution and accuracy of the bathymetry data, the accuracy of the modelled outputs, may also be influenced by the vertical datum. This can typically be based on the mean sea level or the lowest astronomical tide. Whilst this parameter is usually less important in deep water, it can have a significant effect on the assumed water depth in shallow coastal regions, with considerable tidal changes.

Subsequently, tidal variation can be another factor that may require consideration, especially in shallow coastal regions, where tidal variation may correspond to a substantial ratio of the water depth. It is worth noting that tidal variation can be very localised.

2.2.2 Seabed properties

The acoustic properties of the seabed are an important parameter in acoustic propagation modelling in shallow water. In general, they will determine how much sound is reflected from the seabed and how much sound, re-enters the water column after transmission through the seabed. A stratified seabed can, for example, result in bending of the sound waves, and a hard seabed layer, such as rock, can reflect the sound. Both can result in sound energy being retransmitted into the water column.

It is often possible to build the acoustic properties of the sediment (as a half-space, for example), and in some cases the stratification of the seabed, into an acoustic propagation model. However, the accuracy of this is often limited by the availability of the actual data at a sufficient spatial scale and with the necessary resolution such that the data are representative of the actual environment. It can also be challenging, or in some cases not possible, to build the necessary variations with distance into a range dependent acoustic propagation model.

Seabed core data can often provide information of the underlying geology, although the specific characteristic might be localised, and it might not be correct to extrapolate this across a broader region.

Seabed survey data may be used to provide information about the upper sediment layer, such as that provided by EMODnet/EUSeaMap (http://jncc.defra.gov.uk/page-5040). However, this sediment information has to be converted into acoustic properties for the seabed and sufficient information is not always available to correlate with published acoustics properties of various sediment types [e.g. Hamilton and Bachman, 1982; Hamilton, 1980; and 1985; Lurton, 2003; Ainslie, 2010]. [Bockelmann, 2017] provides median grain size of North Sea surface sediments, which best connects to high frequency lab experiments. The sediments in North Sea are predominantly sandy which may have dispersive properties at low frequency [Zhu et al, 2009]. However, there is no measured data at low

frequency (below ~1 kHz) in the area.

2.2.3 Sound speed profile

The sound speed profile can have a significant influence on how the sound propagates, especially in deep water, and also in the regions where there are large salinity changes such as in Baltic sea, and near river estuary. The sound speed profile is dictated by changes in the water temperature, pressure and salinity, with depth and also range to a less degree. Where there is variation in the sound speed with depth, bending and trapping of the sound can occur, which in some cases can lead to the sound travelling substantially further due to reduced spreading and less interaction with the seafloor and sea surface (sound is trapped in the SOFAR channel, for example).

In shallow water, although the sound speed profile may influence propagation through bending of the sound, the bathymetry and sediment acoustic properties generally constitute the more influential propagation parameters.

The sound speed profile may be measured *in situ,* and may also be obtained from global data sets, such as the data available from the World Ocean Atlas (WOA) database (http://www.nodc.noaa.gov/OC5/indprod.html), or, https://marine.copernicus.eu/access-data/ocean-monitoring-indicators, providing information about the geographic and seasonally variability.

2.2.4 Sea surface

The rough sea surface, and associated wind-generated bubbles, is usually characterised by means of a wind speed (at a height of 10 m). The main effects of the rough sea surface on sound propagation are the scattering, absorption of sound by bubbles introduced by breaking waves. The mixture of bubbles with water also reduces sound speed. The conversion, and the resulting effects on propagation, are the subject of ongoing research [Hall 1989; Keiffer et al., 1995; Novarini et al., 1998; Norton and Novarini, 2002; Ainslie, 2005].

2.2.5 Model input data uncertainty

Given that the availability of environmental input data are generally limited, and with some uncertainty on the quality of the data, and some might be critical to the performance of the acoustic propagation model, it is important to understand the influence that the accuracy of the environmental data has on the outputs of the model, i.e. the uncertainty in the modelled output as a function of the uncertainty associated with the input data. In general, the influence of the uncertainty in the environmental input data on the propagation efficiency may be assessed through sensitivity analysis, where the value of a parameter is varied, with other variables fixed for control. The same approach may be employed to assess the effect of data resolution on the modelled output.

2.3 Acoustic sources

There are many underwater acoustic sources, both anthropogenic and natural. Anthropogenic acoustic sources include shipping, geological survey with air guns and sonars, military sonars, navigation sonars (depth sounder), off-shore constructions, etc. Nature sources are for examples, wind, rain, earthquake, ice, biological, etc.

Acoustic sources can be divided into groups of continuous and impulsive. Shipping and wind are continuous, while sonars, airguns are impulsive.

2.4 Acoustic metrics

Sound pressure level (SPL) is a fundamental metrics in environmental noise assessment. It is a function of frequency band and time window dependent on objects of interest. Many other metrics are derived from SPL that provide better presentations of its effects from various prospective. The acoustic metrics used for JOMOPANS are listed in Table 2.1. Although not used in JOMOPANS, Sound exposure level (SEL) is included for its wide applications in noise impact assessment. A more detailed description of some of the metrics that are specifically applied to JOMOPANS is provided in Annex A: Jomopans metrics.

Table 2.1 Acoustic metrics for JOMOPANS

Name	Definition
Sound pressure level	(i) 10 dB times the logarithm to base 10 of the ratio of the mean square sound pressure over a stated time interval to the reference value of sound pressure squared; *or* (ii) 20 dB times the logarithm to base 10 of the ratio of the root mean square sound pressure over a stated time interval to the reference value for sound pressure.
Sound exposure level	The SEL is a representation of sound energy that is defined as 10 dB times the logarithm (base 10) of the sound exposure, which is the integral of the squared sound pressure over some period of time *T*, normalized by a reference squared pressure p_0^2 and reference time T_0,
Percentiles	The value of SPL below which a certain percentage of the observations fall
Excess level	(i) Instantaneous excess of "ambient noise" from all ships and wind over "natural" wind noise (ii) Instantaneous excess of "ambient noise" from all ships and wind over median values of "natural" wind noise over the evaluation time interval.
Dominance	The percentage of evaluation time over which the excess level exceeds a specified cut-off value.
Pressure curve	The cumulative distribution of the percentage of evaluation area as a function of the dominance values.
Pressure Index	A single number index for the area under the pressure curve, quantifying the percentage of the evaluation area as well as the percentage of the evaluation time interval, in the evaluation frequency band, where the excess level exceeds the specified cut-off value.

2.5 Citation of other guidance

JOMOPANS standard for terminology, 2021

ISO 18405:2017. Underwater acoustics — Terminology. International Organization for Standardization, Geneva, Switzerland, 2017.

ISO 17208-1: 2016. Underwater acoustics — Quantities and procedures for description and measurement of underwater sound from ships; Part 1: Requirements for precision measurements in deep water used for comparison purposes. International Organization for Standardization, Geneva, Switzerland, 2016.

ISO 17208-2: 201X. Underwater acoustics — Underwater acoustics — Quantities and procedures for description and measurement of underwater noise from ships — Part 2: Determination of source levels from deep water measurements. International Organization for Standardization, Geneva, Switzerland, 201X.

ISO 17208-3: 201X. Underwater acoustics — Underwater acoustics — Quantities and procedures for description and measurement of underwater noise from ships — Part 3: Determination of source levels from shallow water measurements. International Organization for Standardization, Geneva, Switzerland, 201X.

Folegot T., Clorennec D., Chavanne R., R. Gallou (2016). Mapping of ambient noise for BIAS. Quiet- Oceans technical report QO.20130203.01.RAP.001.01B, Brest, France, December 2016

Ainslie, M. A., de Jong, C. A. F., Martin, B., Miksis-Olds, J. L., Warren, J. D., Heaney, K. D. (2017). Project Dictionary (Terminology Standard). DRAFT. Technical report by TNO for ADEON Prime Contract No. M16PC00003.

Ainslie, M.A., Miksis-Olds, J.L., Martin, B., Heaney, K., de Jong, C.A.F., von Benda-Beckman, A.M., and Lyons, A.P. 2017. ADEON Soundscape and Modeling Metadata Standard. Version 2.0 DRAFT. Technical report by TNO for ADEON.

IWC 2014. Joint workshop report: Predicting sound fields—global soundscape modelling to inform management of cetaceans and anthropogenic noise 15-16 April 2014, Leiden, Netherlands. International Whaling Commission (2014). Available from http://scorint.org/IQOE/Leiden_Report.pdf.

3 Jomopans ambient noise modelling

3.1 Introduction

Jomopans has produced maps of ambient noise in the North Sea, as input for assessment of the environmental status. As specified in the Jomopans objectives, these maps provide "*information on the amount of ambient noise and its spatial distribution as well as the main sources of the noise*." A target was set to provide this information for at least 90 % of the North Sea area.

The ISO 198405 standard for underwater acoustic terminology defines *ambient noise* as "*sound except acoustic self-noise and except sound associated with a specified signal*", where *acoustic self-noise* is the "*sound at a receiver caused by the deployment, operation, or recovery of a specified receiver, and its associated platform*". **Jomopans has adopted the common use of the term 'ambient noise' without reference to a specified signal**.

The EU MSFD indicator 11.2.1 quantifies ambient noise in terms of a sound pressure level, which is a quantity with five dimensions: latitude, longitude, depth, frequency and time. An ambient noise map is a two-dimensional (latitude, longitude) projection of this quantity.

Jomopans [Merchant et al, 2018] has selected the acoustic metric to be monitored according to the specifications described in Table 3.1.

Table 3.1 Jomopans acoustic metric specification.

Attribute	Specification
Physical quantity	Sound pressure level, dB re 1 µPa
Snapshot duration	1 second
Statistics	Percentiles of the sound pressure level distribution measured over one-month periods. Suggested percentiles: 5, 10, 25, 50, 75, 90, 95
Frequency	one-third octave bands, with centre frequencies ranging from 10 Hz to 20 kHz, defined according to the base-ten convention (IEC 61260-1:2014; ANSI 2009)
Geospatial	Depth-averaged value either at the centroid of each grid cell, or as a spatial average of the levels within the grid cell. Grid referenced using the standardised C-square notation (Rees 2003).
Depth	Depth averaged (energy-wise)

The contour of North Sea region considered in the Jomopans projects is shown by the shaded area in

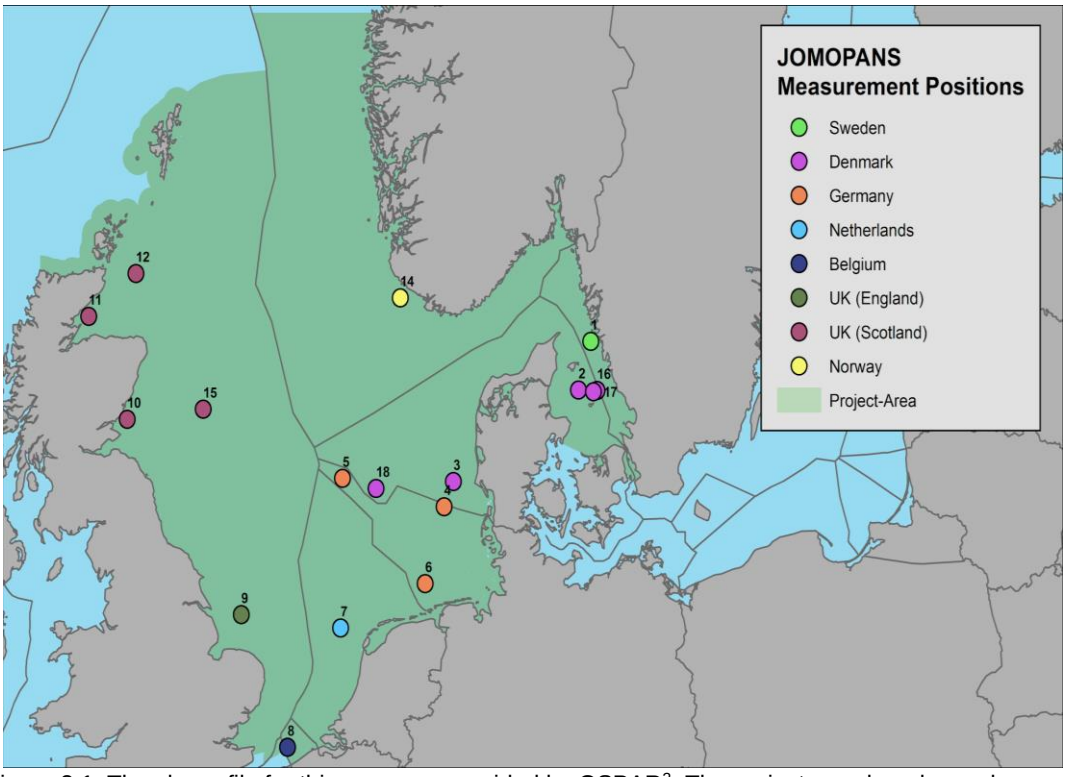

Figure 3.1. The shape file for this area was provided by OSPAR[2]. The project area largely overlaps with OSPAR Region II "Greater North Sea".

Although from a biological perspective a large frequency bandwidth and high resolution in frequency, time and space might be desirable for monitoring this acoustic metric, the corresponding computational complexity set practical limitations. Moreover, not all the required inputs for modelling the acoustic metric are available at such a high resolution.

Jomopans decided to focus on **shipping and wind sound sources only**. These were expected to dominate the North Sea soundscape over most of the evaluation area and time.

For future further development, the ambient noise modelling could be extended to include contributions of other continuous, or possibly also impulsive, sources that may enter into the scope of Descriptor 11.1.2 of the MSFD. Examples of possible sources to be added in the future are:

- other natural sounds (such as rain, snow, hail, lightning, thunder, earthquakes, surf zone wave breaking, current related sounds, marine life)
- impulsive sounds (such as explosions, seismic surveys, marine piling and sonar);
- offshore platforms and structures (such as wind turbine operational noise and oil- and gas pipes).

[2] Provided by email from Chris Moulton (OSPAR) to Niels Kinneging (Jomopans PL) dd 16 January 2018.

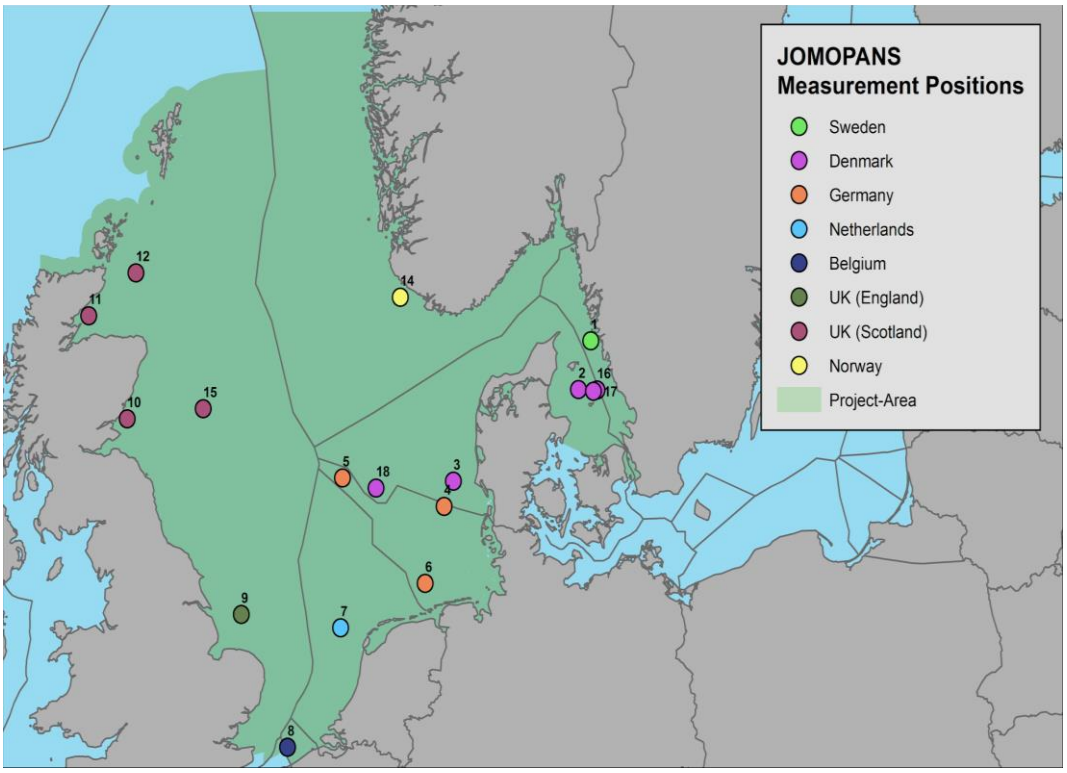

Figure 3.1 Map of the North Sea. The green coloured area is the Jomopans project area. The coloured circles indicate the locations of the Jomopans underwater sound monitoring locations. The Norwegian 'Love' monitoring station is not shown on the map. This station served as a reference station (very low shipping) and is located in the northern area of Norway and outside of the specific project region. Figure from [Fischer et al, 2021]

This chapter provides an overview of the various choices made for the modelling of ambient noise maps for the North Sea area and the selection of model input data and mapping procedures. Chapter 4 describes model verifications and validation. Sections 3.7 and 3.8 refer to the performed model sensitivity studies.

3.2 Jomopans ambient noise modelling

The Jomopans sound maps for shipping and wind are calculated according to the following approach:

1. Obtain ship traffic information (location, speed, ship type and length) from AIS/VMS data (see section 3.7.5), interpolated to a regular time grid (10-min), and to a regular two-dimensional source grid (0.025° resolution).
2. Calculate propagation loss (time-invariant) between source grid locations and locations on a receiver grid (0.05° longitude and 0.025° latitude resolution, averages over 10 equally spaced points over the local water depth), at centre frequencies of one-third octave bands ranging from 10 Hz to 20 kHz, using the Aquarius 3 propagation loss model (see section 3.4). Store the calculated propagation loss in a look-up table.
3. For each ship at each time step, estimate the source level spectrum, at centre frequencies of one-third octave bands ranging from 10 Hz to 20 kHz, using the Jomopans -ECHO source level model (see section 3.3).
4. For each time step, calculate the depth-averaged sound pressure level spectrum at each receiver grid location, by summing the contributions of from all source grid cells (source level minus propagation loss).
5. Obtain wind information (speed at 10 m above the water surface, see section 3.7.4), interpolated to a regular time grid (10-min), and to the receiver grid (0.05° longitude and 0.025° latitude resolution).
6. For each time step, calculate the depth-averaged sound pressure level spectrum due to the wind at each receiver grid location, using a semi-empirical wind source and propagation model (see sections 3.5 and 3.6).
7. For each receiver grid location, determine monthly percentiles of the calculated sound pressure level spectra from ships and wind.

3.3 Jomopans-ECHO ship source model

Robust sound mapping tools not only require accurate models for estimating source levels for large numbers of marine vessels, but also an objective assessment of their uncertainties. The diversity of ship characteristics and the various noise source mechanisms at different operational conditions make it impossible to include an exact prediction of the underwater radiated noise of individual vessels in the calculation of shipping sound maps. Moreover, information available from the vessel tracking data from Automated Identification System (AIS) is limited and not easily related to vessel noise emissions. The need for more coherent underwater radiated noise measurements on commercial vessels, to support the development of reliable statistical ship source level models, was also concluded in two large European research programs, SONIC [Brooker & Humphrey, 2015] and AQUO [Audoly & Rizzuto, 2015].

One such data set, consisting of a large collection of systematic source level measurements for wide variety of vessels, was collected during the Enhancing Cetacean Habitat and Observation (ECHO) program's 2017 vessel slowdown trial in Haro Strait [Trounce et al, 2019]. To support underwater noise studies associated with the trial, JASCO Applied Sciences collected a total of 1862 monopole source level measurements, over a four-month period, on three different hydrophone systems. This data set was used to establish speed scaling relationships for source levels of several different categories of vessels. This data set is unique, not only because it provides a large collection of source levels for many different types of vessels, but also because the voluntary slow down protocol provided a strong experimental control for determining the effects of vessel speed on noise emissions [MacGilivray et al; 2019]. As such, the ECHO project provided an ideal data set for testing speed dependence in statistical source level models.

Based on the ECHO data set, Jomopans has proposed an updated reference spectrum model that incorporates ship type as well as speed and length. The Jomopans-ECHO model [MacGillivray & de Jong, 2021], inspired by the RANDI 3.1 model [Breeding et al, 1996], calculates the ship source level spectrum, as a function of frequency (f), ship speed over ground (V), ship length (l) and ship type (vessel class, C) :

$$L_S\,(f, V, L, C) = L_{S0}(f) + 60\log_{10}(V/V_C)\ \text{dB} + 20\log_{10}(l/l_0)\ \text{dB},$$

where V_{vc} is the reference speed per vessel class and $l_0 = 100$ m is a fixed reference length for all vessel classes. The vessel class (C) is obtained from the AIS 'ship type' parameter, according to Table 3.2, which also presents the reference speed (V_C) per vessel class.

The reference speeds have been obtained from a fit of the RANDI3.1c model variant [de Jong et al, 2020] to the ECHO data-set [MacGillivray et al, 2019], for a fixed reference length $l_0 = 300$ ft.

The baseline spectrum for all vessel classes is given by:

$$L_{S_f,0}(\hat{f}) = K - 20\log_{10}(\hat{f}_1)\ \text{dB} - 10\log_{10}\left(\left(1 - \frac{\hat{f}}{\hat{f}_1}\right)^2 + D^2\right)\ \text{dB},$$

with $K = 191$ dB, $D = 3$ (for all classes, except $D_{\text{cruise vessel}} = 4$) and $\hat{f} = \frac{f}{f_{\text{ref}}}$, $\hat{f}_1 = 480\ \text{Hz}\ \left(\frac{V_{\text{ref}}}{V_C}\right)$, $f_{\text{ref}} = 1$ Hz and $V_{\text{ref}} = 1$ kn

The cargo vessels (container ships, vehicle carriers, bulkers, tankers) have an additional peak below 100 Hz, so that for these types the spectrum at $\hat{f} < 100$ is replaced by:

$$L_{S_f,0}\left(\hat{f} < 100, \text{Cargo}\right) =$$

$$K^{\text{LF}} - 40\log_{10}\left(\hat{f}_1^{\text{LF}}\right)\ \text{dB} + 10\ \log_{10}(\hat{f})\ \text{dB} - 10\log_{10}\left(\left(1 - \left(\frac{\hat{f}}{\hat{f}_1^{\text{LF}}{}_1}\right)^2\right)^2 + (D^{\text{LF}})^2\right)\ \text{dB},$$

with $K^{\text{LF}} = 208$ dB, $D^{\text{LF}} = 0.8$ (container ships and bulkers) or $D^{\text{LF}} = 1.0$ (vehicle carriers and tankers) and $\hat{f}_1^{\text{LF}} = 600\ \text{Hz}\ (V_{\text{ref}}/V_C)$.

NOTE: the above model expressions are for source spectral density level. In the final modelling these have been converted to source level in one-third octave bands by adding $10\log_{10}(0.231\,\hat{f})$ dB.

Table 3.2 ECHO vessel classes, based on AIS ship type ID, with fitted reference speed per vessel class.

Vessel Class (C)	AIS SHIPTYPE ID	Reference speed (V_C) in knots
Fishing vessel	30	6.4
Tug	31,32,52	3.7
Naval vessel	35	11.1
Recreational vessel	36,37	10.6
Government/Research	51,53,55	8.0
Cruise vessel	60-69 (length $l > 100$ m)	17.1
Passenger vessel	60-69 (length $l \leq 100$ m)	9.7
Bulker	70, 75-79 (speed $V \leq 16$ kn)	13.9
Container Ship	71-74 (all speeds) 70, 75-79 (speed $V > 16$ kn)	18.0
Vehicle Carrier	n/a	15.8
Tanker	80-89	12.4
Other	All other type IDs	7.4
Dredger	33	9.5

This model has been fitted to the ECHO database of measured ship source levels [MacGillivray et al, 2019]. The number of ships (n) in the database and the average speed through the water ($\bar{V}$) and (estimated) average length ($\bar{l}$) per vessel class are given in Table 3.3.

Table 3.3 ECHO data per vessel class: number of ships (n), average speed through the water ($\bar{V}$) and (estimated) average length ($\bar{l}$).

Vessel Class	n	$\bar{V}$ (kn)	$\bar{l}$ (m)
Bulker	850	13.5	211
Containership	440	18.8	294
Cruise	54	16.4	268
Fishing	21	10.1	32
Government	2	12.8	58
Naval	9	14.7	79
Other	6	14.0	81
Passenger	2	18.3	52
Recreational	7	15.2	45
Tanker	53	13.5	186
Tug	67	8.1	28
Vehicle Carrier	65	17.0	194

Figure 3.2 compares the Jomopans-ECHO model (dashed lines) with the measured average source level spectra (one-third octave bands) for the six dominant vessel classes in the ECHO database.

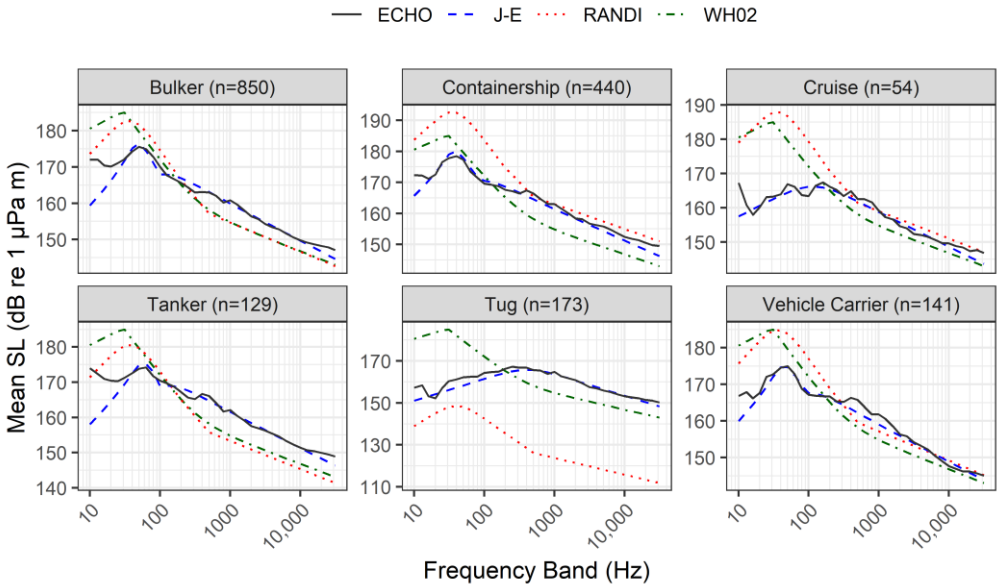

Figure 3.2 Comparison of the mean source level (for a fixed source depth of 6 m) versus frequency predictions of the WH02 [Wales & Heitmer, 2002], RANDI [Breeding et al, 1996] and JOMOPANS-ECHO (J-E) models with mean measured source levels from ECHO data set (black). The n value in each panel indicates the number of measurements that were averaged for the specified vessel type.

Figure 3.3 shows that over the 20 Hz to 20 kHz one-third octave bands the maximum absolute value of the mean residual difference (in one-third octave bands, averaged over all vessels) between the J-E model and the ECHO data is 2 dB, and the mean standard deviation of the residual differences per one-third octave band is 6 dB. The larger deviations observed in the one-third octave bands below 20 Hz is likely due to tonal noise at propeller blade rates and harmonics which are not represented in the statistical source level models. The speed and length trends in the original RANDI model appear to follow the trends observed the ECHO data set and so these coefficients were not modified in the J-E model. The J-E model was found to provide a significantly better match to the ECHO data, when compared with the older RANDI and WH02 models (Figure 3.2).

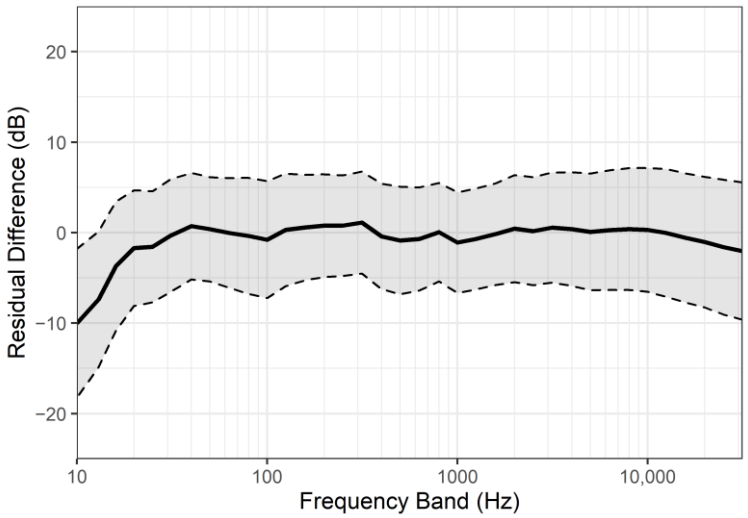

Figure 3.3 Mean residual differences (solid line) versus frequency between JOMOPANS-ECHO model and the ECHO data set. The dashed lines show one standard deviation of the residual differences about the mean. The mean standard deviation of the residual differences is 6 dB over the frequency range 20 Hz to 20 kHz. Over the same frequency range, the mean absolute value and interquartile range of the residual differences are 5 dB and 8 dB, respectively.

Dredgers (AIS type ID 33)

Dredgers are more abundant on the North Sea than in the Haro Strait. The ECHO data set does not include dredgers. TNO has measured the source level for multiple runs of 7 dredgers in a project during the construction of Maasvlakte 2, the Rotterdam port extension [de Jong et al, 2010]. The mean length of these dredgers was 123 m, the mean transit speed 13.8 kn and the mean dredging speed 1.8 kn. The Jomopans-ECHO source level model matches the mean observed source level for transiting dredgers with a fitted reference speed of 9.5 kn. While dredging, the source level is much higher than would be predicted based on the low speed, due to the propeller loading associated with the dredging. However, the JOMOPANS-ECHO source level model for a sailing speed of 14 knots provides a good estimation of the source level when the dredger is dredging (independent of the actual dredging speed). The AIS data available for JOMOPANS do not provide an indication when dredger is dredging, but we may tentatively assume that the dredger is dredging when its speed is lower than 3 knots.

Figure 3.4 shows the average measured source level spectra compared with this implementation of the JOMOPANS-ECHO model. The lower figures show the mean residuals and standard deviation.

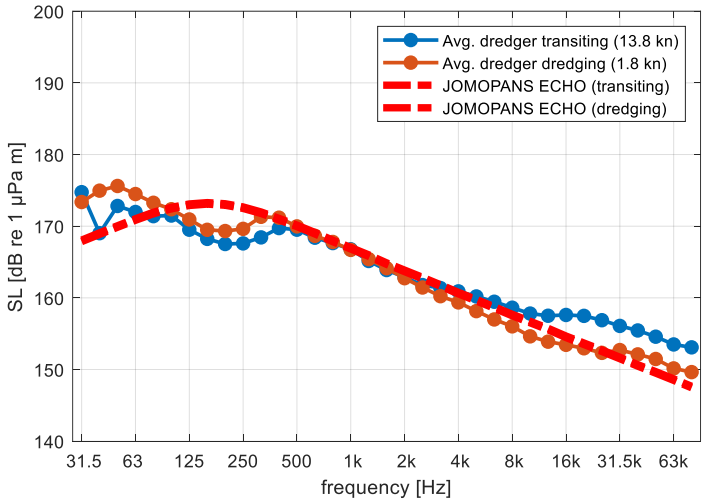

Figure 3.4 Measured average source level spectrum for dredgers (line with ●-markers), transiting and dredging, compared with the Jomopans-ECHO model (dashed lines), for a fixed source depth of 6 m.

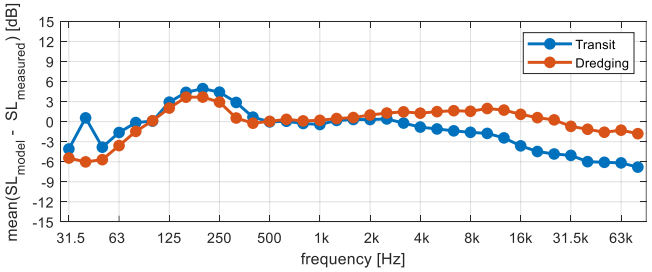

Figure 3.5 Difference between modelled and measured average source level spectrum for dredgers, transiting and dredging.

The Jomopans-ECHO model has been published in the Journal of Marine Science Engineering [MacGillivray & de Jong, 2021].

3.4 Ship noise propagation model

As explained in Chapter 1, various underwater acoustic propagation models are available, but not all of these are suited for mapping broadband ship noise in shallow water at large spatial and temporal scale. To manage the computational complexity, several simplifying assumptions have been made, including the selection of an efficient modelling algorithm.

- The propagation loss for the ship sources was calculated using TNO's Aquarius 3 model, which combines a range-dependent adiabatic normal mode sum for the lower frequency bands with a flux integral model for the higher frequency bands [Sertlek, 2016; Sertlek et al, 2018].
- This model was verified against other models for the T4.2 benchmark test cases, see Section 4.1 and [de Jong et al, 2020].
- AIS ship locations were replaced to the nearest position on a fixed source grid (section 3.8.3), so that the propagation loss between source and receiver locations can be precomputed.
- A so-called '$N \times 2\mathrm{D}$' approach is applied in which the range-dependent propagation loss is calculated along N radial trajectories from each ship source position.
- The model assumes a range dependent environment, with a sea water layer above a semi-infinite 'fluid' sediment (knows as a 'Pekeris' type waveguide).
- The water surface is modelled as a uniform flat pressure release boundary. Effects of surface waves are tentatively neglected.
- The water depth is range dependent.
- The Aquarius 3 approach is based on a stair-step approximation for the bathymetry and the calculation of normal mode eigenvalues for each stair step.
- Aquarius 3 calculates the analytic mode shapes of an equivalent free-free fluid wave guide, using Weston's 'effective depth' approximation, in combination with an approximation of the modal loss factor, as introduced by Kornhauser and Raney [1955].

3.5 Wind source model

The wind noise is calculated with the wind noise source and propagation models based on the semi-empirical expressions described in [Ainslie, 2010, Chapter 8], see [de Jong et al, 2018] and [de Jong et al, 2020]. The method used by the model is described by [Ainslie et al, 2011]. The propagation model is the same for both wind and rain, but only the wind source model was implemented in Aquarius. In the model wind is treated as a uniform sheet source, with a uniform source spectral density per unit area represented by the symbol K_f. The wind source level model uses Eq. 8.206 of [Ainslie, 2010] which gives K_f as a function of wind speed v at 10 m above the water surface, frequency f, and air-sea temperature difference. If the water is warmer than air ($T_{\mathrm{air}} - T_{\mathrm{water}} < 1°\mathrm{C}$) the model is independent of sea-air temperature difference, simplifying (for v_{10} > 1 m/s) in these conditions to:

$$K_f = \frac{10^{4.12}\left(\frac{v_{10}}{1\ \mathrm{m/s}}\right)^{2.24}}{1.5 + \left(\frac{f}{1\ \mathrm{kHz}}\right)^{1.59}}\ \mu\mathrm{Pa}^2\mathrm{Hz}^{-1}$$

This provides a smooth transition between the APL-UW (1994) wind noise source spectrum model, intended for the frequency range 10 kHz to 100 kHz, and the trend observed in measurement data from [Kuperman & Ferla, 1985] at lower frequencies, noting that the behaviour of the wind noise source level at frequencies of order 1 kHz and below is difficult to measure, and hence not well established. The quantity $10\log_{10}\frac{K_f}{\mu\mathrm{Pa}^2\mathrm{Hz}^{-1}}\ \mathrm{dB}$ (wind areic dipole source spectrum level) is plotted as a function of frequency in Figure 3.6.

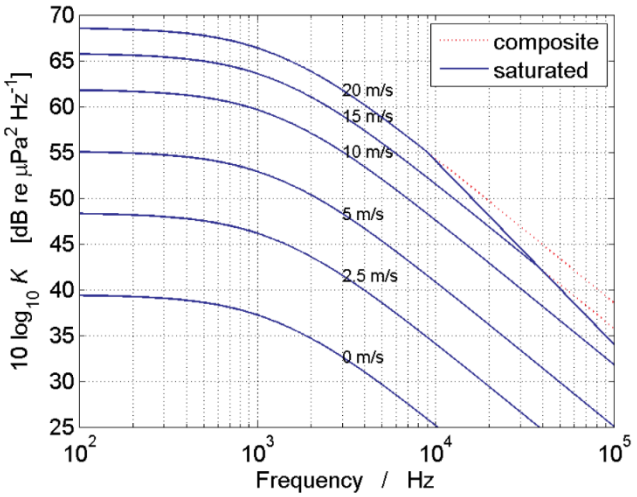

Figure 3.6 Wind noise areic dipole source spectrum level versus frequency (figure 8.17 from [Ainslie, 2010]); "composite"=evaluated using Equation (8.206); "saturated"=composite model, capped using Equation (8.203)).

Ainslie [2010, p.425] suggests: At high frequency and sufficiently high wind speed (above about 30 kHz for a wind speed of 10 m/s, or above 10 kHz for 15 m/s) special attention needs to be given to the absorbing effect of near-surface bubbles. A pragmatic approach is to cap the dipole source level so that it does not exceed the following frequency-dependent value (obtained by inspection of Fig. 17 from [APL-UW, 1994, p. II-43]:

$$10\log_{10}(\pi K_{max}) = 79 - 20\log_{10}\left(\frac{f}{1\ \mathrm{kHz}}\right)$$

This saturation is not yet implemented in Aquarius model.

3.6 Wind noise propagation model

Propagation of the wind noise is modelled by an implementation of Eqs.(10)-(12) from [Ainslie et al, 2011], taking into account multiple reflections of surface noise via the seabed and sea surface, including a low-frequency model of sea surface reflection loss as a function of wind speed, based on the measurements of Weston and Ching; Eq. (8.22) from [Ainslie ,2010].

The sound pressure spectral density level of wind noise at depth d below the water surface is calculated as the sum of direct and reflected path contributions:

$$L_{p,f,\mathrm{wind}} = 10\log_{10}\left(\frac{2\pi K_f(n_\mathrm{D} + n_\mathrm{B})}{1\ \mu\mathrm{Pa}^2/\mathrm{Hz}}\right)\ \mathrm{dB}$$

with n_D and n_B the direct and reflected path contributions, see [Ainslie et al, 2011].

The direct path contribution is

$$n_\mathrm{D} = E_3(2\alpha d)$$

With α the attenuation coefficient of sea water and $E_3(x)$ is the exponential integral of third order, which can be approximated by Eq. 9.157 from [Ainslie, 2010]:

$$n_\mathrm{D} \approx \frac{e^{-2\alpha d}}{2\alpha d + 3 - e^{-0.434(2\alpha d)}}$$

At distances and frequencies where absorption can be neglected this approximates to $n_\mathrm{D} \approx 0.5$.

The contribution of the reflected paths is

$$n_\mathrm{B} = \frac{1}{\eta}\left\{\sin\theta_c - (a-b)^{-1}\left[a^{3/2}\arctan\left(a^{-1/2}\sin\theta_c\right) - b^{3/2}\arctan\left(b^{-1/2}\sin\theta_c\right)\right]\right\}$$

with $a = 2\alpha H/\eta$ (for water depth H) and $b = 1/[2(kd)^2]$ (for wavenumber k).

The seabed and sea surface reflection losses are taken into account by means of an adjustment of the form $\eta = \eta_B + \eta_S$. Here η_B is the seabed reflection loss coefficient (see Eq. 8.86 of [Ainslie, 2010)], p.378):

$$\eta_B = 2w\epsilon\frac{cos^2\,\theta_c}{sin^3\,\theta_c} = 2w\epsilon\,\frac{v}{(v^2-1)^{3/2}}$$

This applies to coarse grained 'fluid' sediments with a sound speed ratio $v = c_{sed}/c_w > 1$, with critical angle $\theta_c = \arccos(1/v)$, density ratio $w = \rho_{sed}/\rho_w$ and attenuation parameter $\epsilon = \frac{\ln 10}{40\pi}\beta_{sed}$, with β_{sed} in decibel per wavelength. The corresponding loss for fine sediments ($v < 1$) (see Eq. (8.86) of Ainslie (2010), p.378) has not (yet) been implemented. Surface loss η_S is calculated as a function of frequency and wind speed v_{10} from a low-frequency sea surface reflection loss model, based on the measurements of [Weston and Ching, 1989] (Eq. 8.22 of [Ainslie, 2010, p.365], which is claimed to be valid up to an acoustic frequency of 4 kHz. The yearly averaged loss parameter is used.

$$\eta_S = 3.4\left(\frac{f}{1\text{ kHz}}\right)^{\frac{3}{2}}\left(\frac{v_{10}}{10\text{ m/s}}\right)^4$$

At high frequency the effects of refraction become less important relative than those of absorption. This effect can be approximately taken into account by imposing an upper limit to the surface reflection loss of 15 dB at normal incidence (see Ainslie, 2010, p.368). This corresponds with $\eta_{S,\max} = 15\ln 10\,/20 \approx 1.7$. At a wind speed of 10 m/s, this limiting value would apply at frequencies above approximately 600 Hz. This upper limit is not implemented in Aquarius model.

3.7 Model inputs used by Jomopans

3.7.1 Bathymetry

The North Sea bathymetry has been downloaded from the European Marine Observation and Data Network[3] (EMODnet). This provides water depth below lowest astronomical tide (LAT) on a 0.125 × 0.125 minute grid, see Figure 3.7. Tidal variations have not been included in the modelling.

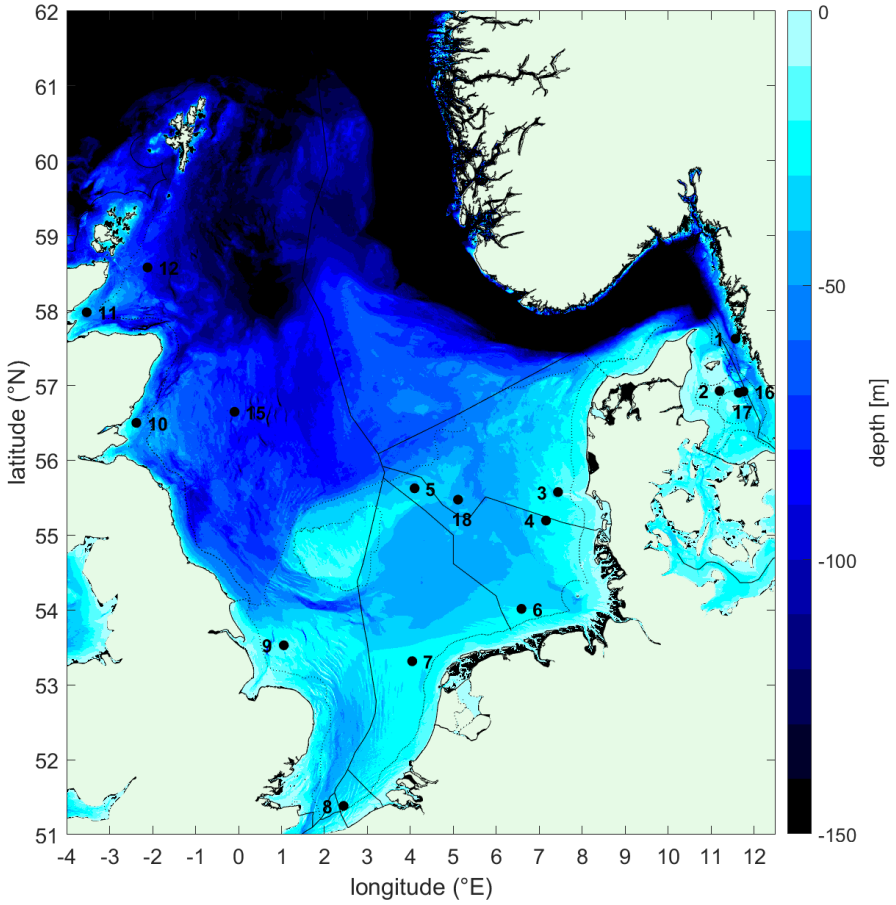

Figure 3.7 Bathymetry (water depth in m relative to LAT) map of the Jomopans area. The numbered black dots indicate the locations of the Jomopans 2019 underwater noise monitoring stations.

[3] https://www.emodnet-bathymetry.eu/

3.7.2 Acoustical properties of seawater

The sound speed and density of the water are assumed to be uniform in depth and range. Constant values are assumed: sound speed $1500\ \mathrm{m/s}$ and density $1000\ \mathrm{kg/m^3}$. These round number values have been arbitrarily chosen, noting that the applied propagation model is not sensitive to small variations in these parameters. [Ainslie, 2010, section 2.1] suggests sound speed $1490\ \mathrm{m/s}$ and density $1027\ \mathrm{kg/m^3}$ as "representative" values for sea water near the surface. Variation of these parameters with less than 10% will affect the calculated propagation loss with much less than $1\ \mathrm{dB}$.

Sound speed variations over the water column have been ignored. Variations of the sound speed with depth can result in a focussing of acoustic energy towards the direction (upwards or downwards) where the sound speed decreases. However, in large parts of the North Sea the shallow water is generally well mixed, so that the sound speed is relatively uniform over the water depth. Hence, sound speed profiles have less effect than in deep water, where sound can be channelled in ducts, strongly affecting the sound propagation. A study for the Dutch part of the North Sea [Sertlek et al 2016] illustrated that neglecting the effect of typical sound speed profiles for summer or winter time leads to an acceptable uncertainty in the propagation loss calculations for shipping noise, of not more than 1-2 dB.

In the Northern North Sea and in the Norwegian trench, where the water depth exceeds 100 m (Figure 3.7), neglecting the effects of sound speed variations over the water depth will cause additional uncertainty in the propagation loss calculations. The same may hold for the Kattegat, because observations of seasonal variability of recorded sound in the Baltic Sea have been attributed to the periodic variations in the sound speed profile of the water column [Mustonen et al, 2019].

Absorption in sea water (in dB/km) is implemented according to [Van Moll et al, 2009], for representative parameters $T = 10\ °C$, $S = 34$ ppt, $\mathrm{pH_{NBS}} = 8$ and $z = 0\ \mathrm{m}$, resulting in the frequency-dependent absorption shown in Figure 3.8.

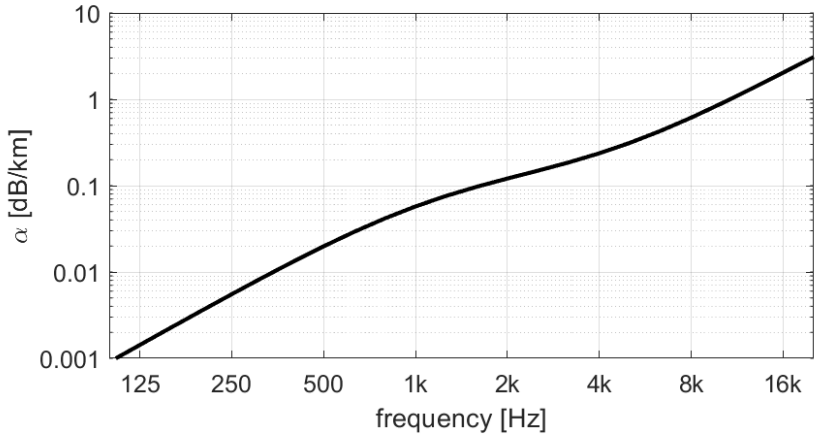

Figure 3.8 Sea water absorption α $[dB/km]$, according to Van Moll et al [2009], as applied in the Aquarius 3 modelling for Jomopans.

3.7.3 Acoustical properties of the seabed

In shallow water, the acoustic properties of the seabed have a major effect on sound propagation. Quoting [Ainslie 2010, section 4.4]: "*The seabed is a complicated layered medium whose acoustical properties vary with depth on length scales from a few millimetres to hundreds of meters. For simplicity it can be convenient to represent this layered medium by means of a uniform seabed with representative depth-averaged properties. However, to be useful the average must be over a depth scale relevant to the frequency of interest—typically a few wavelengths.*"

The upper layers of the North Sea seabed mainly consist of unconsolidated sediments (clay, silt, sand and gravel). Such sediments can be approximated as 'fluid' medium in which sound scattering and propagation is dominated by compressional waves. The effect of sediment shear stiffness on underwater sound propagation may be neglected to first order. Hence the relevant acoustic properties of the sediment are density, sound speed and attenuation coefficient.

So, the seabed is modelled as a fluid half space, with location- and frequency-dependent parameters:

- Sound speed c_s [m/s] (expressed as ratio c_s/c_w to the sound speed c_w in water at the seabed)
- Density ρ_s [kg/m^3] (expressed as ratio ρ_s/ρ_w to water density ρ_w at the seabed)
- Absorption β_s [dB/λ]

The location-dependent seabed properties are determined based on the median grain size of the sediment top layer.

Again quoting [Ainslie 2010, section 4.4]: "*Grain size is a useful descriptor of the acoustical properties of the seabed because it is strongly correlated with sound speed and density and, for a given sediment type, is independent of depth.*" This statement applies to 'pure sediment samples' (i.e., those whose grains all have the same size), but can be tentatively generalized to naturally occurring mixtures of different sediment types. The median grain size of such mixtures can be loosely related to the various sediment classification schemes in terms of descriptions such as for example 'coarse sand' (Udden-Wentworth), 'sandy silt' (Shepard) and 'muddy sandy gravel' (Folk).

Grain size $M(\phi)$ is commonly expressed in ϕ units, a logartithmic measure of grain diameter d:

$$M(\phi) = -\log_2\left(\frac{\overline{d}}{1\ \mathrm{mm}}\right)\ \phi$$

A map of median grain sizes of North Sea surface sediments is available from the World Data Center for Climate portal[4] [Bockelmann, 2017]. The download site notes that "*The underlying data set is a compilation of over 30,000 sediment samples from many national and European surveys conducted over a period of more than 50 years. Due to the vintage of some samples in the database, users are advised to consider the dynamic nature of the seafloor when using the data and when creating derived surrogate based habitat maps. Also, due to the diversity of sources for the point data, users should be aware of the differing methods by which the grain size analyses were conducted. As a consequence, map confidence is not necessarily uniform and thus areas not always comparable, even though interpolation surface may look continuous.*" Uncertainties in the sediment data and the resulting obstacles in harmonization have been described by Van Heteren and Van Lancker [2015].

Nevertheless, the median grain size map, see Figure 3.9, is considered to be the best available consistent data set on a global North Sea scale for characterizing the acoustical properties of the upper layer of the North Sea sediment.

In the Aquarius 3 shipping noise modelling, the median grain size of the sediment at the source grid locations is obtained from linear interpolation of the data from [Bockelmann, 2017]. Variations of sediment properties along the radial trajectories from the source along which the propagation loss is calculated are tentatively ignored.

The acoustic properties of the equivalent 'fluid' sediment are derived from the median grain size, based on conversions provided in Ainslie [2010, section 4.4]. Table 4.17 from [Ainslie, 2010] gives the conversion for near-surface sediment properties, typically applicable in the frequency range 10 kHz to 100 kHz, and Table 4.18 for the bulk properties of the uppermost few meter of sediment, typically applicable in the frequency range 1 kHz to 10 kHz.

At lower frequencies (typically below 1 kHz) the sound penetrates deeper into the seabed, where sediment sound speed and density increase with increasing depth, and the absorption decreases. The increase can be gradual, but it can also exhibit sharp contrasts at transitions between sediment layers, particularly at rock layers that support shear waves as well as compression waves. Moreover, the propagation in porous sediment layers results in dispersion (frequency-dependent sound speed) and nonlinear dependence of attenuation and frequency (see e.g. [Kibblewhite ,1989]).

[4] https://doi.org/10.1594/WDCC/coastMap_Substrate_MGS

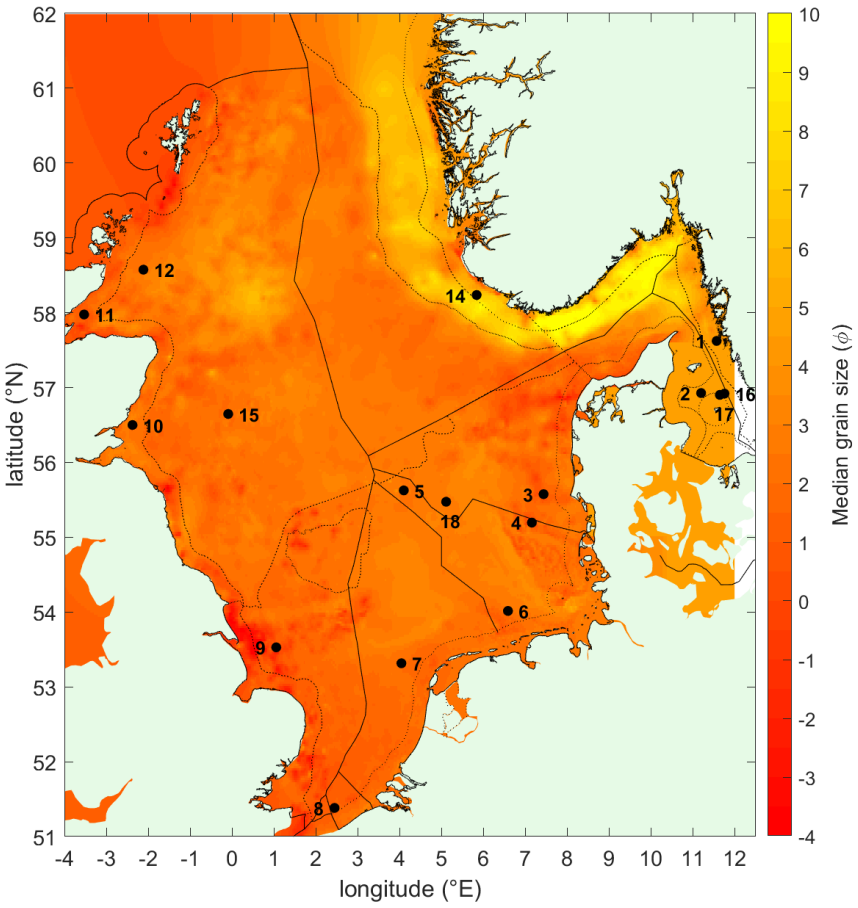

Figure 3.9 Map of the median grain size of North Sea seafloor surface sediments [Bockelmann, 2017]. The constant ϕ-value for the Southern part of the Kattegat (Northeast of Denmark) has been tentatively extrapolated. The numbered black dots indicate the locations of the Jomopans 2019 underwater noise monitoring stations.

Appropriate information on the geoacoustic properties of the North Sea sediment layers in the frequency range relevant for shipping noise (typically 50 Hz to 1 kHz) is lacking. Moreover, the additional numerical complexity of a depth-dependent geoacoustic model is impractical for underwater sound mapping at North Sea scale. Therefore, the Aquarius modelling includes an approximation of the seabed, modelled as a uniform 'fluid-like' half-space, with frequency-dependent acoustic properties.

The frequency dependence of the sediment properties is based on the 'low-frequency geoacoustic model for the effective properties of sandy sea bottoms' published by Zhou et al [2009]. This model was developed from long-range acoustic measurements conducted at 20 shallow water locations in different coastal zones around the world.

Figure 3.10 shows the measured sound speed ratio and attenuation from Zhou et al [2009].

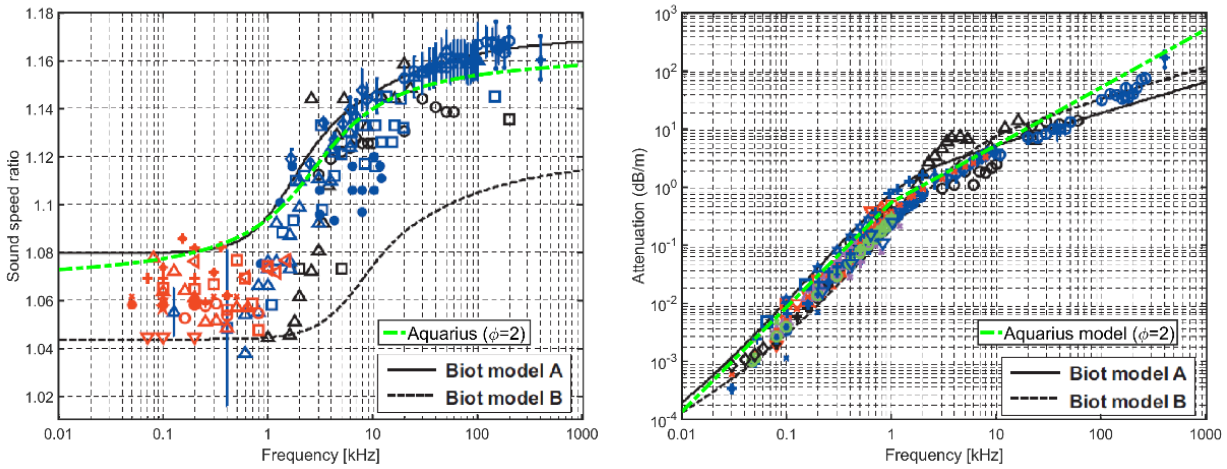

Figure 3.10 Measured broadband sound speed ratio (left) and attenuation (right) in sandy sea bottoms (Markers) compared with the Biot-Stoll model with the input parameters are adjusted to match either the sound speed ratio (Biot model A) or the attenuation (Biot model B), from [Zhou et al, 2009]. The green dashed lines give the results of the geoacoustic model implemented in Aquarius, for medium sand with a median grain size parameter $\phi = 2$.

The effective sound speed ratio c_r of the North Sea seabed applied in the Aquarius model consists of a parametrised inverse tangent curve:

$$c_r(f) = \mathrm{atand}\left(a * \left(\log 10\left(\frac{f}{1\ \mathrm{kHz}}\right) - b\right)\right) * c + d$$

where $\mathrm{atand}(x)$ denotes the inverse tangent function with argument x in degrees.
This curve was fitted to the sound speed ratio data from [Zhou et al 2009]. As no digitised data was available, the fit was carried out to 5 data values selected "by eye" to roughly match the 'Biot model A' curve in Figure 3.10 (left): $c_r(10\ \mathrm{Hz}) = 1.08$,): $c_r(100\ \mathrm{Hz}) = 1.08$,): $c_r(1\ \mathrm{kHz}) = 1.10$,): $c_r(10\ \mathrm{kHz}) = 1.145$,): $c_r(10\ \mathrm{Hz}) = 1.16$. Using the MATLAB curve fitting toolbox (nonlinear least-squares method) the parameters values were solved to be $a = 1.7778$, $b = 0.4508$, $c = 0.000554$ and $d = 1.1208$.

For the attenuation coefficient, the Aquarius model follows [Zhou et al 2009] by decreasing the absorption parameter in proportion with $f^{0.8}$, for frequencies below 1 kHz. No frequency dependence is proposed for the density ratio, in alignment with [Zhou et al 2009].

Although the Zhou et al [2009] paper and data do not indicate a clear dependence on median grain size, the Aquarius model was parametrized to include a grain size dependence, to match the tabulated geoacoustic parameters as a function of grain size for frequencies above 1 kHz, as provided in Ainslie [2010, section 4.4].

The sound speed ratio is adjusted by adding a constant value to the parametrised inverse tangent curve such that $c_r(10\ \mathrm{kHz})$ is equal the sound speed ratio $(c_{\mathrm{HF}}(\phi)/c_w)$ from Table 4.17 [Ainslie, 2010]. To avoid a sound speed ratio smaller than 1, which is not supported by the Aquarius propagation model, the low-frequency part of the curve is limited to a fixed minimum value of 1.01. Though the sound speed ratio at the seabed surface can be lower than one, low-frequency sound penetrates deeper into the seabed, where sediment sound speed increases with increasing depth. The value 1.01 is selected as a tentative choice for implementing this effect. It is not supported by evidence or data, but it resulted in a good model-data agreement for the Vinga site [Merchant et al, 2021].

For the attenuation coefficient, the Aquarius model takes the value $\beta_{\mathrm{HF}}(\phi)$ from Table 4.17 [Ainslie, 2010] for the frequency range above 1 kHz and calculates $\beta(f) = (f/1\ \mathrm{kHz})^{\,0.8}\beta_{\mathrm{HF}}(\phi)$ for frequencies below 1 kHz.

The frequency-dependent geoacoustic modelling that is implemented in the Aquarius model reduces the overestimation of low-frequency propagation loss that was observed in the first model-data comparisons [Merchant et al, 2021], without direct fitting of the model to the North Sea shipping observations. Note, however, that model development was outside the scope of the Jomopans project and that the proposed geoacoustic model has not been further investigated or validated.

More accurate modelling of the underwater sound propagation in the North Sea at low frequencies would require more research and data acquisition, particularly in regions with a muddy seabed, such as the Kattegat.

3.7.4 Surface wind

The ERA5 hourly data from the Copernicus website[5]: are used for the wind noise modelling. The amplitude of the wind speed vector is computed from the 10-minute averages of the U- and V-components of the wind speed vector measured at 10 m above the sea surface wind speed:

$$v_{1\mathrm{h}} = \sqrt{v_U^2 + v_V^2}$$

This data set provides the selected wind data on a one-hour timescale and on a 0.25º × 0.25º spatial grid. This is linearly interpolated to the (every 10 min) time steps and to the (0.05º × 0.025º) mapping grid for the sound pressure level predictions.

Note that the model predictions of the Jomopans acoustic metric would require much more detailed input data for the wind modeling than currently available, in spatial and temporal resolution as well as in averaging time. The uncertainty associated with this shortcoming is likely reduced by the statistical representation of the SPL in monthly percentiles, but it has not been further investigated quantitatively.

3.7.5 AIS data

Ship traffic at sea is monitored by AIS (Automatic Identification System) and VMS (Vessel Monitoring System) services. The International Maritime Organization's International Convention for the Safety of Life at Sea requires AIS to be fitted aboard international voyaging ships with 300 or more gross tonnage (GT), and all passenger ships regardless of size. AIS is intended, primarily, to allow ships to view marine traffic in their area and to be seen by that traffic. Under the European Union legislation, VMS is a legal requirement for commercial fishing vessels in excess of 15 metres, to allow environmental and fisheries regulatory organizations to track and monitor the fishing activities.

Because the information from AIS and VMS is not created for the purpose of sound mapping, there are several uncertainties in this input to the modelling (see Annex A).

Firstly, the information does not include all ships. Many small ships do not carry AIS transponders and ships can turn off their AIS transponders, for a variety of reasons. Moreover, land-based AIS receivers have a limited reception range (a few tens of kilometres, depending on location and weather conditions) and satellite-based receivers offer larger spatial coverage but poor temporal coverage.

Secondly, information from AIS provides an imperfect means of identifying vessel class and estimating source levels. For example, container ships and vehicle carriers cannot be distinguished from other types of cargo vessels through their AIS ship type identification. AIS broadcasts are not free from errors in vessel length, ship type ID, and speed, and vessel design details that truly relate to noise emissions, such as the speed at which the propellers start to develop cavitation and the type and power of the propulsion engines, are entirely absent from AIS data.

For the North Sea sound mapping, Jomopans has acquired processed AIS/VMS data of the North Sea shipping from Quiet Oceans[6]. These are based on land- and satellite-based AIS data, supplemented with VMS data, though the VMS data could not be obtained from all North Sea countries, due to national restrictions. The processing included check of validity and consistency and interpolation of the individual ship trajectories to a regular temporal resolution of 10 minutes. To further enhance the data, TNO applied an additional, apparently less restrictive, trajectory interpolation and speed check, see Annex A.

3.8 Map resolution

Numerical modelling of underwater soundscape maps requires selection of a model resolution in space, time and frequency.

3.8.1 Spatial resolution

Selection of the spatial resolution at which the sound maps are to be produced depends on the resolution interest to the user of the maps, on the available resolution of the model input data, and on the manageability of the numerical calculations and data.

Depth resolution

For the Jomopans sound maps of the North Sea, the depth averaged mean square sound pressure is calculated over 10 uniformly spaced points between 1 m above the seabed and 1 m below the sea

[5] https://cds.climate.copernicus.eu/cdsapp#!/dataset/reanalysis-era5-single-levels?tab=form
[6] https://www.quiet-oceans.com/

surface. To avoid the large uncertainties associated with sound propagation in very shallow water, the sound maps are limited to locations where the water depth exceeds 5 m.

Horizontal resolution
The Jomopans sound maps for the North Sea area were calculated at a horizontal resolution of 0.05° longitude × 0.025° latitude, corresponding with approximately square grid cells of about 3.2 × 2.8 km^2. This was considered sufficient to resolve the main shipping lanes, while at the same time keeping the number of grid points manageable.

The Jomopans receiver grid covers the longitudes between -5.2 and 13.2 degrees East and the latitudes between 50.9 and 62.1 North. At the given resolution this results in 369x449 (=165681) grid points.

The World Meteorological Organization (WMO) divides the chart of the world into grid cells of 10° latitude by 10° longitude. WMO square 1500 covers the longitudes between 0 and 10 degrees East and the latitudes between 50 and 60 North. WMO squares are used as the basis for the c-squares (concise spatial query and representation system) spatial indexing system [Rees, 2003], which further divides 10°×10° WMO squares into smaller units of 5°×5°, 1°×1°, 0.5°×0.5°, 0.1°×0.1°. The c-squares strings describing the four 0.1° squares in the outer corners of the Jomopans receiver grid are:

1501:103:392 | 1601:123:112 | 7500:205:392 | 7600:225:112

3.8.2 Spatial processing for sound maps

In order to reduce the computational complexity of the modelling, sound maps are generally obtained using an "$N \times 2\mathrm{D}$ approach" for the source locations, implying that the modelling results are obtained by means of two-dimensional linear interpolation between radial transects (slices/radials) from each source. Furthermore, the modelling range (i.e. the length of the transects) has a large effect on the computational complexity.

Number of radials
For environments with a high spatial variability (e.g. strong variations in water depth or seabed properties) a large number of radials may be needed; while for more homogenous environments a smaller number can be sufficient. Because the environment varies gradually over large fraction of the North Sea area, it was suspected that using a limited number of radials transects is sufficient for most of the North Sea area (with the exceptions of source locations near coastal areas and strong bathymetric features, e.g. near the Skagerrak). The effect of the choice for the number of radials was determined by calculating a single time step ship noise map for the North Sea with two different numbers of radials (16 and 36 radials respectively, uniformly distributed over 360°), **see Annex D.1**. The simulation results indicate that using a reduced number of radials (16 instead of 36) has a small (< 1 dB) effect on the predicted SPL for the majority of North Sea region. Somewhat larger local differences occur in coastal regions and at locations with a large depth variation and low shipping density, such around the Dogger Bank. To keep the calculation time for the North Sea maps manageable, it was decided to limit the calculations to 16 radials.

Maximum length of radials
Sound generated by a ship may contribute up to many kilometres, depending on frequency, environment and background noise produced by other sources (including wind and other ships). In order to reduce the computational complexity of the modelling, it is desirable to limit the maximum computation range where possible. The effect of the choice for the length of the radials was determined by calculating a single time step ship noise map for the North Sea with different radial lengths (from 25 km up to 500 km), **see Annex D.2**. As expected, these simulations indicated that the largest radial distances are required for low-frequency ship noise simulations in areas with a low shipping density. For the Jomopans North Sea sound maps, it was decided to extend the radials to 400 km for all frequencies and all source locations. The added value of using different radial lengths for different frequencies was not worth the software implementation effort, thanks to the effective vectorization of TNO's Aquarius propagation model, which has a frequency-independent computation time. For more complex ray and parabolic equation type models, however, it might be beneficial to reduce the radial length for higher frequencies.

Spatial resolution along radials
The propagation loss calculation along the radials is calculated at a horizontal spatial resolution of 100 m, from a location at 100 m from the source grid location to the maximum distance of 400 km. Radials are ended where the water depth is smaller than 5 m. The bathymetry along the radial is linearly interpolated from the bathymetry map (section 3.7.1).

3.8.3 Source grid

The computation time can be reduced significantly by means of source gridding. This enables repeated use of stored data (look-up table) from a single calculation of propagation loss between predefined source and receiver grids for shipping sound map calculations over multiple time steps. This requires that the environmental properties do not vary significantly over the time window over which the look-up table is used. Actual ship locations from AIS are relocated to the nearest source grid position.

The effect of the source gridding was studied for the calculated monthly statistics of SPL for the area around the Vinga measurement location, by comparing gridded scenarios against the reference solution without source gridding, **see Annex D.3**. It was concluded that the application of a source grid with a resolution similar to the receiver grid resolution, but shifted by one half of the grid resolution to avoid overlap, results in negligibly small differences of the monthly SPL statistics compared to the reference solution, except in the close vicinity of shipping lanes.

For the Jomopans North Sea sound maps, it was decided to apply a source grid based on the receiver grid, shifted by one half of the grid resolution and slightly refined by adding intermediate source grid positions at 0.025° latitude resolution, while avoiding overlap with the receiver grid points, see Annex D.3.

The spatial extent of the Jomopans source grid area overlaps with the Jomopans receiver grid area. For future applications, the source grid should be selected greater than the receiver grid, so that all ships within the maximum length of the radials are included. This means that AIS input area should also be selected greater. This was not possible with the AIS data acquired for Jomopans, but should be taken into consideration for future ship noise mapping efforts. As a consequence, the SPL values near the outer edges of the Jomopans North Sea sound maps for 2019 are likely too low.

3.8.4 Temporal resolution

A minimum number of temporal ‘snapshot’ calculations is required to get a reliable and robust calculation of the monthly percentile maps. The AIS data have been provided at a 10 minute resolution, the wind data at a 60 minute resolution. In order to get a better understanding of the sensitivity of the calculated SPL percentiles for the selected temporal resolution, the statistical sound maps were calculated for time resolutions of 20, 30 and 60 minutes respectively, **see Annex D.4**.

The simulations showed that using a 60 minute temporal resolution instead of 10 minutes mainly affected the higher percentiles of SPL. At some locations, the error in the 95% temporal percentile was found to be of the order of 2 dB. The median SPL values were not significantly affected by reducing the temporal resolution from 10 minutes to 60 minutes.

The Jomopans North Sea sound maps were calculated at a 10 minute resolution.

3.8.5 Frequency resolution

The Jomopans acoustic metric is calculated in one-third octave (base-10) bands. Acoustic modelling in the frequency domain applies to single frequencies. To limit the computation time, the one-third octave band levels must be calculated from a minimum number of single frequency calculations per band. The effect of including more than one frequency per band was tested for the verification scenario described in section 4.1.2, see [de Jong et al 2020]. In the calculation of the broadband SPL the effect is less than 1 dB. In the individual one-third octave bands SPLs at fixed distances (10 and 40 km), differences between the single frequency and band average results are up to 2 dB in the bands that dominate the broadband SPL. At the lower and higher frequencies, where the calculated SPL values contribute less to the broadband SPL, the difference is substantially larger (>10 dB). Using one frequency per one-third octave band is likely an acceptable reduction of the calculation effort, at the cost of an approximate uncertainty of 2 dB in the calculated depth averaged SPL in one-third octave bands. If one is interested in levels at a specific receiver depth, the error associated with using a single frequency per band can be significantly larger.

For the Jomopans North Sea sound maps, the one-third octave bands SPL spectra were calculated at the centre frequencies.

3.8.6 Jomopans resolution settings

Table 3.4 describes the model resolution settings that were selected for the Jomopans shipping and wind noise maps for the North Sea in 2019.

Table 3.4 Model resolution for the Jomopans North Sea sound maps

Parameter	Setting
Time steps	Every 10 minutes (e.g. 4464 snapshots for May 2019)
Frequencies	One-third octave (base-10) band centre frequencies, from 10 Hz to 20 kHz
Receiver grid	0.05 degrees longitude and 0.025 degrees latitude (about 3 km × 3 km) Depth average over 10 equally spaced grid points
Ship source grid	the same resolution as the receiver grid, but shifted by one half of the grid resolution, with additional intermediate grid positions added
Number of radials	16
Length of radials	400 km
Resolution along radials	100 m
Interpolation from radials to receiver grid	2D linear interpolation

3.9 Calculation time for Jomopans sound maps

A dedicated PC running 64-bit windows 10 has been used to do the calculations with an Intel Xeon 4114 CPU @ 2.2 GHZ (10 cores) and 128 GiB of memory installed. A large part of the time we also had access to another heavier PC with 20 cores and 512 GiB of memory which was considerably more efficient to calculate the month statistics.

Most calculations are setup in a way that if anything goes wrong and they are restarted and continue from where they were. On the rare occasions that something goes wrong and a process halts the time waiting for the user to restart will have to be added to the calculation lead time.

Calculating the fine source grid propagation loss lookup table using 16 radials and 400 km distance for the JOMOPANS area on a dedicated machine takes about 7 days using three parallel MATLAB sessions which gave the optimal performance as MATLAB is able to automatically use multiple cores per session (80-95 % CPU usage in this scenario). Using only 1 core it would take about 14 days.

Calculating SPL levels for one snapshot in time takes about 10 minutes, using the propagation loss look-up table. A 10-minute resolution and 1 month of shipping data this results in about 4320 snapshots. That would take about 32 days when using 1 MATLAB session. Using 6 sessions results in about 9 days of computation. When upscaling to multiple MATLAB sessions the usage of a secondary hard drive was required for storing the snapshot results while reading the source gridded propagation losses from the first hard drive.

Reshuffling the data and calculating the percentiles and excesses takes about 2 days using a single MATLAB session. Most of that time was spent on reading and writing the data.

Table 3.4 Calculation time and data volume for Jomopans North Sea sound maps for the 12 months of 2019 using the optimal number of sessions for the TNO dedicated computer.

	Computation time	Data size
Calculate propagation loss	7 days	Prop loss database 768 GB
Calculate snapshots of SPL levels for 12 months	12 * 9 days	wind 2250 GB ships 4800 GB
Reshuffle snapshots into areas	7 days	4800 GB
Calculate month statistics	12 days	50 GB
Calculate year statistics	12 days	6 GB
Total	**146 days**	**13 TB**

4 Verification and validation of modelling

The credibility of the modelled underwater sound maps depends on an appropriate verification and validation of the applied models. Jomopans [Robinson & Wang, 2020] uses the term '*verification*' for demonstrating that the numerical models are correctly implemented in software and calculate the correct outputs for specified inputs. '*Validation*' refers to demonstrating that the model outputs reflect an adequate representation of physical reality. This evidence of adequate representation of reality comes from comparison to physical measurements.

Section 4.1 describes two benchmark scenarios that have been developed by Jomopans for verification of the selection of an appropriate underwater acoustic propagation model for creating shipping noise maps in shallow water, including a verification of the correct model implementation.

These scenarios and the solutions (provided in Annex E) provide a highly recommended benchmark for model verification for future sound mapping efforts.

4.1 Model verification: benchmark cases for shallow water propagation

Jomopans has developed two benchmark scenarios to verify the implementation of underwater acoustic propagation models. These benchmarks have been published and presented at the 5th Underwater Acoustics Conference and Exhibition UACE2019, Hersonissos, Crete, Greece [Binnerts et al, 2019], see also [de Jong et al, 2020]

4.1.1 Benchmarked propagation models in Jomopans

Table 4.1: overview of models that have been compared, a description of the model type and an indication of the frequency range of applicability

	Model name	Model type	Frequency range	Remark
TNO	Aquarius 3	Range-dependent hybrid analytical mode sum + flux integral model	32 Hz-20 kHz	High precision configuration used for benchmarking
	Aquarius 4	Range-dependent numerical mode model using mode lookup table	10 Hz-20 kHz	Contribution from leaky modes neglected
	RAM	Range-dependent split-step Padé PE	10-500 Hz	Double precision
QO	RAM-Surf	Range-dependent split-step Padé PE	10 Hz - 2 kHz	High precision configuration used for benchmarking. Bellhop used for 2 kHz one-third octave band.
	Bellhop	Range-dependent coherent Gaussian rays	2 kHz - 20 kHz	
	Quonops	Hybrid RAM-Surf & Bellhop	10 Hz – 20kHz	
FOI	JEPE	Range-dependent Jeltsch energy-conserving PE	32 Hz - 10 kHz	
	XRAY	2D hybrid raytracing and plane wave	200 Hz - 20 kHz	
	REV3D	3D hybrid raytracing and plane wave	200 Hz - 20 kHz	Coherent and Incoherent
	XFEM	range-independent, wave number integration/ normal modes	10 Hz - 20 kHz	
	RPRESS	range-independent, wave number integration/ normal modes	10 Hz -10 kHz	
NPL	OASES	Wavenumber integration	10 Hz - ~20 kHz	Range-dependent version limited to ≤1 kHz (test case 2)
JASCO	Marine Operations Noise Model (MONM)	Range-dependent split-step Padé PE	10 Hz - ~20 kHz	

Note that all of these models have their own specific implementations of the acoustic wave equations

and their own specific settings. For example: normal mode model settings include the number of modes and the root finding algorithm applied to find these modes, ray model settings include the number of rays and the type of rays and parabolic equation model settings include number of Padé terms [Jensen et al, 2011]. In the JOMOPANS model benchmarking, the selection of model settings was left to the model operators. Several model settings were adapted after a first iteration of comparing the results for the two test cases described below, generally leading to a reduction of the differences between the model results.

4.1.2 Test case 1: Ship noise propagation in a range-independent environment

The basic test case 1 is adapted from the 'single ship' scenario from the AQUO-SONIC workshop [Colin et al, 2015], which was based on a test case defined in the Weston sonar performance modelling workshop (WMW) [Zampolli et al, 2010], see also [Sertlek & Ainslie, 2014] and [Sertlek et al, 2018].

The test case involves the two-dimensional (axisymmetric) modelling of propagation loss in a 'range-independent' shallow water (Pekeris) waveguide and the calculation of sound pressure levels due to the sound spectrum radiated by a ship, represented by an omnidirectional point source at 5 m below the sea surface. The scenario is sketched in Figure 4.1. This scenario deviates from the original WMW scenario by a different source depth (5 m instead of 30 m) and water depth (50 m instead of 100 m) and by an extension towards lower frequencies (down to the 10 Hz frequency band). This makes the scenario more representative for ship noise (source close to sea surface and low frequency noise) and for the North Sea environment (mainly shallow water). Although no benchmark results are available for this altered scenario, wave number integration and normal modes, such as RPRESS, XFEM and OASES, have been sufficiently tested for a range independent environment, to have confidence that these provide a "trusted solution".

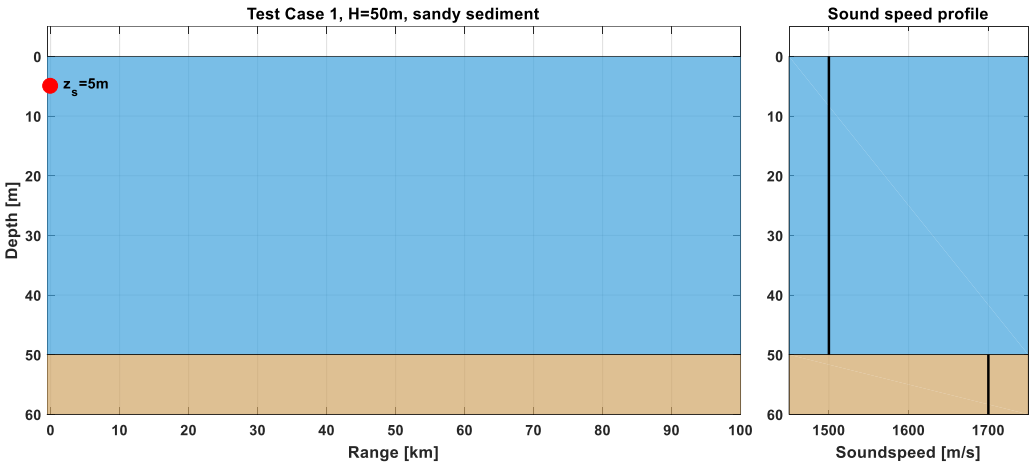

Figure 4.1 Schematic representation of the Test Case 1 environment. The red dot indicates the source position at 5 m depth

Sea surface

- Smooth (perfectly compliant) sea surface.
  - Zero wind speed
  - Zero surface roughness

Water:

- Iso-velocity water
  - uniform sound speed $c_0 = 1500\,\mathrm{m/s}$
  - uniform fluid density $\rho_0 = 1000\,\mathrm{kg/m^3}$
- Absorption α_0 in sea water, in dB/km, (Ainslie-McColm model, from [Ainslie, 2010], p 29):

$$\alpha_0 = \frac{20\ dB}{ln10}\left(\alpha_1 \frac{\hat{f}^2}{\hat{f}^2 + \hat{f}_1^2} + \alpha_2 \frac{\hat{f}^2}{\hat{f}^2 + \hat{f}_2^2} + \alpha_3 \hat{f}^2\right)$$

  - Here $\hat{f}$ is the frequency in kHz, and $\hat{f}_1 = 1.15$ and $\hat{f}_2 = 75.6$ are relaxation frequencies in kHz. The coefficients α_i are: $\alpha_1 = 1.40 \times 10^{-2}$, $\alpha_2 = 5.58$ and $\alpha_3 = 3.90 \times 10^{-5}$.

Sea floor:

- Uniform water depth $H = 50\,\mathrm{m}$.

- Homogeneous half space, sandy sediment
  - Fluid model for the sediment: only compression, no shear
  - Compressional wave velocity $c_s = 1700\,\mathrm{m/s}$ (sound speed ratio $c_s/c_0 = 1.1333$)
  - Density $\rho_s = 2000\,\mathrm{kg/m^3}$ (density ratio $\rho_s/\rho_0 = 2$)
  - The sediment absorption coefficient (β), in units of decibels per wavelength, is 0.5, corresponding to an absorption coefficient per unit frequency (β/c_s) of 0.294118 dB/(m kHz). The sediment absorption coefficient is related to fractional imaginary part ϵ of the complex sediment wave number $k_s(1 + \mathrm{i}\epsilon)$ by means of $\epsilon = \beta \ln(10)/40\pi$ [Sertlek et al, 2018].

Source

- Source depth $z_s = 5\ \mathrm{m}$
- Source directivity: omnidirectional (monopole)
- Average shipping source level spectrum as suggested by [Colin et al, 2016] based on [Wales & Heitmeyer, 2002], extrapolated outside its range of validity below 30 Hz and above 1.2 kHz, using the following formula for the mean monopole source spectral density level (in $\mathrm{dB\ re\ 1\ \mu Pa^2\ m^2/Hz}$)

$$L_{S,f}(f) = 230\ dB - 10log_{10}\left(\left(\frac{f}{1\ Hz}\right)^{3.594}\right)\ dB + 10log_{10}\left(\left(1 + \left(\frac{f}{340\ Hz}\right)^2\right)^{0.917}\right)\ dB \quad (5\text{-}1)$$

  - At frequencies of 30 Hz and below, a constant value of $L_{S,f}(f)$ is used, equal to the right hand side of Eq. (2), evaluated at 30 Hz.
- The one-third octave ('OTO') band source level $L_{S,\mathrm{OTO}}$ is approximated by the level of the product of the spectral density at the band centre frequency and the bandwidth of each band:

$$L_{S,OTO}(f_n) \approx L_{S,f}(f_n) + 10\,log_{10}\left(0.231\frac{f_n}{1\ Hz}\right)dB \quad (5\text{-}2)$$

- The one-third octave (base 10)[7] bands are defined by ISO 18405, with centre frequencies:

$$f_n = 10^{\frac{n}{10}} \times 1\ kHz, \quad \text{for} \quad n = -20{:}\,1{:}\,13 \quad (5\text{-}3)$$

Output specification

The quantity to be calculated is the sound pressure level (SPL) spectrum $L_{p,\mathrm{OTO}}(f_n, r, z)$ in one-third octave bands ranging from 10 Hz to 20 kHz , with f_n the centre frequency of the n-th band, in Hz, and (r, z) the range and depth of the receiver positions, in m.

- The SPL is calculated as the difference of the single ship source level and the calculated propagation loss (PL) between the reference position of the source and the receiver positions:

$$L_{p,OTO}(f_n, r, z) = L_{S,OTO}(f_n) - N_{PL}(f_n, r, z) \quad (5\text{-}4)$$

- Calculations for the Test Case 1 scenario are compared at the band centre frequency with calculations for a single frequency.
- The total broadband SPL in the 10 Hz to 20 kHz one-third octave bands is calculated by summation of the spectral contributions:

$$L_{p,BB}(r, z) \approx 10\,log_{10}\left(\sum_{n=-20}^{n=13} 10^{\frac{L_{p,OTO}(f_n,r,z)}{10\ dB}}\right)\ dB \quad (5\text{-}5)$$

- The receiver ranges r of interest are between 100 m and 100 km from the source. A minimum requirement is to calculate the SPL at ranges of 0.1, 0.2, 0.5, 1, 2, 5, 10, 20, 50 and 100 km. If possible, a higher range resolution may be useful, e.g. to produce continuous graphs of SPL versus distance with a 100 m receiver range resolution.
- A minimum requirement is to calculate the depth averaged value of the squared sound pressure over the local water depth H at the receiver. The user defines and reports the depth resolution in the calculations.

Results

Figure 4.2 shows the model predictions of the depth averaged broadband SPL as a function of range for the test case 1 scenario.

[7] JOMOPANS always uses the one-third octave (base 10) bands, i.e., decidecade (or one-tenth decade) bands, even when the '(base 10)' is not mentioned explicitly.

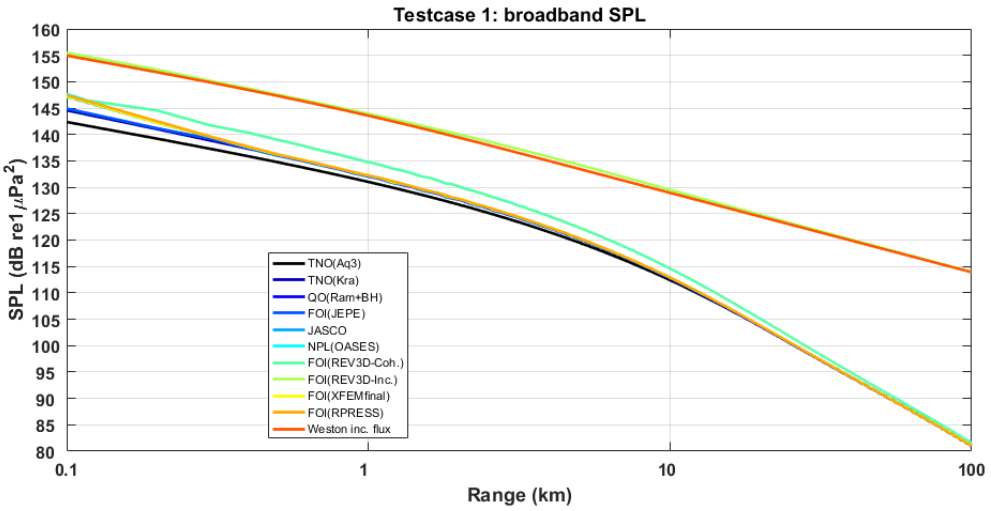

Figure 4.2 Calculated depth-averaged broadband SPL in dB re 1 μPa^2 as a function of range (horizontal distance to the source) for test case 1 for the various models (see legend).

Figure 4.2 shows the one-third octave band spectra of the SPL as a function of frequency and distance from the source for test case 1 predicted by the various models

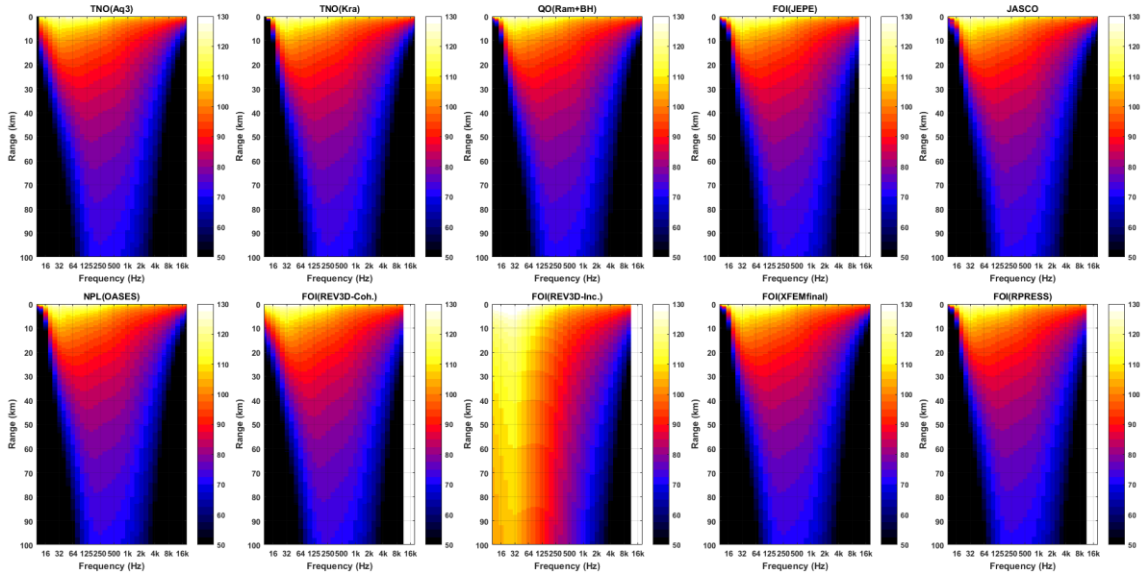

Figure 4.3 Depth-averaged SPL in dB re 1 μPa^2 as a function of frequency (one-third octave bands) and range, as calculated by the various models for test case 1.

The results for test case 1 benchmark show that an agreement of the broadband SPL (<1 dB) can be achieved by using the correct model configuration at ranges beyond 500 m. At shorter ranges, larger deviations can be observed, associated with the specific approximations in the different modelling approaches. These differences are of little concern for the long range sound propagation loss calculations for the shipping noise maps.

Because the wavenumber integration approach involves the least approximation, the solution from FOI's XFEM model is offered as a reference solution for this first benchmark case. Selected values are tabulated in Annex E.

4.1.3 Test case 2: ship noise propagation in an environment with an upslope bathymetry

The second test cease is range-dependent, meaning that it incorporates the effects of a varying water depth (bathymetry) on sound propagation. Details on the origin of the scenario can be found in [Sertlek et al, 2018, Case 4]. The geometry is shown in Figure 4.4. The source depth and other input parameters and the output specification for this scenario are identical to test case 1 (section 4.1.2).

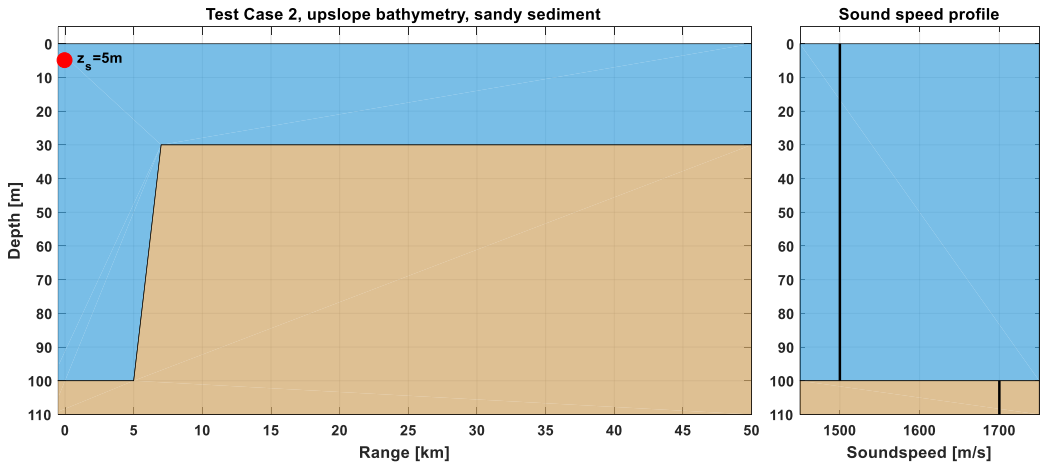

Figure 4.4 Schematic representations of the test case 2 environment with a 5 m source depth (red dot) to be representative for ship generated noise and an iso-velocity sound speed gradient, similar to the test case 1 environment.

Results

Figure 4.5 shows the model predictions of the depth averaged broadband SPL as a function of range for the test case 2 scenario.

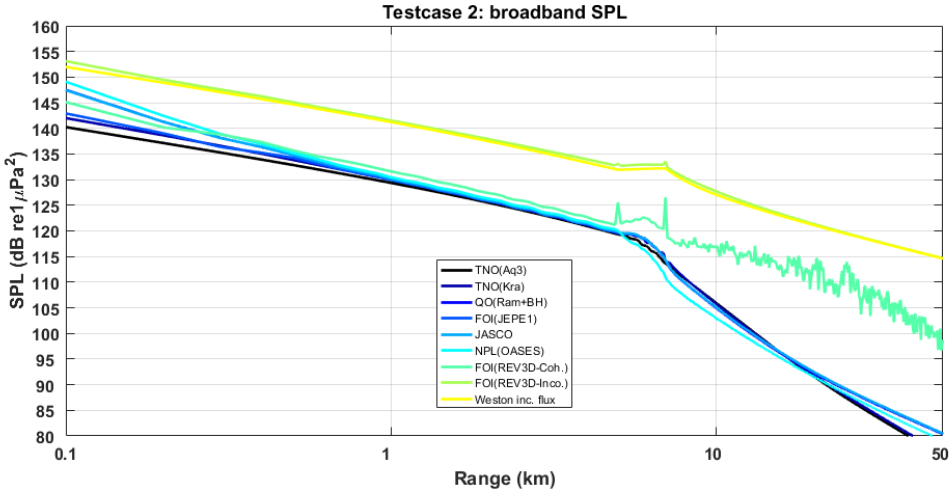

Figure 4.5 Calculated depth-averaged broadband SPL in dB re 1 μPa^2 as a function of range (horizontal distance to the source) for test case 2 for the various models (see legend).

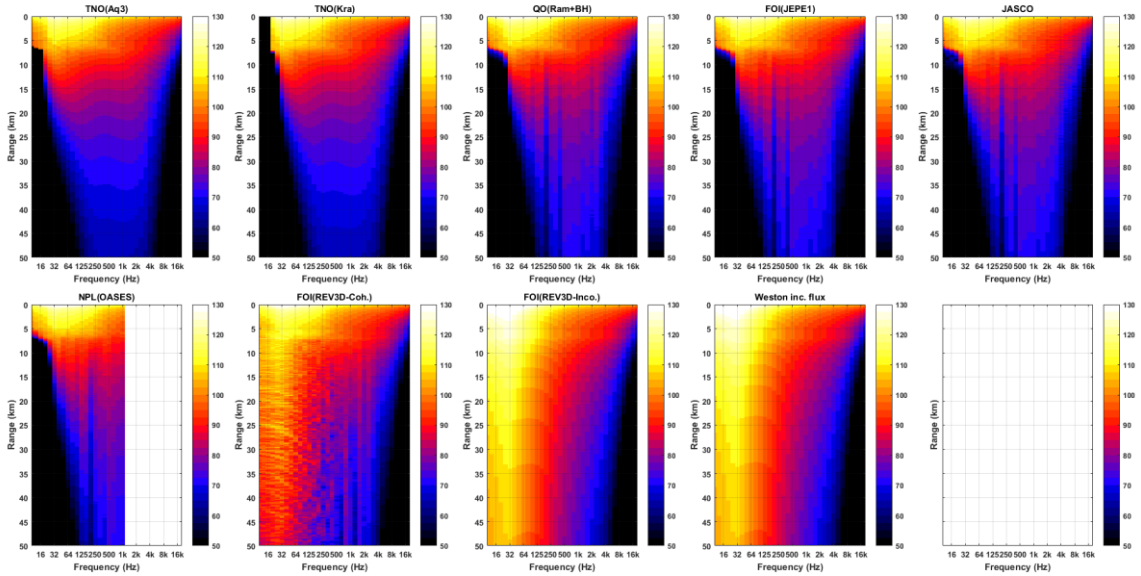

Figure 4.6 Depth-averaged SPL in dB re 1 μPa^2 as a function of frequency (one-third octave bands) and range, as calculated by the various models for test case 2.

The results for test case 2 benchmark show that an agreement of the broadband SPL (<2 dB at ranges beyond about 1 km from the source up to about 20 km) can be achieved for this range-dependent scenario by using the correct model configuration. Also, it is observed that the Aquarius models, that make use of the adiabatic approximation, deviate from the parabolic equation models (RAM, JEPE and MONM), leading to a lower SPL at large distances (up to about 5 dB at 50 km).

In contrast with the range-independent test case 1, where the wavenumber integration models provide a trusted solution, there is no fully trusted solution for this second, range-dependent, benchmark case. As a compromise, the (power-) average of the solutions of the three parabolic equation models, which differ very little, is proposed as a reference solution. Selected values are tabulated in Annex E.

4.2 Model validation: comparison with 2018 and 2019 data from Jomopans measurement stations

The overall pattern of observed differences between measured and predicted monthly SPL percentiles at the JOMOPANS measurement stations [Fisher et al, 2021], [Putland et al, 2021] was that the model predicted sound levels which were lower than the measurements at low frequencies (< 2 kHz), while the model more closely agreed with the measurements at higher frequencies (> 2 kHz).
WP6 [Putland et al, 2021] concluded: “Overall, the analysis did not identify consistent uncertainties in noise maps, rather uncertainties may be caused by a complex combination of factors, including sediment uncertainty and additional sources of noise in the measurements such as operational wind farms, vessels not on AIS/VMS records and seismic surveys..

5 Uncertainties and recommendations

To be able to model the monthly statistics of underwater sound at North Sea scale, many assumptions and approximations have to be made. This inevitably leads to uncertainties. The uncertainty can be partially assessed by comparison of model predictions to measurements from local monitoring stations, provided that uncertainty in the measurements is limited and can be quantified. The lesson learned from the measurements (WP5) and model-data comparisons (WP6) in Jomopans is that it is very difficult to separate the multiple causes for uncertainties in measurements and modelling. Consequently, it is not yet possible to quantify the uncertainty in the modelled underwater sound maps, particularly at locations that are not close to measurement stations. Nevertheless, this chapter provides an overview of the various possible sources of uncertainty that have been identified in Jomopans studies and discussions.

Annex B to this report gives a general introduction into the analysis of the combined uncertainty in the statistical underwater noise estimates produced by the modelling which derive from the uncertainties in the input quantities to the model. This approach could not be further developed within the Jomopans project, but deserves further development in possible follow-on projects.

The following sections describe the various sources of uncertainty. These are grouped in uncertainties associated with completeness of the model and input data (section 5.1), with uncertainties in the models (section 5.2) and in the input data (section 5.3).

5.1 Uncertainties due to incompleteness of models and input data

The Jomopans modelling started with the hypothesis that the relevant monthly statistics of the underwater noise in the North Sea are dominated by noise from ships and wind.

Other sources
Incompleteness of the modelling due to the omission of other sound sources may explain part of the model-data deviations that have been observed at some Jomopans measurement stations. This has not yet been further investigated. In principle, more sources could be added to the modelling, for example:

- other natural sounds (such as rain, snow, hail, lightning, thunder, earthquakes, surf zone wave breaking, current related sounds, marine life)
- impulsive sounds (such as explosions, seismic surveys, marine piling and sonar); though these are covered in the scope of Descriptor 11.1.2 of the MSFD, there may be areas where these contribute to the monthly SPL statistics.
- offshore platforms and structures (such as wind turbine operational noise and oil- and gas activities).

The feasibility to include these additional sources depends on the availability of appropriate models and input data.

Ship traffic data (AIS/VMS)
The available ship traffic data is inherently incomplete. Many small ships do not carry AIS transponders and ships can turn off their AIS transponders, for a variety of reasons. Moreover, land-based AIS receivers have a limited reception range (a few tens of kilometres, depending on location and weather conditions) and satellite-based receivers offer larger spatial coverage but poor temporal coverage. Limits in coverage can be somewhat compensated by interpolation of individual ship tracks, but ships without AIS are excluded from the modelling. This leads to an underestimation of the underwater noise at locations where the noise is not dominated by the larger vessels with AIS coverage, as has been observed for Scottish and Danish measurement stations [Putland et al, 2021]. It is not possible to quantify the underestimation at locations far from measurement stations.

Moreover, AIS provides incomplete information for identifying vessel class and estimating source levels. For example, container ships and vehicle carriers cannot be distinguished from other types of cargo vessels through their AIS ship type identification. Vessel design details that truly relate to noise emissions, such as the speed at which the propellers start to develop cavitation and the type and power of the propulsion engines, are entirely absent from AIS data.

Ideally, the source grid and AIS/VMS data should extend at least 100 km outside the map area (receiver grid), to avoid underestimation of the SPL near the outer edges of the maps. The Jomopans sound maps are based on calculations with source and receiver grids of the same size.

Wind speed data
Calculating the Jomopans acoustic metrics at the selected mapping grid would require more detailed input data for the wind speed than currently available, in spatial and temporal resolution as well as in averaging time. The uncertainty associated with this shortcoming is likely reduced by the statistical representation of the SPL in monthly percentiles, but it has not been further investigated to what extent. Moreover, the uncertainty in the Copernicus wind speed data is not specified.

Sound speed profile
The Jomopans sound maps are based on propagation loss calculations in which the effects of variations of the sound speed over the water depth (the sound speed profile) are ignored.

In model sensitivity studies carried out in the Kattegat area (Vinga measurement station) it was observed that a fresh water top layer, with significantly lower salinity, can result in upward refraction of the sound, causing a reduced propagation loss due to reduced seabed reflection losses. The presence of fresh water may also reduce propagation loss at higher frequency, due to the lower absorption. This local effect could be included in the sound map modelling, at the cost of applying a more complex propagation loss model (e.g. parabolic equation), collecting more input data (sound speed profiles) and carrying out more propagation loss calculations to describe the time-varying sound speed profile effects.

Surface waves
The Jomopans shipping sound maps are based on propagation loss calculations in which the effects of wind-driven surface waves (including air bubbles entrained by wave breaking) are ignored.

Surface waves and bubbles (resulting in stratification of the sound speed near the surface) will mainly influence the propagation of sound at high frequency. The wind-driven surface loss was therefore included in the wind noise model, which is more important at higher frequencies. Because of the dominating lower frequencies, the effect of the surface loss is less important for ship noise modelling. To limit the computational complexity, it was decided to discard the effect of wind-driven surface waves on shipping noise and use only a single lookup table. This may have led to an overestimation of the ship noise predictions at some locations.

Tidal water depth variations
The Jomopans sound maps are based on propagation loss calculations in which the effects of tidal variations of the water depth are ignored. The effect of tidal variations will be mainly relevant at shallow locations where the variations are not negligible compared to the water depth. Sound level predictions at these shallow locations are more uncertain than in deeper water, not only due to ignoring the tidal variations, but also due to the uncertain modelling of very shallow water propagation.

Seabed properties
The Jomopans sound maps are based on propagation loss calculations in which the combined effects of the layered structure of the seabed, of gradients in the layer properties, of dispersion in the porous sediment layers and of shear waves in seabed layers are not explicitly modelled, but approximated by a modelled uniform half-space that supports compressional waves with a frequency-dependent sound speed and absorption.

5.2 Uncertainties in the models

Ship source level model

- The Jomopans-ECHO ship source level model suggests an estimated statistical uncertainty in the predicted source level spectra of 6 dB, based on the standard deviation of the deviation between the model and the ECHO measurement data.
- The ECHO ship source level dataset is limited to ships in transit, for which the acoustic source level is generally dominated by propeller cavitation noise. Hence, the model uncertainty may be substantially larger for ships that are manoeuvring, sailing at low speed, or anchored at sea.
- The statistical uncertainty in the predicted source level spectra does not significantly contribute to the statistical uncertainty in the predicted monthly SPL percentiles, as demonstrated by a Monte Carlo simulation for the Vinga area, see Annex D.5. In this case study, an assumed 7 dB standard deviation of the source levels was reduced to a standard deviation of less than 1 dB in the monthly median SPL, and less than 3 dB in the highest (95%) percentile. The large extra computational effort associated with the Monte Carlo modelling approach for evaluating the effect of this uncertainty on the maps of the monthly SPL statistics can therefore be avoided. Note however that the source level uncertainty is significant when comparing time series of model and measurements.

Wind source level model
- The uncertainty of the semi-empirical wind noise model is not specified.
- The relatively good model-data agreement the Jomopans stations for frequencies above 1 kHz suggests that the combined uncertainty of models and input data for the monthly SPL statistics of wind noise above 1 kHz is generally less than 6 dB (the observed model-data difference for the 2019 stations [Putland et al, 2021]).

Propagation model
- Uncertainties in shallow water propagation loss modelling are generally dominated by uncertainties in the input data (section 5.3), provided that the models are properly configurated and benchmarked (see section 4.1).

5.3 Uncertainties in the input data

AIS/VMS data input to the ship source level model
- AIS/VMS broadcasts are not free from errors in ship type ID, ship length and ship speed.
- AIS/VMS data interpolation may lead to uncertainties as well.
- These errors and uncertainties can result in unspecified uncertainty in the predicted source level, but it is unlikely that this enhances the statistical uncertainty in the predicted source level spectra, which already amounts to 6 dB.

Bathymetry
- The uncertainty in the bathymetry maps is not specified.

Seabed acoustic properties
- The uncertainty in the median grain size maps is not specified.
- Variation of the median grain size parameter by $\pm 2\phi$ in the model-data comparison (2018) for the Texel and Vinga sites led to a variation of the predicted median SPL spectra at the station location up to 20 dB at dominant shipping noise frequencies (one-third octave bands 10 Hz to 1 kHz).
- The conversion from median grain size maps to a geo-acoustic model of the seabed with frequency dependent sound speed and absorption is uncertain. Quantifying this uncertainty was not possible within the scope of Jomopans.
- The frequency-dependent geoacoustic modelling that is implemented in the Aquarius model reduces the overestimation of low-frequency propagation loss that was observed in the first model-data comparisons [Merchant et al, 2021], without direct fitting of the model to the North Sea shipping observations.
- More accurate modelling of the underwater sound propagation in the North Sea at low frequencies would require more research and data acquisition, particularly in regions with a muddy seabed.

5.4 Combined uncertainties in the Jomopans sound maps

- From the model-data comparisons of the monthly SPL percentiles at the JOMOPANS measurement stations [Putland et al, 2021] it was observed that the model predicted sound levels were lower than the measurements at low frequencies (< 1 kHz), while the model more closely agreed with the measurements at higher frequencies (> 1 kHz). WP6 [Putland et al, 2021] concluded: “Overall, the analysis did not identify consistent uncertainties in noise maps, rather uncertainties may be caused by a complex combination of factors”
- Evaluation of the combined uncertainty in the statistical sound maps from ships and wind produced by Jomopans (see Annex B to this report) deserves further investigation in follow-on projects, aimed at quantifying the various factors that contribute to this uncertainty, including model simplifications as well as uncertain input data.

5.5 Recommendations

- Further evaluation of the measurement data in terms of contributions of different sources (modelled and not-modelled) would be needed to derive relevant data for quantifying model uncertainties, see [Putland et al, 2021].
- The geo-acoustic properties of the North Sea seabed in the frequency range relevant for shipping noise (typically the 20 Hz – 2 kHz decades) are not well established. These could be further investigated by means of geoacoustic inversion techniques. It is recommended to seek collaboration with researchers involved with oil- and gas exploration and geotechnical site surveys.
- Sound speed profile effects may be important in regions with strong stratification, such as the fresh water top layer observed in the Kattegat. These local effects can be quantified by more detailed modelling in those areas?
- The measurement data suggest that wind-generated surface waves may have a relevant effect on

the propagation of shipping sound. It is recommended to quantify the effect and then further investigate whether this effect can be quantified and included in the modelling, if that is found to be relevant.

- The proposed depth-average SPL may not be the most appropriate metric for underwater ambient noise in deeper parts of the North Sea (such as the Norwegian trench). It is recommended to further explore the relevance of calculating other, depth-weighted metrics, in close cooperation with studies into various types of impact on marine life.
- The uncertainty in the predicted Jomopans sound maps in areas that are not covered by measurement stations is unknown. It is recommended to review the possibilities for providing a more complete spatial coverage of measurements for model validation. It may be acceptable to sacrifice temporal coverage for this, because the Jomopans sound maps for 2019 do not show a large variation over the months.
- The comparison between model predictions and measurements suggests that it is worthwhile considering extending the modelling capability to other sound sources, next to ships and wind, such as seismic surveys and operational sound from offshore platforms and structures.

6 Jomopans sound maps and indicators

Jomopans has developed a framework for monitoring the North Sea underwater soundscape by calculating spatial maps of the sound produced by shipping and wind. Furthermore, Jomopans has proposed using these maps for calculating an 'ambient noise pressure indicator' for the implementation of the assessment of 'good environmental state' (GES) in accordance with the EU Marine Strategy Framework Directive (MSFD).

Jomopans has illustrated the application of this monitoring framework for the year 2019.

6.1 Jomopans sound map types

The maps represent monthly or annual percentiles of sound pressure level (SPL) and excess level (EL) and Dominance, as specified in Table 2.1.

A brief reminder:

Excess Level (EL) is calculated for each time step as the difference between the total SPL from all ships and wind and the SPL from wind alone. Two different versions of EL are provided, (i) representing the instantaneous excess of the "ambient noise" from all ships and wind over "natural" wind noise and (ii) representing the instantaneous of "ambient noise" from all ships and wind over median values of "natural" wind noise over the month (or year).

Dominance represents the percentage of evaluation time over which the excess level exceeds a specified cut-off value. Two different cut-off values have been selected: 6 dB and 20 dB.

16 different types of maps are produced:

1. 50th percentile (median) SPL from wind
2. 50th percentile (median) SPL from all ships
3. 50th percentile (median) SPL from fishing ships
4. 50th percentile (median) SPL from cruise/ferry ships
5. 50th percentile (median) SPL from bulkers
6. 50th percentile (median) SPL from container ships
7. 50th percentile (median) SPL from tankers
8. 50th percentile (median) SPL from dredgers
9. 50th percentile (median) EL from ships and wind over instantaneous wind noise
10. 50th percentile (median) EL from ships and wind over monthly median wind noise
11. Dominance based on EL over instantaneous wind noise with a 6 dB cut-off value
12. Dominance based on EL over instantaneous wind noise with a 20 dB cut-off value
13. Dominance based on EL over monthly median wind noise with a 6 dB cut-off value
14. Dominance based on EL over monthly median wind noise with a 20 dB cut-off value

Each of these maps is calculated for 6 different frequency bandwidths:

i. 'Broadband', covering the 10 Hz to 20 kHz one-third octave bands
ii. 'Decade 1', covering the 20 Hz to 160 Hz one-third octave bands
iii. 'Decade 2', covering the 200 Hz to 1.6 kHz one-third octave bands
iv. 'Decade 3', covering the 2 kHz to 16 kHz one-third octave bands
v. 63 Hz one-third octave band
vi. 125 Hz one-third octave band

The three decades are broadly aimed at the hearing sensitivity of different animal groups. For example, fish are generally sensitive to sound in the lowest band (20 Hz to 160 Hz), while harbour porpoises are mainly sensitive to shipping sound in the highest band (2 kHz to 16 kHz). 63 Hz and 125 Hz are the bands selected for EU descriptor D11C2.

All maps have been produced for the 12 months of 2019 and for the full year of 2019.

In total this has resulted in 16 (map types) × 6 (frequency bands) × 13 (evaluation periods) = 1248 maps, that can be downloaded from and displayed in the Jomopans GES Tool[8].

6.2 SPL percentile maps

[8] Hosted at https://jomopans.michaelcarder.co.uk/en/ until the end of 2022.

Map types 1 to 8 (section 6.1) present the spatial distribution of a temporal percentile of the calculated SPL, for various specific combinations of sound sources.

6.2.1 Wind

Figure 6.1 to Figure 6.3 show maps of the annual median wind noise in the six frequency bands.

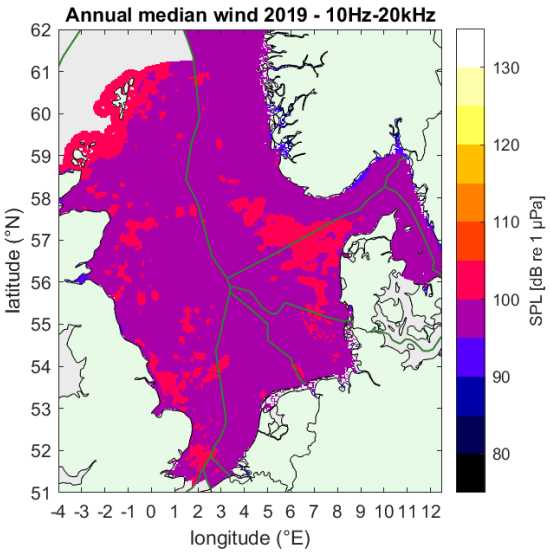

Figure 6.1 Map of the annual median (50th percentile) of depth-averaged SPL in dB re 1 µPa² of broadband wind-generated noise in the North Sea region in 2019.

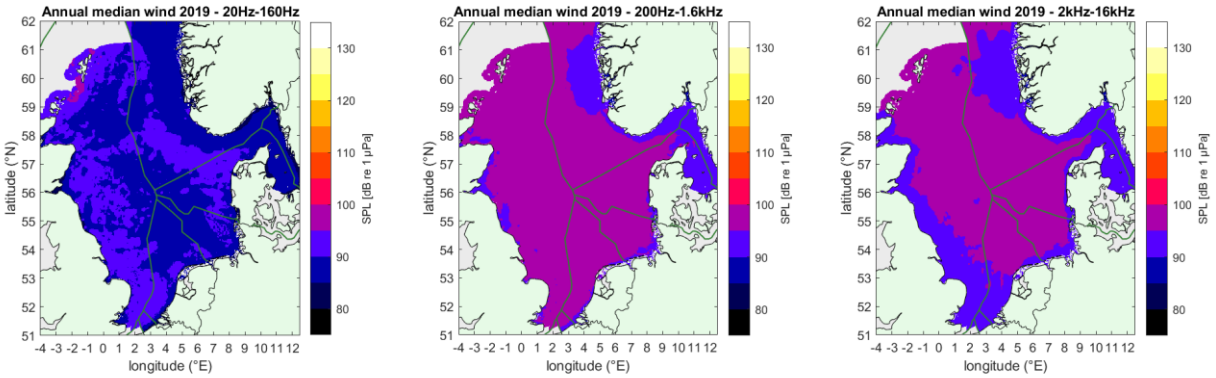

Figure 6.2 Maps of the annual median (50th percentile) of depth-averaged SPL in dB re 1 µPa² of wind-generated noise in the North Sea region in 2019 in the three decade bands.

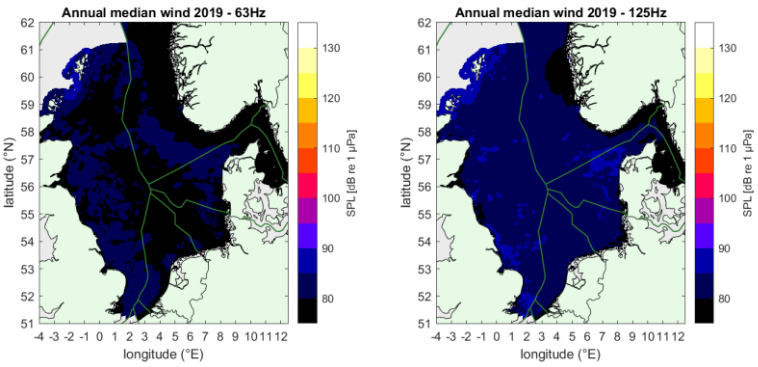

Figure 6.3 Map of the annual median (50th percentile) of depth-averaged SPL in dB re 1 µPa² of wind-generated noise in the North Sea region in 2019 in the two one-third octave bands (left: 63 Hz, right: 125 Hz) for EU descriptor D11C2.

Figure 6.4 shows maps of the monthly median broadband wind noise. As expected, the wind noise is generally higher in the winter months than in the summer months.

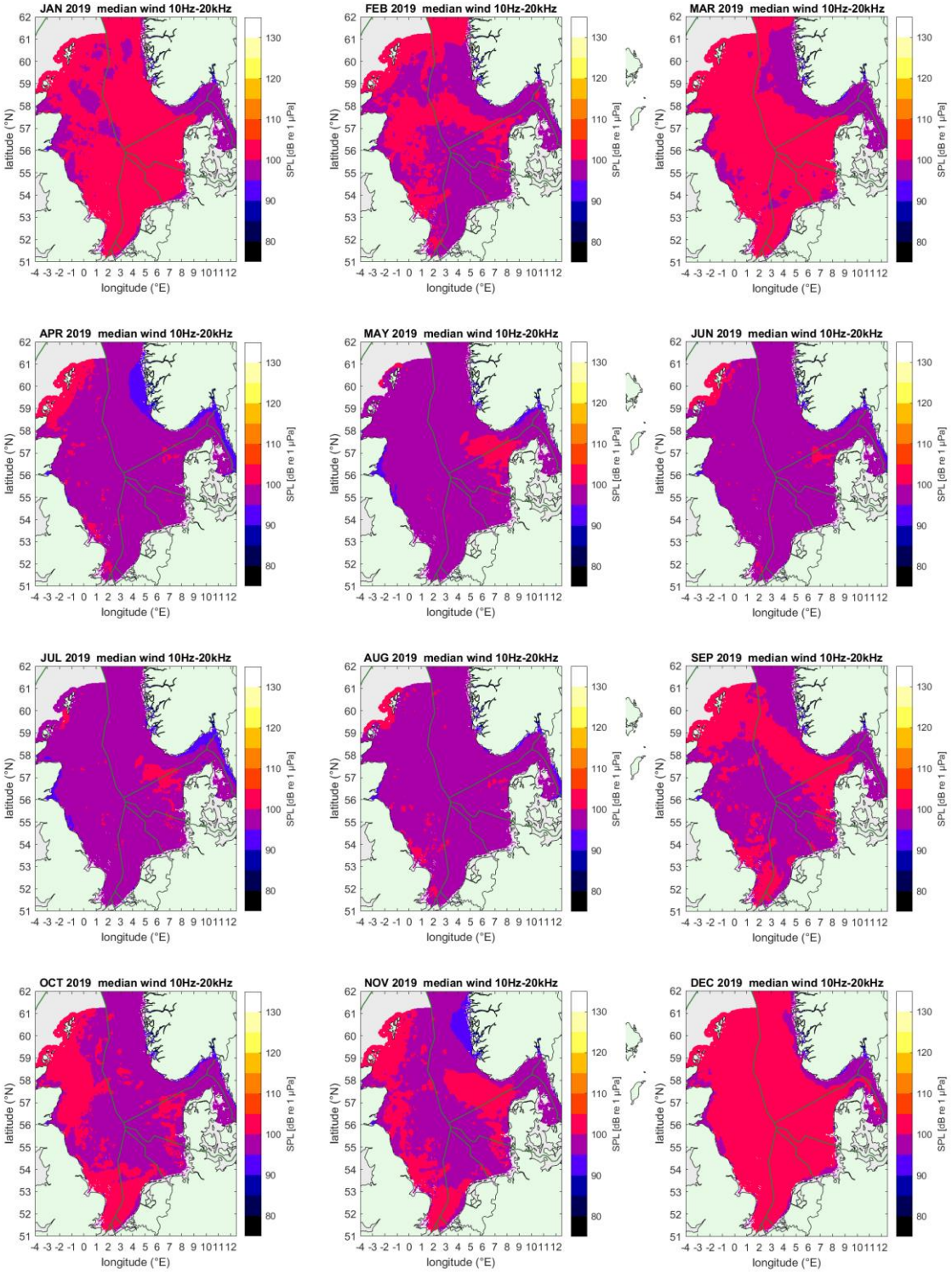

Figure 6.4 Maps of the monthly median (50th percentile) of depth-averaged SPL in dB re 1 µPa² of broadband wind-generated noise in the North Sea region for the 12 months of 2019.

6.2.2 Shipping + Wind

Figure 6.5 to Figure 6.7 show maps of the total annual median noise generated by shipping and wind, in the six frequency bands. Shipping noise increases the ambient noise significantly at nearly all map locations, except at frequencies above 1 kHz (see Figure 6.6).

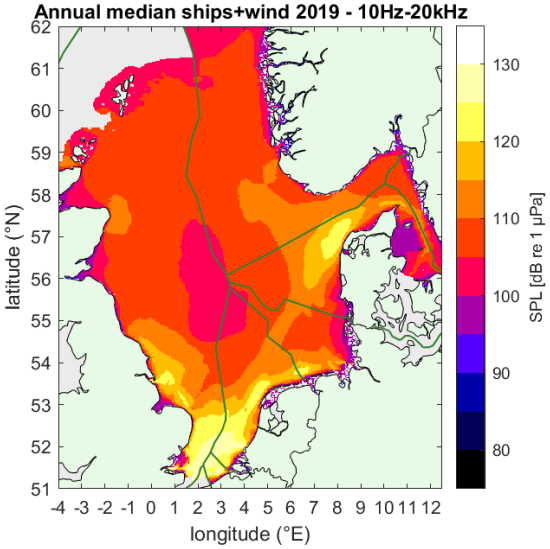

Figure 6.5 Map of the annual median (50th percentile) of depth-averaged SPL in dB re 1 µPa² of broadband noise generated by shipping and wind in the North Sea region in 2019.

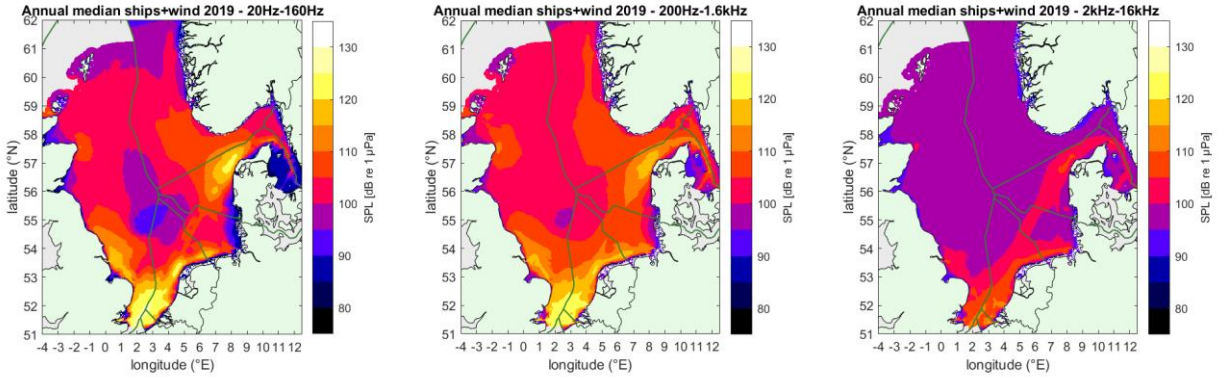

Figure 6.6 Maps of the annual median (50th percentile) of depth-averaged SPL in dB re 1 µPa² of noise generated by shipping and wind in the North Sea region in 2019 in the three decade bands.

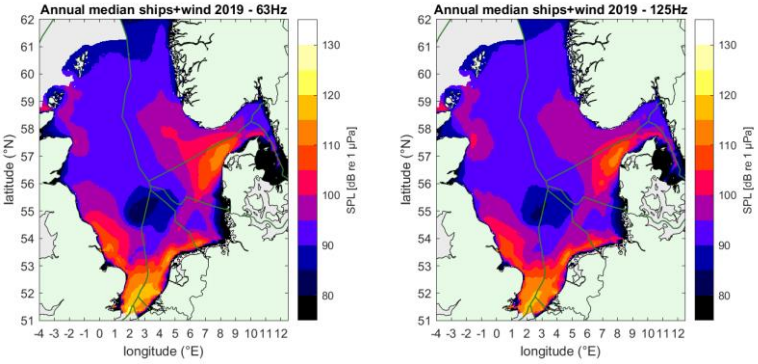

Figure 6.7 Map of the annual median (50th percentile) of depth-averaged SPL in dB re 1 µPa² of noise generated by shipping and wind in the North Sea region in 2019 in the two one-third octave bands (left: 63 Hz, right: 125 Hz) for EU descriptor D11C2.

Figure 6.8 shows maps of the monthly median broadband noise generated by shipping and wind.

Shipping noise dominates over wind and the median shipping noise varies little over the months.

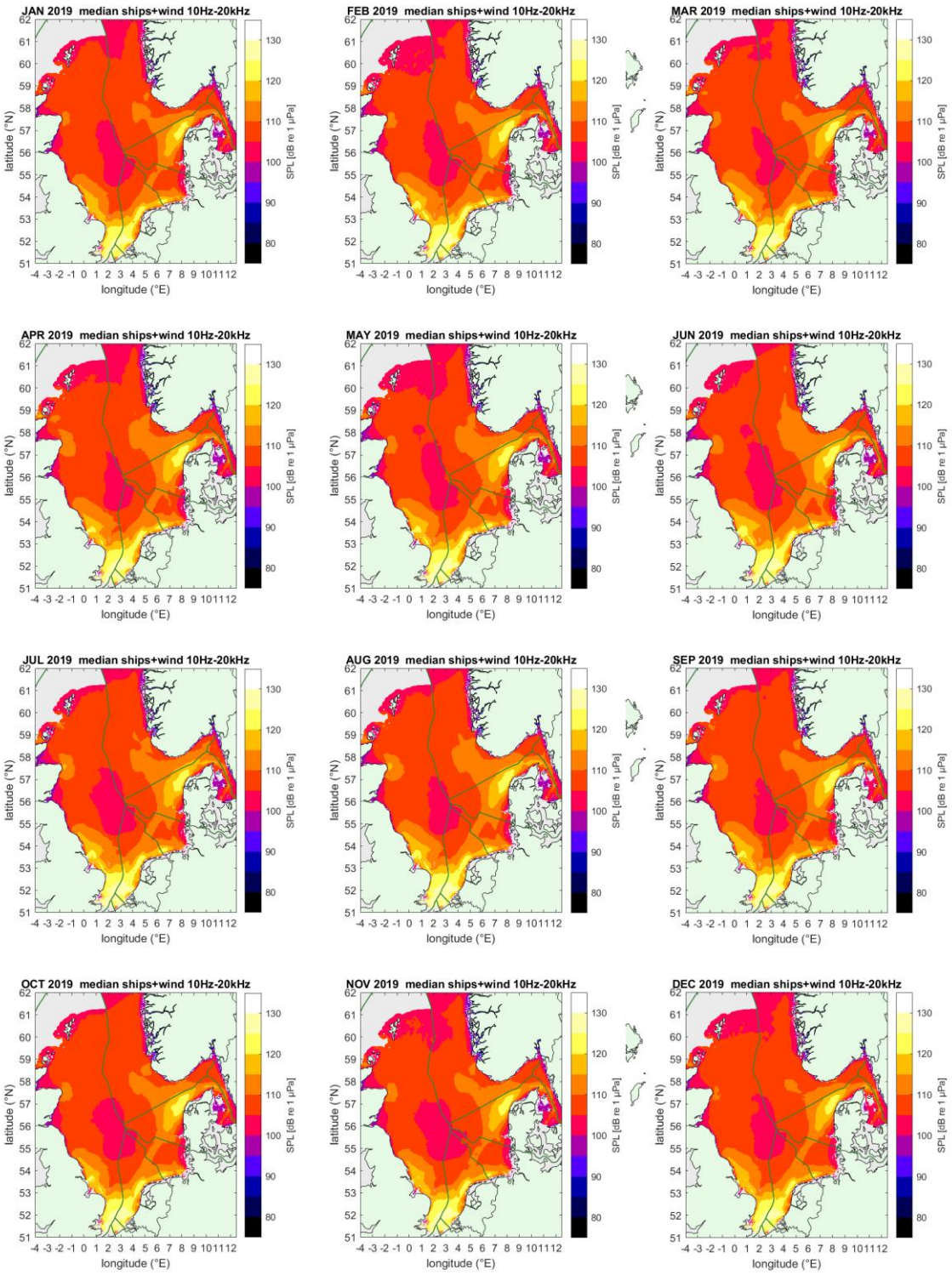

Figure 6.8 Maps of the monthly median (50th percentile) of depth-averaged SPL in dB re 1 µPa² of broadband wind-generated noise in the North Sea region for the 12 months of 2019.

6.2.3 Individual ship type contributions

Figure 6.9 shows maps of the annual median broadband noise generated by six individual ship types. Bulkers, tankers and container ships have the largest presence in the AIS data and dominate the soundscape.

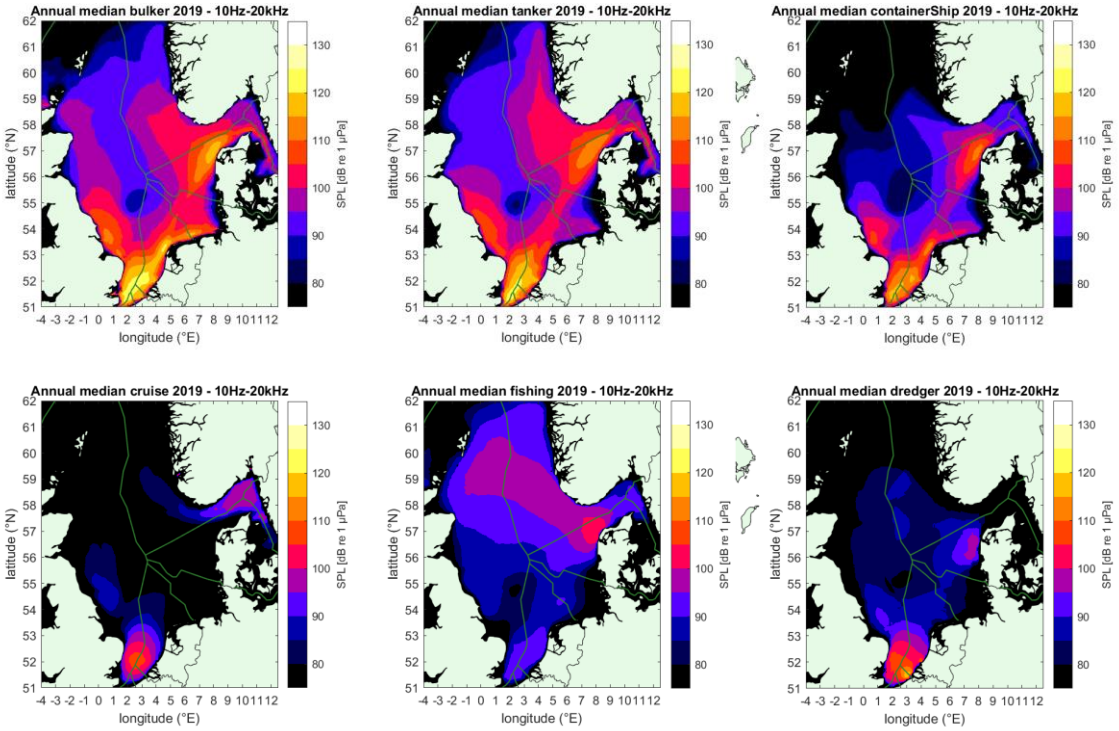

Figure 6.9 Map of the annual median (50th percentile) of depth-averaged SPL in dB re 1 μPa^2 of broadband noise generated by six different ship types (bulkers, tankers, container ships, cruise ships/ferries, fishing[9] boats and dredgers, see the header of the subplots) in the North Sea region in 2019.

[9] Note that not all fishing boats are represented in AIS and that VMS data were supplied for Norway, Sweden, Denmark and Germany only, see Annex C.

6.3 Excess Level

Figure 6.10 to Figure 6.12 show maps of the annual median excess level of noise generated by shipping and wind over wind noise in the six frequency bands. This illustrates that low-frequency shipping noise dominates over wind noise over most of the North Sea area during 50% of the time. At higher frequencies (the 2 kHz to 16 kHz decade), positive excess is limited to the areas around the main shipping lanes in the Southern North Sea, Skagerrak and Kattegat.

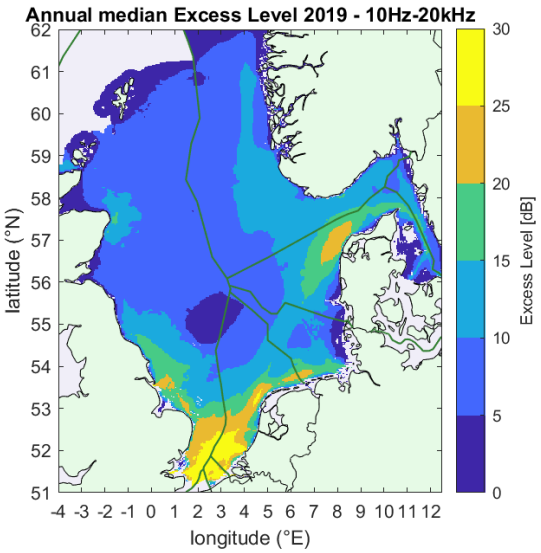

Figure 6.10 Map of the annual median (50th percentile) broadband excess level (in dB) in the North Sea region in 2019.

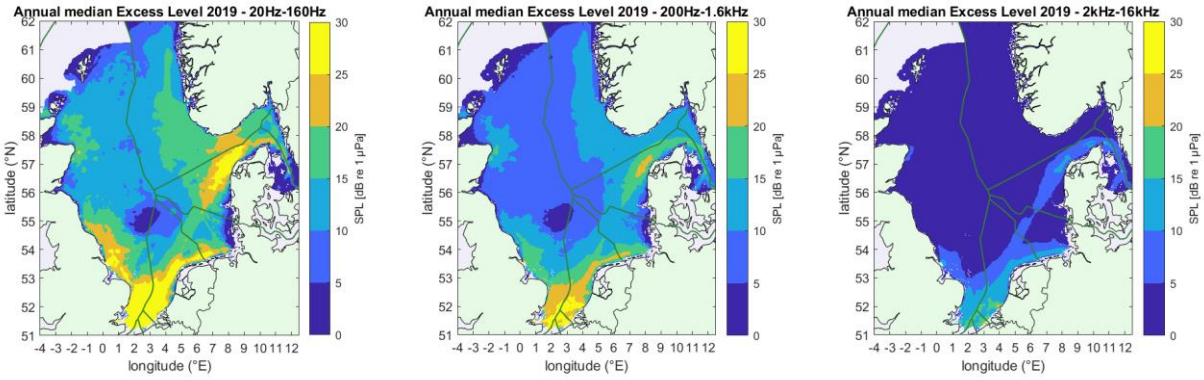

Figure 6.11 Maps of the annual median (50th percentile) excess level (in dB) in the North Sea region in 2019 in the three decade bands.

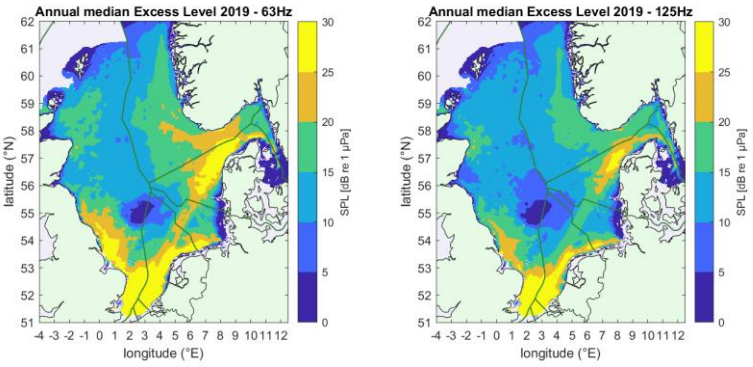

Figure 6.12 Map of the annual median (50th percentile) excess level (in dB) in the North Sea region in 2019 in the two one-third octave bands (left: 63 Hz, right: 125 Hz) for EU descriptor D11C2.

6.4 Dominance

Figure 6.13 shows maps of the annual dominance, quantifying the percentage of the time over which the broadband excess level of noise generated by shipping and wind over wind noise is above a cut-off value of 6 dB (left figure) and 20 dB (right figure). Under the simplifying assumption of spherical spreading loss of the communication signals and insignificant absorption, a 6 dB excess level translates into a decrease in maximum communication distance by 50% and a 20 dB excess translates into a decrease in maximum communication distance by 90% (see WP7 report). The 6 dB cut-off value is exceeded over a large part of the North Sea are most of the time. The only exception is seen in the Dogger Bank area (central North Sea, around 3°E and 55°N). The 20 dB cut-off value is positive excess is mainly exceeded in the areas around the main shipping lanes in the Southern North Sea, Skagerrak and Kattegat.

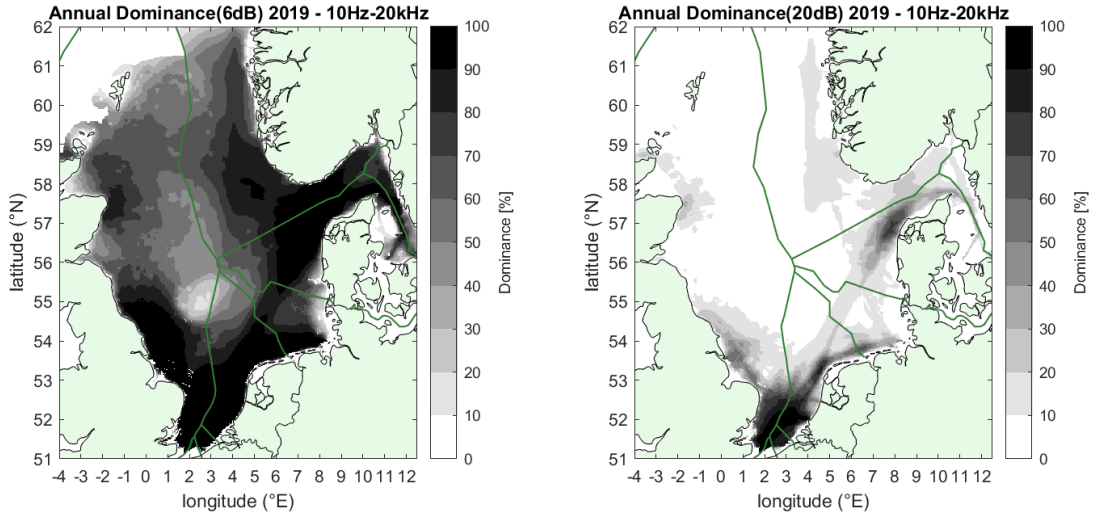

Figure 6.13 Map of the annual broadband dominance for an excess level cut-off of 6 dB (left) and 20 dB (right), in the North Sea region in 2019.

Figure 6.14 shows that the dominance of shipping noise occurs mainly at lower frequencies. It is very limited in the highest decade band (the 2 kHz to 16 kHz decade).

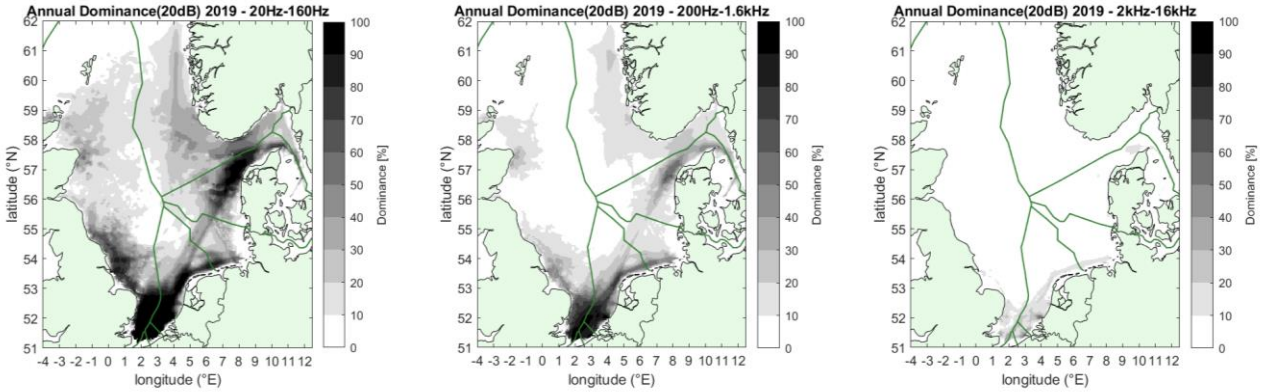

Figure 6.14 Maps of the annual dominance for an excess level cut-off of 20 dB, in the North Sea region in 2019 in the three decade bands.

Figure 6.15 shows maps of the monthly dominance, quantifying the percentage of the time over which

the broadband excess level of noise generated by shipping and wind over wind noise is above a cut-off value 20 dB. The dominance percentages are higher in the summer months, mainly because of the lower wind noise levels in that period (Figure 6.4), while the ship noise levels vary little over the months (Figure 6.8).

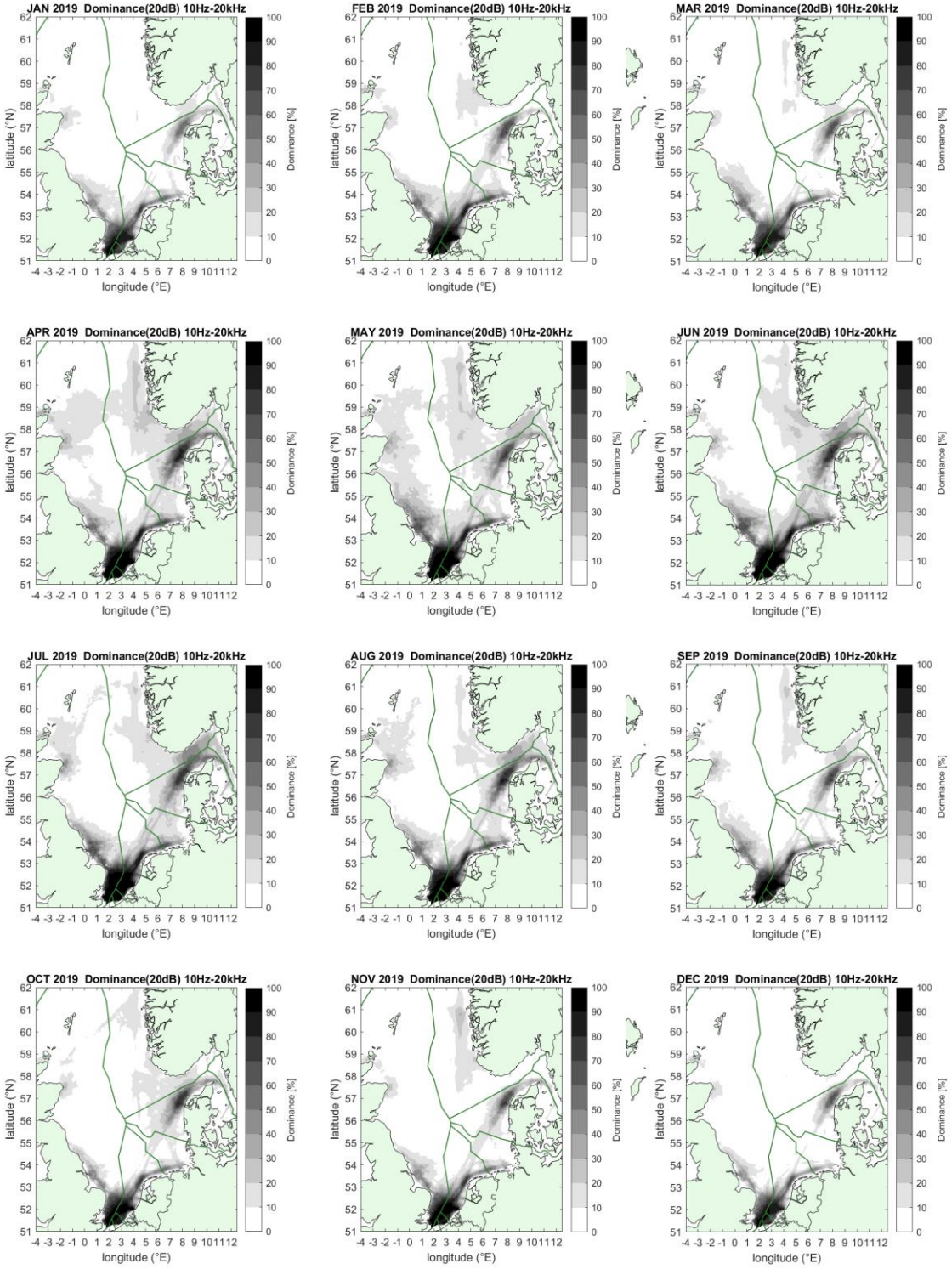

Figure 6.15 Map of the monthly broadband dominance for an excess level cut-off of 20 dB, in the North Sea region for the 12 months of 2019.

6.5 Pressure curve and pressure index

The dominance maps (section 6.4) can be evaluated in terms of the cumulative distribution of the percentage of the evaluation area as a function of the dominance values. The resulting **'*pressure curve*'** (defined in Table 2.1 and Annex A, also referred to as **'*pressure function*'**) illustrates the percentages of the time and of the area over which the excess level of noise generated by shipping and wind over wind noise is above a specified cut-off value. Figure 6.16 shows the pressure curves for a cut-off value of 6 dB (blue area) and 20 dB (red area), for the six frequency bands.

The (shaded) area under the pressure curve quantifies the percentage of the evaluation area as well as the percentage of the evaluation time interval, in the evaluation frequency band, where the excess level exceeds the specified cut-off value. Jomopans has defined **'*pressure index*'** as the ratio (here expressed as a percentage) of this area to the total area (100%×100%) of the pressure curve graph. The legends to the graphs in Figure 6.16 give the corresponding values of the pressure index.

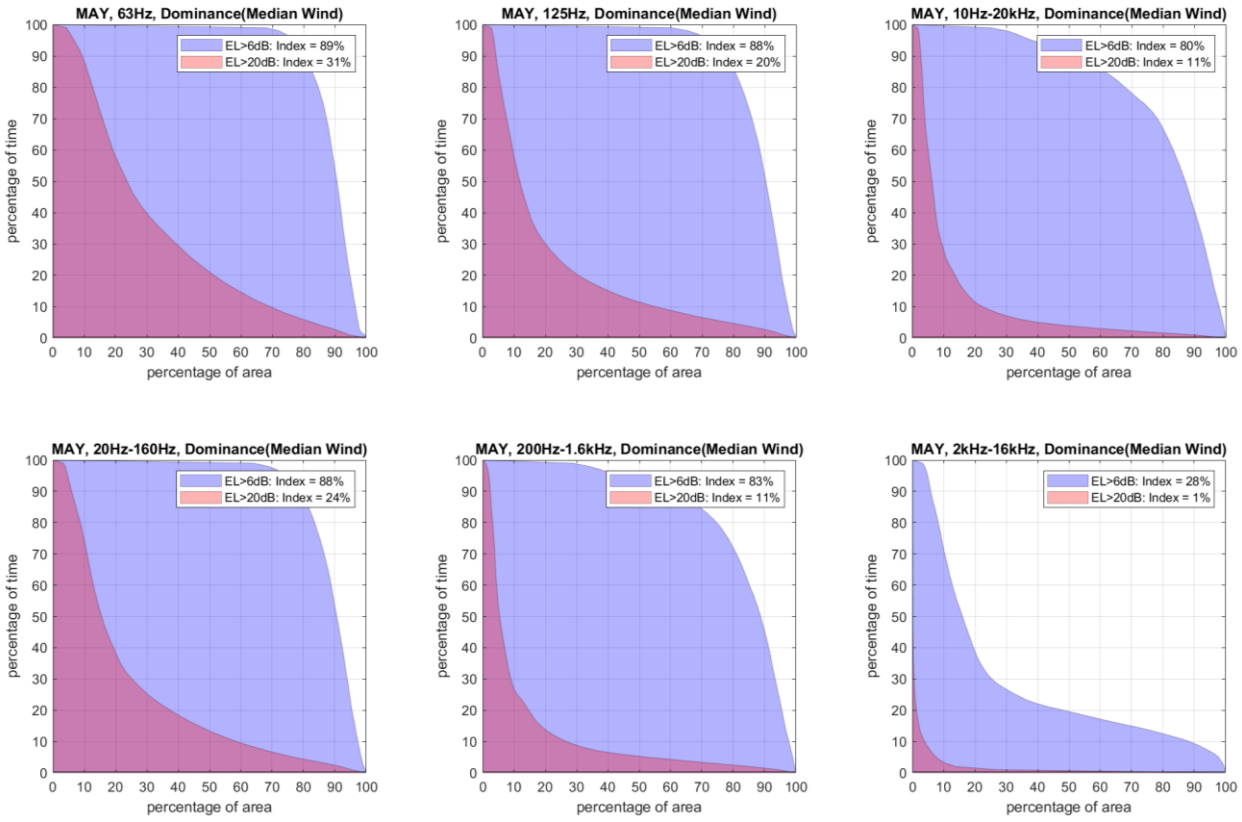

Figure 6.16 Pressure curves, illustrating the percentages of the time and of the area over which the excess level of noise generated by shipping and wind over (monthly median) wind noise is above a cut-off value of 6 dB (blue area) and 20 dB (red area), for the six Jomopans frequency bands. The assessment area for these pressure curves is the full North Sea area and the assessment period is the month of May 2019.

Figure 6.17 illustrates how the calculated pressure index for the full North Sea area varied over the twelve months of 2019. The pressure index appears to be higher during the summer months than during winter. Analysis of the SPL percentile maps of wind noise (section 6.2.1) and shipping + wind noise (section 6.2.2) led to the conclusion that this variation of the pressure index is mainly due to the variation of the wind over the months. The shipping noise is relatively constant over the months, while the wind noise is lower in the summer months when the wind speeds are generally lower.

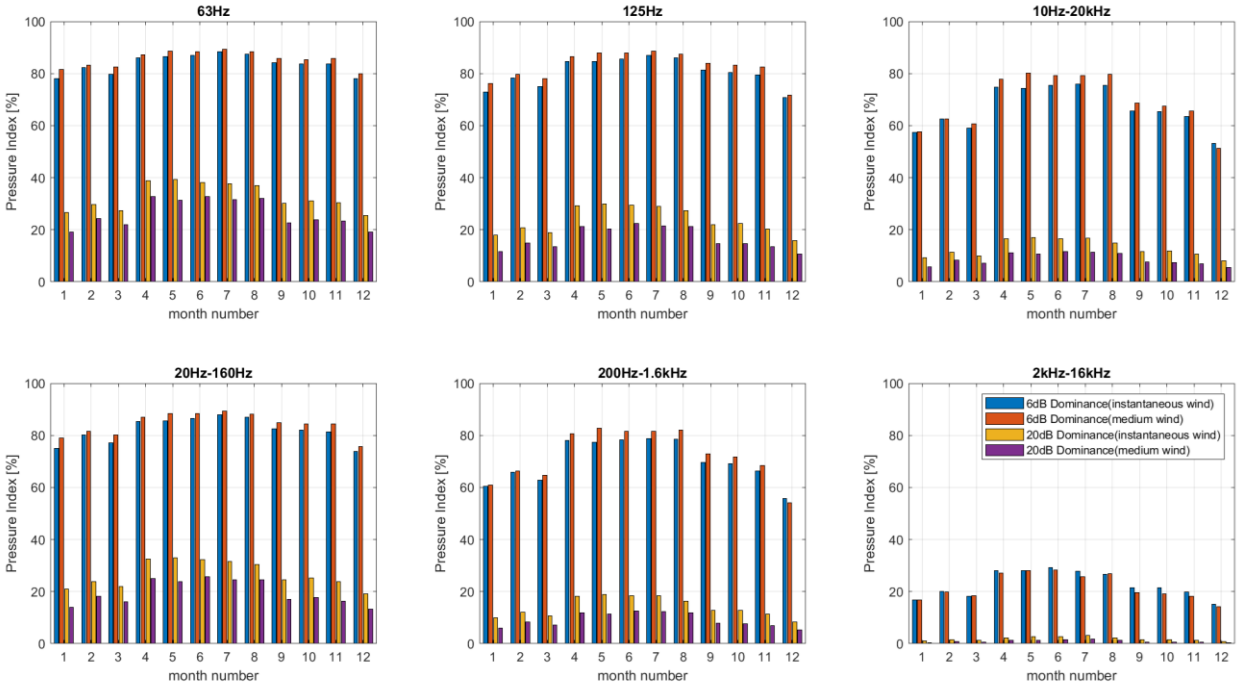

Figure 6.17 Pressure index variations over the 12 months of 2019, for the full North Sea area and for the six Jomopans frequency bands. The four bars per month represent the pressure index based on respectively: an excess of 6 dB or more over the instantaneous or monthly median wind noise and an excess of 20 dB or more over the instantaneous or monthly median wind noise.

Starting from the dominance maps, the pressure index can also be assessed for selected regions. To illustrate this application, we have selected the OSPAR subregions, shown in Figure 6.18.

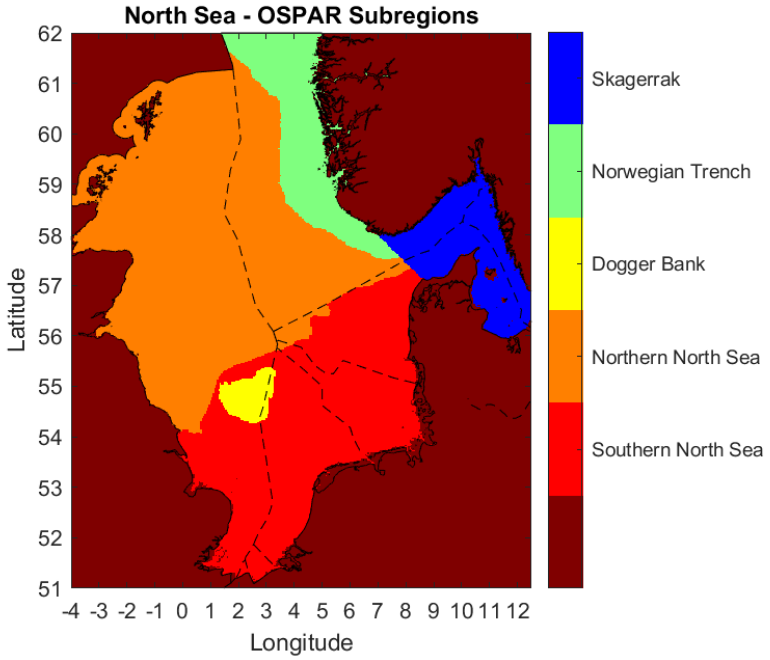

Figure 6.18 Map of the five subregions of OSPAR Region II 'Greater North Sea'. The dashed black lines show the borders of the national exclusive economic zones.

Figure 6.19 shows the pressure curves for the five OSPAR subregions, for May 2019 and for the three decade frequency bands, and Figure 6.20 shows the corresponding pressure index values.

This illustrates that the excess level in the lowest decade bands is 20 dB or more during 100% of the time in more than 10% of the Southern North Sea area, due to the busy shipping lanes to and from the English Channel. The Kattegat, with the shipping lanes to and from the Baltic Sea has the next highest pressure index. The Dogger Bank, a shallower area in the central North Sea, is remote from shipping lanes, resulting in the lowest pressure index. The pressure indices in the 2 to 16 kHz frequency band is much lower than the pressure indices in the lower bands, indicating that shipping noise does not dominate as much over wind noise at these higher frequencies.

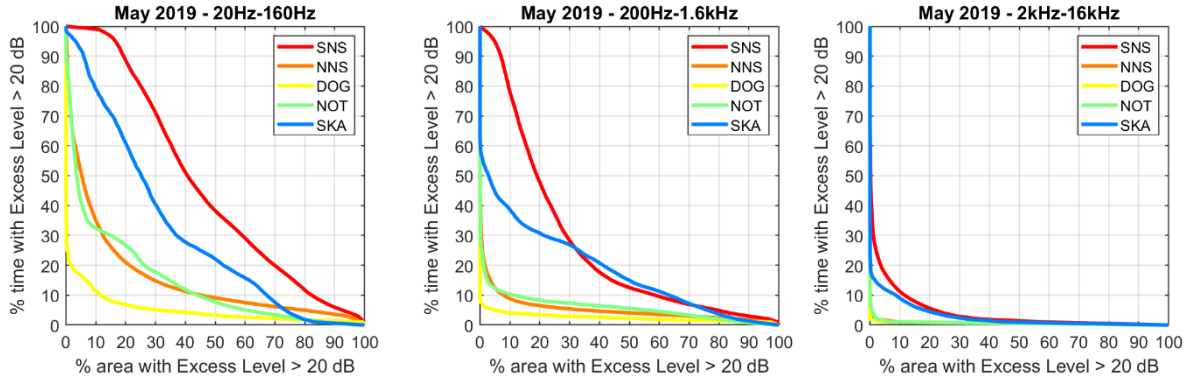

Figure 6.19 Pressure curves for the five OSPAR subregions, for May 2019 and for a cut-off value for excess level of 20 dB in the three decade frequency bands.

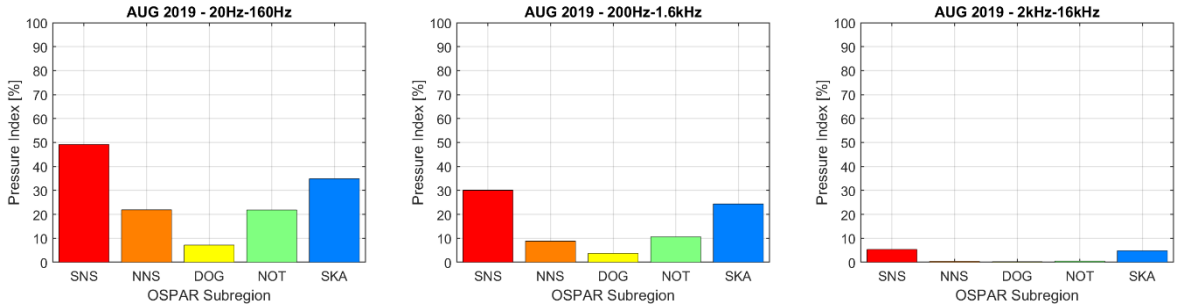

Figure 6.20 Pressure index for the five OSPAR subregions for May 2019 and for a cut-off value for excess level of 20 dB in the three decade frequency bands.

7 Guidelines for soundscape modelling

Monitoring the ambient sound in the sea via numerical modelling has many advantages over direct measurements. Modelling is much cheaper than measurements at sea, it offers a wider spatial and temporal coverage and it provides direct insight in the contributions of different sound sources. However, there are many uncertainties and being able to model ambient sound with confidence requires careful consideration of the various modelling choices as well as model validation by measurements.

Figure 7.1 illustrates the steps to be taken for the soundscape modelling process. The list below provides guidelines for sound map modelling based on the lessons learned in the Jomopans project.

Project area and acoustic metric definition

- Select the project area, assessment period, the required spatial resolution of the maps and the frequency range and resolution
- Define source and receiver grids

Environmental data portals

- Obtain input data for the acoustic modelling of the environment:
    - Bathymetry
        - EMODnet provides bathymetry data for European waters
    - Seabed properties (Folk class or median grain size)
        - A map of median grain sizes of North Sea surface sediments is available from the World Data Center for Climate portal [Bockelmann, 2017].
        - Convert to (frequency-dependent) density, compressional wave speed, and absorption (see section 3.7.3)
    - Sea water properties (density, sound speed and absorption)
        - Standard uniform sea water properties provide an appropriate first-order approximation for many shallow water environments
        - In deeper water and in shallow water with significant stratification of temperature and/or salinity, it may be necessary to incorporate sound speed gradient effects.
    - Wind speed (speed at 10 m above the water surface, see section 3.7.4)
        - The Copernicus website[10] provides ERA5 hourly wind speed data
        - Interpolate to a regular time grid and to the receiver grid.
        - Note that the 10-minute averaging time of the wind data leads to uncertainty in the calculated statistics of SPL-metrics with a shorter averaging time. Higher resolution wind data would be required but is not available.

AIS data

- Obtain ship traffic information (location, speed, ship type and length) from AIS/VMS data
    - Check the quality of the input data, and, where possible, supplement missing data by means of track interpolation (see section 3.7.5 and Annex C)
    - Interpolate to a regular time grid and (optionally) to a regular two-dimensional source grid
    - Ideally, the source data should extend well outside the received grid, to avoid underestimation of the shipping noise at the outer edges of the receiver grid.

Propagation loss model configuration and verification

- Select an appropriate propagation loss model
    - For low-frequency (< 2 kHz) shipping noise in a shallow-water environment, such as the main North Sea area, models based on normal modes, parabolic equation or wavenumber integration are appropriate.
- Select appropriate model configuration settings (see section 3.8)
- Verify the model implementation and model configuration settings (for shallow-water propagation models) by running the proposed benchmark scenario's (section 4.1).

[10] https://cds.climate.copernicus.eu/cdsapp#!/dataset/reanalysis-era5-single-levels?tab=form

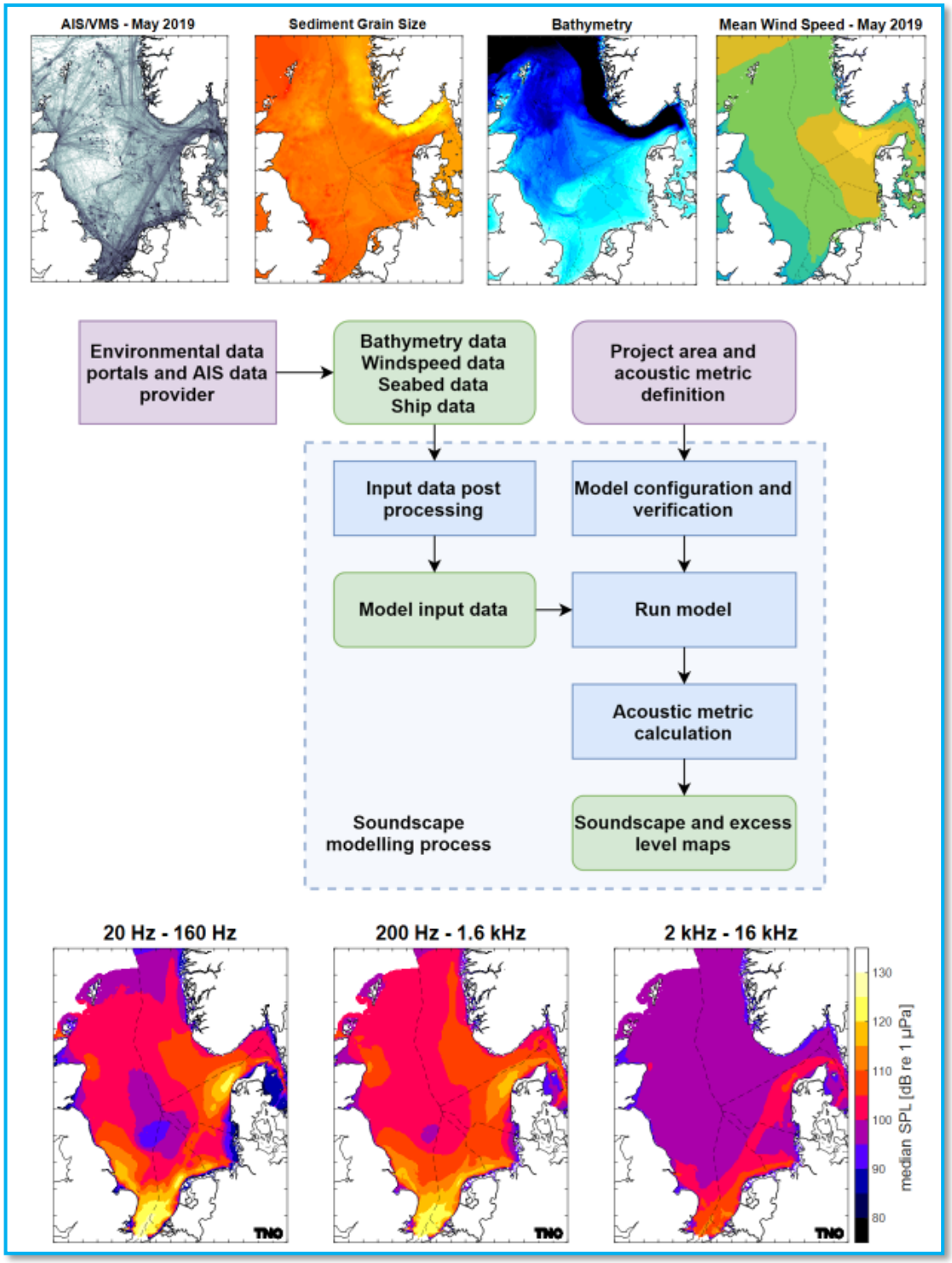

Figure 7.1 Schematic illustration of the soundscape modelling process, with example maps of input data (upper graphs) and resulting soundscape maps (bottom graphs).

Run model

- Calculate the propagation loss between source grid and receiver grid locations averaged over the local water depth (section 3.8.1), at the selected frequencies (section 3.8.5).
    - If temporal variations of the environment can be ignored, these calculations can be made computationally efficient by precomputing the propagation loss between the source grid receiver grid locations and storing the calculated propagation loss in a look-up table.
    - The calculations can also be made computationally more efficient by calculating propagation loss along radials from the source location (section 3.8.2) and then interpolating the results to the receiver grid locations.
- For each ship at each time step, estimate the source level spectrum, at the selected frequencies, using the Jomopans -ECHO source level model (see section 3.3).
- For each time step, calculate the depth-averaged sound pressure level spectrum at each receiver grid location, by summing the contributions from all source grid cells (source level minus propagation loss).
- For each time step, calculate the depth-averaged sound pressure level spectrum due to the wind at each receiver grid location, using a wind source and propagation model (see sections 3.5 and 3.6).

Acoustic metric calculation

- For each receiver grid location, calculate monthly percentiles of the sound pressure level spectra from ships and wind.
- For each receiver grid location, calculate monthly percentiles of the excess level spectra (the difference between the sound pressure level from the total of ships and wind and from wind noise alone) and dominance (the percentage of evaluation time over which the excess level exceeds a specified cut-off value).

Reporting

- All steps in the soundscape modelling process need to be detailed when reporting soundscape maps, where possible motivated:
    - Project description (selected area and acoustic metrics),
    - Selected spatial, temporal and frequency range and resolution,
    - Selected input data (sources and environment), with spatial and temporal resolution,
    - Any processing applied to the input data (e.g. interpolation or extrapolation)
    - Selected models (source level and propagation loss)
    - Applied model configurations (parameter settings)
    - Applied postprocessing (e.g. interpolation, statistics, etc.)

Discussion and conclusion

- The Jomopans sound maps provide an unprecedented insight in the relevance of shipping for the North Sea sound scape.
- If models and input data are available, a similar approach can be applied for other sources of ambient underwater noise than shipping and wind, such as operational wind turbines, seismic surveys, oil- and gas platforms, etc.
- The quality of the produced sound maps depends to a large extent on the quality of the available input data. None of the sources of input data used in this study has been developed for the purpose of underwater ambient noise mapping. Hence, AIS/VMS coverage is generally incomplete and the conversion of available seabed properties to acoustic model parameters is uncertain.
- There are still many remaining issues to be solved to be able to quantify and possibly reduce uncertainties in the modelled soundscape maps. The main issues are incompleteness (missing sources) and uncertainty in the input data and uncertainties associated with the model
- Recommendations for further research are summarized in section 5.5
- The Jomopans soundscape modelling capability provides the possibility to carry out scenario studies: A desk study of the effects of slow steaming for reducing emissions as well as underwater radiated noise from marine traffic on the North Sea, commissioned by the Belgian Marine Environment Service, was presented at the seminar[11] “Solutions for underwater noise from shipping”.

[11] https://www.health.belgium.be/en/news/solutions-underwater-noise-shipping

8 References

Ainslie, M. A. (2005) Effect of wind generated bubbles on fixed range acoustic attenuation in shallow water at 1-4 kHz, J. Acoust. Soc. Am., 118, 3513-3523

Ainslie, M. A. (2010) *Principles of sonar performance modeling*. Berlin: Springer-Praxis.

Ainslie, M. A., Harrison, C. H. and Zampolli, M. (2011) An Analytical Solution for Signal, Background and Signal to background Ratio for a Low Frequency Active Sonar in a Pekeris Waveguide Satisfying Lambert's Rule.

APL-UW High-Frequency Ocean Environmental Acoustic Models Handbook. *Applied Physics Laboratory, University of Washington, APL-UW TR* 9407 (1994).

Audoly, C.; Rizzuto, E. (2015) Ship Underwater Radiated Noise Patterns; Technical Report AQUO European Collaborative Project Deliverable D2.1; AQUO Project Consortium: Val-de-Reuil, France.

Aulanier, F.; Simard, Y.; Roy, N.; Gervaise, C.; Bandet, M. (2017) Effects of shipping on marine acoustic habitats in Canadian Arctic estimated via probabilistic modeling and mapping. Mar. Pollut. Bull. 125, 115–131.

Binnerts, B, de Jong, CAF, Karasalo, I, Östberg, M, Folegot, T, Clorenneq, D, Ainslie, MA, Warner, G, Wang, L (2019) Model benchmarking results for ship noise in shallow water. Proceedings of the 5th Underwater Acoustics Conference and Exhibition UACE2019, Hersonissos, Crete, Greece

Binnerts, B, de Jong, CAF, von Benda-Beckmann, S, de Krom, P. Östberg, M, Folegot, D, Ainslie, MA, Welch, S (2021) Model predictions 2018 measurement sites. Report of the EU INTERREG Joint Monitoring Programme for Ambient Noise North Sea (JOMOPANS).

Bockelmann, F.-D., Puls, W., Kleeberg, U., Müller, D. and Emeis, K.-C. (2018), “Mapping mud content and median grain-size of North Sea sediments – A geostatistical approach”, Marine Geology 397, 60–71

Bockelmann, Frank-Detlef (2017). Median grain size of North Sea surface sediments. World Data Center for Climate (WDCC) at KRZ. https://doi.org/10.1594/WDCC/coastMap_Substrate_MGS

Breeding, J.E., Pflug, L.A., Bradley, M., Hebert Walrod, M & McBride, W. (1996) Research Ambient Noise Directionality (RANDI) 3.1 Physics Description. report NRL/FR/7176-95-9628

Brooker, A.G.; Humphrey, V.F. (2015) Noise Model for Radiated Noise/Source Level (Intermediate); Document Number FP7-314394-SONIC, Deliverable 2.3. Tech. Rep.; SONIC, Suppression of Underwater Noise Induced by Cavitation Consortium: The Amsterdam, The Netherlands

Bucker, H. P. (1976) Use of calculated sound fields and matched-filed detection to locate sound sources in shallow water, J. Acoust. Soc. Am., 59, 368-373

Buckingham, M. J. (1992) Ocean-acoustic propagation models, J. Acoustique, 223-287

Chion, C.; Lagrois, D.; Dupras, J. A (2019) Meta-Analysis to Understand the Variability in Reported Source Levels of Noise Radiated by Ships from Opportunistic Studies. Front. Mar. Sci. 6, 714

Colin, M., Ainslie, M. Binnerts, B, de Jong, C., Sertlek, Ö, Karasalo, I., Östberg, M., Folegot, T. and Clorennec, D. (2015), “Definition and results of test cases for shipping sound maps”, Proc. IEEE OCEANS 2015 – Genova

Collins, M. D. (1993) A split-step Pade solution for the parabolic equation method, J. Acoust. Soc. Am., 93, 1936-1942

Collins, M. D., McDonald, B. E., Heaney, K. D. and W. A. Kuperman (1995) Three-Dimensional Effects in Global Acoustics, J. Acoust. Soc. Am., 97, 1567-1575

Cornuelle, B. D., Munk, W. and P. F. Worcester (1989) Ocean acoustic tomography from ships, J. Geophys. Res., 94, 6232-6250

de Jong, C., Ainslie, M., Dreschler, J., Jansen, E., Heemskerk, E. and Groen, W. (2010) Underwater noise of Trailing Suction Hopper Dredgers at Maasvlakte 2: Analysis of source levels and background noise. Report TNO-DV 2010 C335.

de Jong, C.A.F., Binnerts, B., Östberg, M., Folegot, T. and Ainslie, M.A. (2018) *Jomopans model and data inventory*. Report of the EU INTERREG Joint Monitoring Programme for Ambient Noise North Sea (JOMOPANS).

de Jong, C.A.F., Binnerts, B., Östberg, M., Karasalo, I., Folegot, T., Clorennec, D., Ainslie, M.A., MacGillivray, A., Warner and G., Wang, L. (2020) *Jomopans model benchmarking and sensitivity studies.* Report of the EU INTERREG Joint Monitoring Programme for Ambient Noise North Sea (JOMOPANS)

Dekeling, R.P.A., Tasker, M.L., Van der Graaf, A.J., Ainslie, M.A, Andersson, M.H., André, M., Borsani, J.F., Brensing, K., Castellote, M., Cronin, D., Dalen, J., Folegot, T., Leaper, R., Pajala, J., Redman, P., Robinson, S.P., Sigray, P., Sutton, G., Thomsen, F., Werner, S., Wittekind, D., Young, J.V. (2014) Monitoring Guidance for Underwater Noise in European Seas, Part II: Monitoring Guidance Specifications, JRC Scientific and Policy Report EUR 26555 EN, Publications Office of the European Union, Luxembourg

Erbe, C.; MacGillivray, A.O.; Williams, R. (2012) Mapping cumulative noise from shipping to inform marine spatial planning. J. Acoust. Soc. Am. 132, EL423–EL428. [

Erbe, C.; Schoeman, R.P.; Peel, D.; Smith, J.N. (2021) It Often Howls More than It Chugs: Wind versus Ship Noise UnderWater in Australia's Maritime Regions. J. Mar. Sci. Eng. 9, 472. https://doi.org/10.3390/jmse9050472

Etter, P. C. (2013) *Underwater Acoustic Modeling and Simulation*, 4th ed, CRC Press

Farcas, A.; Powell, C.F.; Brookes, K.L.; Merchant, N.D. (2020) Validated shipping noise maps of the Northeast Atlantic. Sci. Total Environ. 735, 139509.

Fischer, J.; Kühnel, D. and Basan, F. (2021) *Jomopans Measurement Guidelines*. Report of the EU INTERREG Joint Monitoring Programme for Ambient Noise North Sea (JOMOPANS)

Folegot, T., Clorennec, D., Baudin, E., and Audoly, C. (2015) AQUO D5.7 Assessment of the solutions to reduce impact on marine life, rev1.0

Folegot T., Clorennec D., Chavanne R., R. Gallou (2016) Mapping of ambient noise for BIAS. Quiet-Oceans technical report QO.20130203.01.RAP.001.01B, Brest, France, December 2016

Gervaise, C., Aulanier, F., Simard, Y. and Roy, N. (2015) Mapping probability of shipping sound exposure level, J. Acoust. Soc. Am. 137 (6), EL429-435

Hall, M. V. (1989) A comprehensive model of wind-generated bubbles in the ocean and prediction of the effects on sound propagation at frequency up to 40 kHz, J. Acoust. Soc. Am., 86, 1103-1117

Hamilton, E. L. (1980) Geoacoustic modelling of the sea floor. J. Acoust. Soc. Am., 68(5), 1313-1340

Hamilton, E. L. and R. T. Bachman (1982) Sound velocity and related properties of marine sediments, J. Acoust. Soc. Am., 72, 1891-1904

Hamilton, E. L. (1985) Sound velocity as a function of depth in marine sediments, J. Acoust. Soc. Am., 78, 1348-1355

Hannay, D.E.; Mouy, X.; Li, Z. (2016) An Automated Real-Time Vessel Sound Measurement System for Calculating Monopole Source Levels Using a Modified Version of ANSI/ASA S12.64-2009. Can. Acoust. 44, 166–167

Harrison, C. H. (1989) Ocean propagation models, App. Acoustics, 27, 163-201

Heaney, K. D., Kuperman, W. A. and B. E. McDonald (1991) Perth-Bermuda sound propagation, 1960, Adiabatic mode interpretation, J. Acoust. Soc. Am., 90, 2586-2594

Heaney, K. D., Campbell, R. L. and J. J. Murray (2012) Comparison of hybrid three-dimensional modeling with measurements on the continental shelf, J. Acoust. Soc. Am., 131,

1680-1688

Heitmeyer, R. M. (2006) A probabilistic model for noise generated by breaking waves, J. Acoust. Soc. Am., 119, 3676-3693

Helble, T. A., D'Spain, G. L., Hildebrand, J. A., Campbell, G. S., Campbell, R. L. and K. D. Heaney (2013) Site specific probability of passive acoustic detection of humpback whale calls from single fixed hydrophones, J. Acoust. Soc. Am., 134, 2556-2571

Holland, C. W. (2010) Propagation in a waveguide with range-dependent seabed properties, J. Acoust. Soc. Am., 128, 2596-2609

Jalkanen, J.-P.; Johansson, L.; Liefvendahl, M.; Bensow, R.; Sigray, P.; Östberg, M.; Karasalo, I.; Andersson, M.; Peltonen, H.; Pajala, J. (2018) Modelling of ships as a source of underwater noise. Ocean Sci. 14, 1373–1383

Jansen, H.W.J & de Jong, C.A.F. (2017) Experimental assessment of underwater acoustic source levels of different ship types, IEEE Journal of Oceanic Engineering, Vol. 42, No. 2

Jensen, F.B., Kuperman, W.A., Porter, M.B. and Schmidt, H. (2011) *Computational Ocean Acoustics*, 2nd ed., Springer, New York

Jiang, P.; Lin, J.; Sun, J.; Yi, X.; Shan, Y. (2020) Source spectrum model for merchant ship radiated noise in the Yellow Sea of China. Ocean Eng. 216, 107607

Joy, R.; Tollit, D.; Wood, J.; MacGillivray, A.; Li, Z.; Trounce, K.; Robinson, O. (2019) Potential Benefits of Vessel Slowdowns on Endangered Southern Resident Killer Whales. Front. Mar. Sci. 6, 34

Karasalo, I., Östberg, M., Sigray, P., Jalkanen, J.-P., Johansson, L., Liefvendahl, M. and Bensow, R. (2017), “Estimates of source spectra of ships from long term recordings in the Baltic sea”, Frontiers in Marine Science

Keiffer, R. S., Novarini, J. C. and Norton, G. V. (1995) The impact of the background bubble layer on reverberation-derived scattering strengths in the low to moderate frequency range, J. Acoust. Soc. Am. 97, 227-234

Kibblewhite, A.C. (1989) “Attenuation of sound in marine sediments: a review with emphasis on new low-frequency data”, J. Acoust. Soc. Am. 86(2), 716-738

Kuperman, W. A., & Ferla, M. C. (1985) A shallow water experiment to determine the source spectrum level of wind-generated noise. *The Journal of the Acoustical Society of America*, *77*(6), 2067-2073.

Küsel, E.T. and Siderius, M., (2019) Comparison of Propagation Models for the Characterization of Sound Pressure Fields, IEEE Journal of Oceanic Engineering

Lichte, H. (1919) Über den Einfluß horizontaler Temperaturschichtung des Seewassers auf die Reichweite von Unterwasserschallsignalen, Physikalische Zeitschrift, 17, 385-389

MacGillivray, A., McPherson, C., Izett,J., Gosselin, J., Zizheng, L. and Hannay, D. (2014) Modelling underwater shipping noise in the Great Barrier Reef Marine Park using AIS vessel track data, Proc. Internoise 2014, Melbourne

MacGillivray, A. and Z. Li. (2018) Vessel Noise Measurements from the ECHO Slowdown Trial: Final Report. Document 01518, Version 3.0. Technical report by JASCO Applied Sciences for Vancouver Fraser Port Authority ECHO Program

MacGillivray, A.O., Li, Z., Hannay, D.E., Trounce, K.B. and Robinson, O.M. (2019) Slowing deep-sea commercial vessels reduces underwater radiated noise. J. Acoust. Soc. Am. 146 (1), 340–351

MacGillivray, A.O. and de Jong, C.A.F. (2021) A Reference Spectrum Model for Estimating Source Levels of Marine Shipping based on Automated Identification System data. J. Mar. Sci. Eng. 2021, 9, 369. https://doi.org/ 10.3390/jmse9040369

McDonald, M. A. and C. G. Fox (1999) Passive acoustic methods applied to fin whale population density estimation, J. Acoust. Soc. Am., 105, 2643-2652

McKenna, M.F.; Ross, D.; Wiggins, S.M.; Hildebrand, J.A. (2012) Underwater Radiated

Noise from Modern Commercial Ships. J. Acoust. Soc. Am. 131, 92–103

Merchant, N. D., Blondel, P., Dakin, D. T. and D. T. Dorocicz (2012) Averaging underwater noise levels for environmental assessment of shipping, J. Acoust. Soc. Am., 132(4), EL343-349

Merchant, N. & Farcas, A. (2018) Acoustic metric to be monitored by JOMOPANS. Report of the EU INTERREG Joint Monitoring Programme for Ambient Noise North Sea (JOMOPANS).

Munk, W. and C. Wunsch (1979) Ocean acoustic tomography: a scheme for large scale monitoring, Deep Sea Res. (A), 26, 123-161

Mustonen, Mirko, Aleksander Klauson, Mathias Andersson, Dominique Clorennec, Thomas Folegot, Radomił Koza, Jukka Pajala, Leif Persson, Jarosław Tegowski, Jakob Tougaard, Magnus Wahlberg and Peter Sigray (2019) Spatial and temporal variability of ambient underwater sound in the Baltic Sea, Sci. Rep. 9, 13237. https://doi.org/10.1038/s41598-019-48891-x

Norton, G. V. and Novarini, J. C. (2002) Including attenuation and dispersion in time domain modeling of broadband sound propagation in dispersive oceanic media, J. Acoust. Soc. Am., 111 (5), 2352-2352

Novarini, J. C., Keiffer, R. S., Norton, G. V. (1998) A model for variations in the range and depth dependence of the sound speed and attenuation induced by bubble clouds under wind-driven sea surfaces, IEEE Journal of Oceanic Engineering, 23, 423 – 438

Porter, M.B. and Henderson, L.J. (2014) Modeling ocean noise on the global scale, Proc. Internoise 2014, Melbourne

Potter, J. R., Mellinger, D. K. and C. W. Clark (1994) Marine mammal call discrimination using artificial neural networks, J. Acoust. Soc. Am., 96, 1255-1362

Preisig, J. C. and T. F. Duda (1997) Coupled Acoustic Mode Propagation Through Continental-Shelf Internal Solitary Waves, IEEE J. Ocean Eng., 22, 256-270

Prins, H.J., Flikkema, M.B., Bosschers, J., Koldenhof, Y., de Jong, C.A.F., Pestelli, C., Mumm, H., Bretschneider, H., Humphrey, V. and Hyensjö, M. (2016), Suppression of underwater noise induced by cavitation: SONIC, Transportation Research Procedia 14, 2668 – 2677

Putland, R, Farcas, A. Merchant, N. de Jong, CAF, Binnerts, B. (2021) Validation report: 2019 data. Report of the EU INTERREG Joint Monitoring Programme for Ambient Noise North Sea (JOMOPANS).

Redfern, J.V., Hatch, L.T., Caldow, C., DeAngelis, M.L., Gedamke, J., Hastings, S., Henderson, L., McKenna, M.F., Moore, T.J. and Porter, M.B. (2017) Assessing the risk of chronic shipping noise to baleen whales off Southern California, USA, Endang Species Res Vol. 32: 153–167

Rees, T. (2003) “C-squares”, a new spatial indexing system and its applicability to the description of oceanographic datasets. Oceanography, 16(1), 11–19

Robinson, S. and Wang, L. (2020), “Standard for Terminology”, Report of the EU INTERREG Joint Monitoring Programme for Ambient Noise North Sea (JOMOPANS).

Sertlek, H.Ö. and Ainslie, M.A. (2014), “A depth-dependent formula for shallow water propagation”, J. Acoust. Soc. Am. 136 (2), pp. 573–582

Sertlek, H.Ö. (2016) “Aria of the Dutch North Sea - Propagation, source and sound mapping simulations for the Dutch North Sea”, PhD Thesis, Leiden University

Sertlek, H.Ö., Ainslie, M.A. and Heaney, K.D. (2018), “Analytical and Numerical Propagation Loss Predictions for Gradually Range-Dependent Isospeed Waveguides”, IEEE Journal of Oceanic Engineering

Simard, Y.; Roy, N.; Gervaise, C.; Giard, S. (2016) Analysis and modeling of 255 source levels of merchant ships from an acoustic observatory along St. Lawrence Seaway. J.

Acoust. Soc. Am. 140, 2002–2018

Simons, D., McHugh, R., Snellen, M., McCormick, N. H. and E. A. Lawson (2001) Analysis of Shallow-Water Experimental Acoustic Data Including Comparison With a Broadband Normal Mode Propagation Model, IEEE J. Ocean Eng., 26(3), 308-323

Stafford, K. M., Fox, C. G. and D. S. Clark (1998) Long-range acoustic detection and localization of blue whale calls in the northeast Pacific Ocean, J. Acoust. Soc. Am., 104, 3616-3625

Tappert, F, D. (1977) The parabolic approximation method, in Wave Propagation and Underwater Acoustics. vol. 70, J. B. Keller and J. S. Papadakis, Eds., 224-287

Thode, A. (2004) Tracking sperm whale (Physer macrocephalus) dive profiles using a towed passive acoustic array, J. Acoust. Soc. Am., 116, 245-254

Thorp, W.H. (1967) Analytic Description of the Low-Frequency Attenuation Coefficient. J. Acoust. Soc. Am. 42, p. 270

Tindle, C. T. and Z. Y. Zhang (1997) An adiabatic normal mode solution for the benchmark wedge, J. Acoust. Soc. Am., 101, 606-609

van Heteren, S. and Van Lancker, V. (2015), Collaborative Seabed-Habitat Mapping: Uncertainty in Sediment Data as an Obstacle in Harmonization, Chapter 8 of Collaborative Knowledge in Scientific Research Networks, ed. Diviaccio et al, IGI Global, Hershey PA, USA

van Moll, C.A.M., Ainslie, M.A. and van Vossen, R. (2009) A simple and accurate formula for the absorption of sound in seawater. IEEE Journal of Oceanic Engineering 34(4), 610-616

Veirs, S.; Veirs, V.; Wood, J.D.(2016) Ship noise extends to frequencies used for echolocation by endangered killer whales. PeerJ 4, e1657

Wales, S.C.and Heimeyer, R.M. (2002) An ensemble source spectra model for merchant ship-radiated noise, J. Acoust. Soc. Am. 111 (3), 1211-1231

Wang, L., Heaney, K., Pangerc, T., Theobald, P., Robinson, S. and Ainslie, M. (2014) Review of underwater acoustic propagation models. NPL Report AC 12.

Wenz, G. M. (1962) Acoustic ambient noise in the ocean: spectra and sources, J. Acoust. Soc. Am., 34, 1936-1956

Weston, D. E. (1959) Guided propagation in a slowly varying medium. Proceedings of the Physical Society, 73(3), 365

Weston, D. E. (1968) Sound Focusing and beaming in the interference field due to several shallow-water modes, J. Acoust. Soc. Am., 44, 1706-1712

Worcester, P. F., Cornuelle, B. D., Dzieciuch, M. A., Munk, W. H., Howe, B. M., Mercer, J. A., Spindel, R. C., Colosi, J.A., Metzger, K., Birdsall T.G., and A. B. Baggeroer (1999) A test of basin-scale acoustic thermometry using a large aperture vertical array at 3250 km range in the eastern North Pacific Ocean, J. Acoust. Soc. Am., 105, 3185-3201

Zampolli, M., Ainslie, M. A., & Schippers, P. (2010). Scenarios for benchmarking range-dependent active sonar performance models. Proc. Institute of Acoustics, 32 (Pt 2), pp.53-63

Zhou, J.-X., Zhang, X.-Z. and Knobles, D. (2009) ‘Low-frequency geoacoustic model for the effective properties of sandy sea bottoms’, J. Acoust. Soc. Am. 125(5): 2847-2866

Annex A Jomopans metrics

This provides a concise overview of the mathematical formulas that convert (measured or calculated) sound pressure into the metrics reported by Jomopans.

Sound pressure: $p(\boldsymbol{X}, z, t)$

- Geographic (lat-lon) coordinates $\boldsymbol{X} = (x, y)$
- Depth z
- Time t

Fourier transform over observation window Δt, at time T:

$$P(\boldsymbol{X}, z, T, f) = \frac{1}{\Delta t} \int_{T}^{T+\Delta t} p(\boldsymbol{X}, z, t) e^{-2\pi i f t} \mathrm{d}t$$

- Frequency f

Energy spectral density: $E_f(\boldsymbol{X}, z, T, f) = 2|P(\boldsymbol{X}, z, T, f)|^2$

Energy evaluated in frequency band between f_{lower} and f_{upper}, with bandwith $\Delta f = f_{upper} - f_{lower}$, denoted by evaluation frequency F_{ev}:

$$E(\boldsymbol{X}, z, T, F_{ev}) = \int_{f_{lower}}^{f_{upper}} E_f(\boldsymbol{X}, z, T, f) \mathrm{d}f$$

Depth average, over water depth $H(\boldsymbol{X})$

$$E_H(\boldsymbol{X}, T, F_{ev}) = \int_{0}^{H(\boldsymbol{X})} E(\boldsymbol{X}, z, T, F_{ev}) \mathrm{d}z$$

Sound pressure level (depth-average and in evaluation frequency band F_{ev})

$$L_p(\boldsymbol{X}, T, F_{ev}) = 10 \log_{10} \left(\frac{E_H(\boldsymbol{X}, T, F_{ev})}{p_0^2} \right) \mathrm{dB}$$

- Reference pressure $p_0 = 1$ µPa

The distribution of values of $L_p(\boldsymbol{X}, T, F_{\mathrm{ev}})$ over the evaluation time interval T_{ev} is expressed by the probability density function $\mathrm{PDF}_T\{L_p(\boldsymbol{X}, T, F_{\mathrm{ev}})\}$, for which:

$$\int_{\min\{L_p\}}^{\max\{L_p\}} PDF_T\{L_p(\boldsymbol{X}, T, F_{ev})\} \mathrm{d}L_p = 1$$

The c% temporal percentile $L_{p,c\%}(\boldsymbol{X}, T_{ev}, F_{\mathrm{ev}})$ expresses the value below which L_p falls during c% percent of the evaluation time interval T_{ev}, so that:

$$\int_{\min\{L_p\}}^{L_{p,c\%}} \mathrm{PDF}_T\{L_p(\boldsymbol{X}, T, F_{ev})\} \mathrm{d}L_p = \frac{c\%}{100\%}$$

L_p consists of contributions from different sources:

- 'Natural' wind noise:

$$L_p(\boldsymbol{X}, T, F_{ev}, \mathrm{wind}) = 10 \log_{10} \left(\frac{E_H(\boldsymbol{X}, T, F_{ev}, \mathrm{wind})}{p_0^2} \right) \mathrm{dB}$$

- 'Anthropogenic' ship noise, from multiple ships s_i:

$$L_p(\boldsymbol{X}, T, F_{ev}, \mathrm{ships}) = 10 \log_{10} \left(\frac{\sum_{s_i} E_H(\boldsymbol{X}, T, F_{ev}, s_i)}{p_0^2} \right) \mathrm{dB}$$

- 'Ambient noise' from all ships and wind:

$$L_p(\boldsymbol{X}, T, F_{ev}, \mathrm{wind + ships}) = 10\, log_{10} \left(\frac{E_H(\boldsymbol{X}, T, F_{ev}, \mathrm{wind}) + \sum_{s_i} E_H(\boldsymbol{X}, T, F_{ev}, s_i)}{p_0^2} \right) \mathrm{dB}$$

JOMOPANS has defined ***Excess Level*** $\mathrm{EL}(\boldsymbol{X}, T, F)$ to express the instantaneous excess of 'ambient noise' from all ships and wind over 'natural' wind noise:

$$\begin{aligned}\mathrm{EL}(\boldsymbol{X}, T, F_{\mathrm{ev}}) &= L_p(\boldsymbol{X}, T, F_{\mathrm{ev}}, \mathrm{wind} + \mathrm{ships}) - L_p(\boldsymbol{X}, T, F_{\mathrm{ev}}, \mathrm{wind}) \\ &= 10\log_{10}\left(\frac{E_H(\boldsymbol{X}, T, F_{ev}, wind) + \sum_{s_i} E_H(\boldsymbol{X}, T, F_{ev}, s_i)}{E_H(\boldsymbol{X}, T, F_{ev}, wind)}\right)\mathrm{dB}\end{aligned}$$

Note: JOMOPANS has proposed an alternative option to define an excess level $\mathrm{EL}_{\mathrm{m}}(\boldsymbol{X}, T, F_{\mathrm{ev}})$ that expresses the excess of 'ambient noise' from all ships and wind over the median value of the 'natural' wind noise over evaluation time interval T_{ev}:

$$\mathrm{EL}_{\mathrm{m}}(\boldsymbol{X}, T, F_{\mathrm{ev}}) = L_p(\boldsymbol{X}, T, F_{\mathrm{ev}}, \mathrm{wind} + \mathrm{ships}) - L_{p,T_{ev},50\%}(\boldsymbol{X}, F_{\mathrm{ev}}, \mathrm{wind})$$

JOMOPANS has defined ***Dominance*** $D(\boldsymbol{X}, T_{\mathrm{ev}}, F_{\mathrm{ev}})$ to express the percentage of the evaluation time over which the excess level exceeds a cut-off value $\mathrm{EL}_{\mathrm{co}}$:

$$D(\boldsymbol{X}, T_{\mathrm{ev}}, F_{\mathrm{ev}}) = \int_{\mathrm{EL}_{\mathrm{co}}}^{\max\{\mathrm{EL}\}} \mathrm{PDF}_T\{\mathrm{EL}(\boldsymbol{X}, T, F_{\mathrm{ev}})\}\mathrm{dEL}$$

JOMOPANS has defined the ***Pressure Curve*** (or *Pressure Function*) $\mathrm{PC}(D_{\mathrm{ev}}, \boldsymbol{X}_{\mathrm{ev}}, T_{\mathrm{ev}}, F_{\mathrm{ev}})$ to express the percentage of the evaluation area $\boldsymbol{X}_{\mathrm{ev}}$ within which the dominance exceeds the evaluation dominance values D_{ev}.

$$\mathrm{PC}(D_{\mathrm{ev}}, \boldsymbol{X}_{\mathrm{ev}}, T_{\mathrm{ev}}, F_{\mathrm{ev}}) = \int_{D_{\mathrm{ev}}}^{100\%} \mathrm{PDF}_{\boldsymbol{X}}\{D(\boldsymbol{X}, T_{\mathrm{ev}}, F_{\mathrm{ev}})\}\mathrm{d}D$$

Note: JOMOPANS graphs of the pressure curve plot temporal percental D_{ev} along the y-axis and spatial percentage $\mathrm{PC}(D_{\mathrm{ev}}, \boldsymbol{X}_{\mathrm{ev}}, T_{\mathrm{ev}}, F_{\mathrm{ev}})$ along the x-axis.

JOMOPANS has defined the ***Pressure Index*** $\mathrm{PI}(\boldsymbol{X}_{\mathrm{ev}}, T_{\mathrm{ev}}, F_{\mathrm{ev}})$ to provide a single number index for the dominance in the evaluation area $\boldsymbol{X}_{\mathrm{ev}}$, over the evaluation time interval T_{ev}, and in the frequency band F_{ev}. PI expresses the area under the pressure curve:

$$\mathrm{PI}(\boldsymbol{X}_{\mathrm{ev}}, T_{\mathrm{ev}}, F_{\mathrm{ev}}) = \int_0^{100\%} \mathrm{PC}(D_{\mathrm{ev}}, \boldsymbol{X}_{\mathrm{ev}}, T_{\mathrm{ev}}, F_{\mathrm{ev}})\ \mathrm{d}D_{\mathrm{ev}}$$

Annex B Uncertainty Analysis

Annex B.1 Uncertainties on input quantities

There are a number of contributions to the combined uncertainty in the statistical estimates produced by the modelling which derive from the uncertainties in the input quantities to the model. Examples of these include the source levels of the many vessels, source levels of the wind noise (and inputs to the wind noise model), and the environmental parameters which govern the sound propagation (properties of the seabed, etc).
Some of these contributions will be uncorrelated and can be represented as a random statistical distribution of values which are amenable to a simple treatment using sensitivity analysis (for example, using a Monte-Carlo approach with a simple evaluation model where the values are subject to independent and identically distributed random errors). Examples that may be treated this way would be vessel source level spectra where a reasonable assumption would be that the actual source levels are randomly distributed about an assumed mean spectral curve. Evaluating the effect of this source level uncertainty on the combined uncertainty using a Monte-Carlo approach for one instant of time with a large number of repeated calculations is likely to lead to lower estimates of uncertainty on the statistical outputs of the modelling than the initial uncertainty estimates of the input source level spectra.
However, the uncertainty on some of these inputs may be correlated rather than independent, and some may contribute a systematic bias to the modelling output estimates. Such contributions require a slightly different treatment, and the effect on the combined uncertainty may not be reducible in the manner described above. In addition, the temporal correlations that occur between individual estimates of the model outputs due to temporal correlations in the input quantities can produce an irreducible effect on the statistical estimates of the model outputs derived over multiple time instants. This temporal correlation is more difficult to account for.
In practice, we expect the uncertainty assessment to be subject to a mixture of random and systematic effects, and it is expected that the standard uncertainty of the estimate will have a component that is reducible and a component that is irreducible. The next section provides a more formal statement of the above.
The principles for the assessment of uncertainty are outlined in a number of standard documents which provide general guidance [1 – 4].

Annex B.2 A treatment of uncertainty contributions

Suppose values $y_i, i = 1, \dots, m,$ satisfy

$$y_i = y + e_i,$$

where the e_i are samples drawn independently from a probability distribution having mean zero and variance σ^2. Then, it is well-known that the sample mean $\bar{y}$ is an unbiased estimate of y with associated standard uncertainty $\sigma/\sqrt{m}$, and it follows that the standard uncertainty can be made arbitrarily small by choosing m to be sufficiently large. In contrast, if

$$y_i = y + e_0,$$

for a single sample e_0 drawn from a probability distribution having zero mean and variance σ_0^2 then the sample mean has standard uncertainty σ_0, independent of m. The first case describes a scenario where the values are subject to independent and identically distributed random errors, and the second a scenario where the values are subject to a single common, systematic error (and, consequently, must be equal).
In practice, we can expect something between two these extremes, with values satisfying

$$y_i = y + e_i + e_0,$$

subject to a mixture of random and systematic effects. In this case, the (so-called) *generalized weighted mean* is an unbiased estimate of y having a standard uncertainty that comprises a component derived from the random effects that is reducible by increasing m and a component derived from the systematic effect that is irreducible. The generalized weighted mean can be obtained as the solution to a *generalized least-squares* problem defined by the values $y_i, i = 1, \dots, m,$ and their associated covariance matrix, given here *explicitly* by

$$V_y = \sigma^2 I + \sigma_0^2 \mathbf{1}\mathbf{1}^{\mathrm{T}},$$

where I is the identity matrix of dimension m and $\mathbf{1}^{\mathrm{T}} = (1,1, \dots,1)$, a vector of length m.
Now consider the situation where y_i is the result of a model evaluation in terms of values $\boldsymbol{x}_i$ of input or influence quantities that are different for each i by virtue of being subject to random errors and values $\boldsymbol{x}_0$ of input or influence quantities that are the same for each i by virtue of being subject to systematic errors:

$$y_i = f(\boldsymbol{x}_i, \boldsymbol{x}_0), \qquad i = 1, \ldots, m.$$

For example, the values $y_i, i = 1, \ldots, m,$ might constitute a time series of values provided by a numerical model of noise propagation. Using knowledge of the probability distributions for the random and systematic effects, a Monte Carlo method can be used to obtain an approximation to the *joint* distribution for the values $y_i, i = 1, \ldots, m,$ and, in particular, their associated covariance matrix. This information can then be used to formulate and solve a generalized least-squares problem to provide a (single) summary estimate of the time series. As above, it can be expected that the standard uncertainty of the estimate will have a component that is reducible and a component that is irreducible. The step of formulating and solving a generalized least-squares problem can be replaced by a further Monte Carlo calculation using the "mean function" as the evaluation model. In this way, the analysis might be extended to treat other summary statistics, such as percentiles, derived from the values.

Annex B.3 References

[1] BIPM, IEC, IFCC, ILAC, ISO, IUPAC, IUPAP and OIML 2008 *Guide to the expression of uncertainty in measurement* (Sevres, France: Joint Committee for Guides in Metrology)

[2] BIPM, IEC, IFCC, ILAC, ISO, IUPAC, IUPAP and OIML 2008 *Evaluation of measurement data – Supplement 1 to the "Guide to the expression of uncertainty in measurement"–Propagation of distributions using a Monte Carlo method* (Sevres, France: Joint Committee for Guides in Metrology)

[3] Cox M G and Siebert B R L 2006 The use of a Monte Carlo method for evaluating uncertainty and expanded uncertainty *Metrologia* **43** pp S178--188

[4] Cox M G and Harris P M 2010 SS*f*M Best Practice Guide No 6, Uncertainty evaluation *Technical Report MS 6* (Teddington, UK: National Physical Laboratory)

Annex C AIS processing and data quality

The Jomopans maps of the underwater sound of shipping on the North Sea are calculated using information from the AIS and VMS ship tracking systems. For this purpose, Jomopans has acquired processed AIS/VMS data of the North Sea shipping in 2019 from Quiet Oceans. The processing included:

1. Quality Check and Cleaning
   - Check the validity of the MMSI vessel numbers from a static external database;
   - Check the validity of the length of the vessels by comparing with external databases;
   - Check the consistency of the date and time;
   - Check the consistency of the trajectory;
   - Check the consistency of the speed;
   - Remove non vessel data.
2. Trajectory interpolations to a regular temporal resolution of 10 minutes.

Quiet Oceans has not revealed the source of the raw data, nor details about their processing.

This annex describes the results of a review of the processed data and the additional processing that has been applied to improve the data quality.

Annex C.1 AIS and VMS

AIS (Automatic Identification System)

The International Maritime Organization's International Convention for the Safety of Life at Sea requires AIS to be fitted aboard international voyaging ships with 300 or more gross tonnage (GT), and all passenger ships regardless of size. AIS is intended, primarily, to allow ships to view marine traffic in their area and to be seen by that traffic.

AIS data gathering is subject to various uncertainties:

- Land and ship based VHF receivers have a reception range of a few tens of kilometres, depending on location and weather conditions.
- Satellite-based receivers offer larger spatial coverage but poor temporal coverage since they are on board polar satellites following low-altitude orbits with repetition periods of the order of 90 minutes.
- For a variety of reasons, ships can turn off their AIS transponders
- AIS transponders can be moved from one vessel to another
- Many small-sized vessels do not carry AIS transponders
- AIS parameters that depend on user input are not always correct

VMS (Vessel Monitoring Systems)

VMS is a general term to describe systems that are used in commercial fishing to allow environmental and fisheries regulatory organizations to track and monitor the activities of fishing vessels. Under the European Union legislation, VMS is a legal requirement for vessels in excess of 15 metres. Since 2005, all Community vessels automatically transmit vessel identification, date, time, position, course and speed either hourly or every 2 hours
Different VMS systems use different communication technologies, including AIS, Inmarsat, Iridium and Argos depending on the functionality required by the particular VMS system. VMS data availability is limited by national regulations.

Annex C.2 Jomopans AIS data deliveries

The 2019 data were delivered for Jomopans in a number of iterations.

The first delivery was based on AIS data alone, because VMS data were not timely available. These data were used by TNO to produce the first North Sea shipping sound maps, that were presented at the Jomopans Midterm Event. Figure C-1 illustrates the shipping density for January 2019 according to this first delivery.

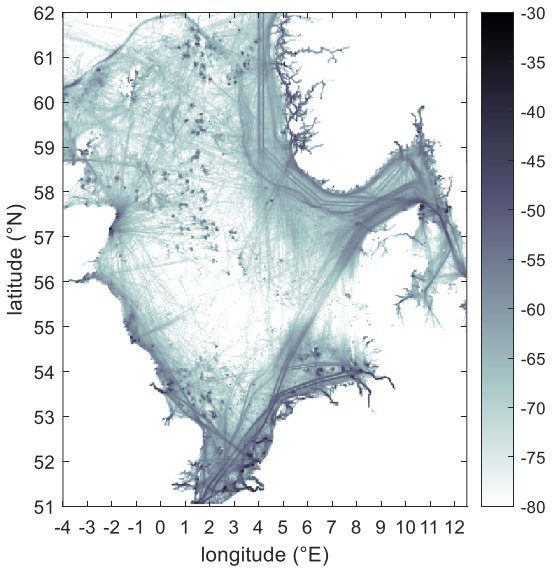

Figure C-1 Shipping density map for the month of January 2019, based on the first delivery of AIS data. The colour scale represents $10log_{10}(\#AIS\ messages\ per\ grid\ cell/\#vessels/\#timesteps)$, *where '#' stands for 'total number of' and the grid cells have dLon = 0.0228 deg and dLat = 0.0191 deg.*

This density map revealed a clear data gap in Danish and German waters. The local decrease of shipping densities in the major shipping lanes in these waters is unrealistic. In a second delivery, Quiet Oceans reduced this problem by including additional raw data in their processing, see Figure C-2. Figure C-3 illustrates where data were added.

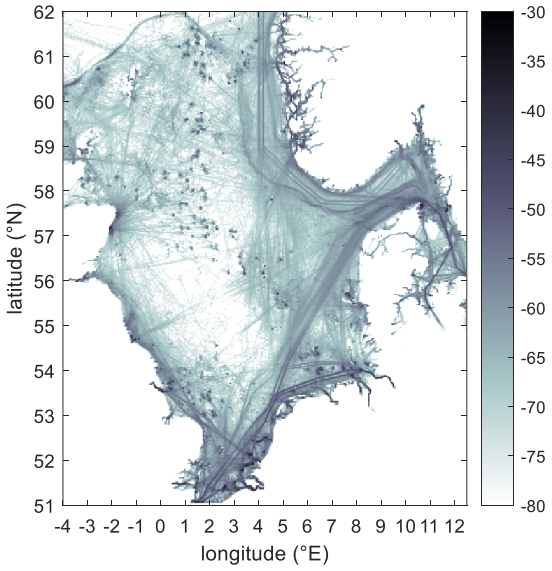

Figure C-2 Shipping density map for January 2019, based on the second delivery of AIS data.

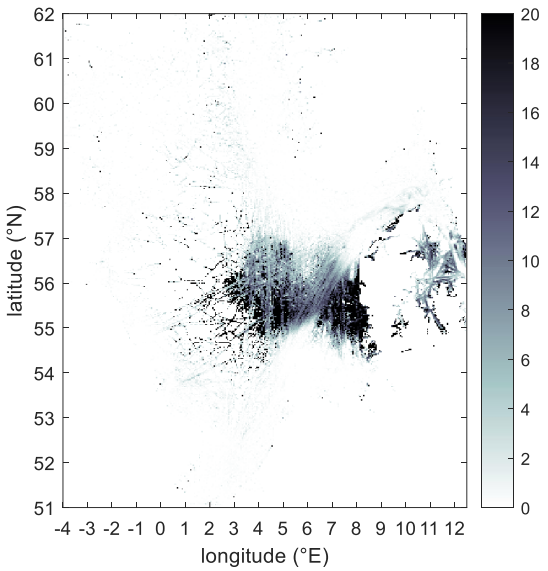

Figure C-3 Increase in ship density due to addition of extra data (delivery 2) for January 2019: $10log_{10}(\#AIS\ messages\ \ delivery\ 2\ /\#AIS\ messages\ \ delivery\ 1)$ *per grid cell.*

Next, raw VMS data for the national waters were made available by Norway, Sweden, Denmark and Germany. Quiet Oceans provided a third delivery in which these VMS data were merged with the AIS data, see Figure C-4. Figure C-5 illustrates where data were added. A substantial part of the added VMS data concerns fishing vessels.

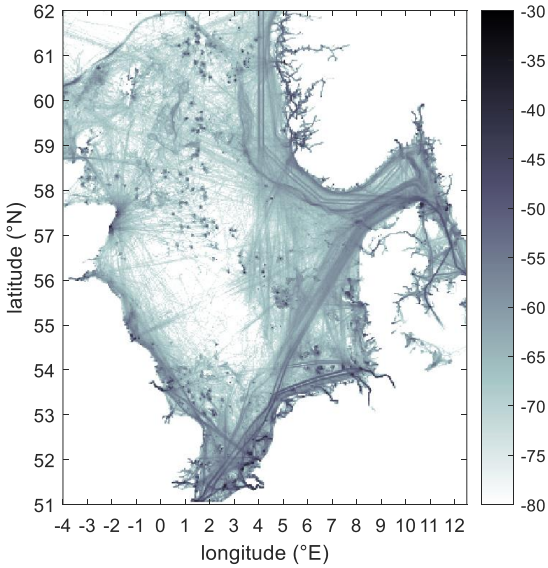

FigureC-4 Shipping density map for January 2019, based on the third delivery of merged AIS and VMS data.

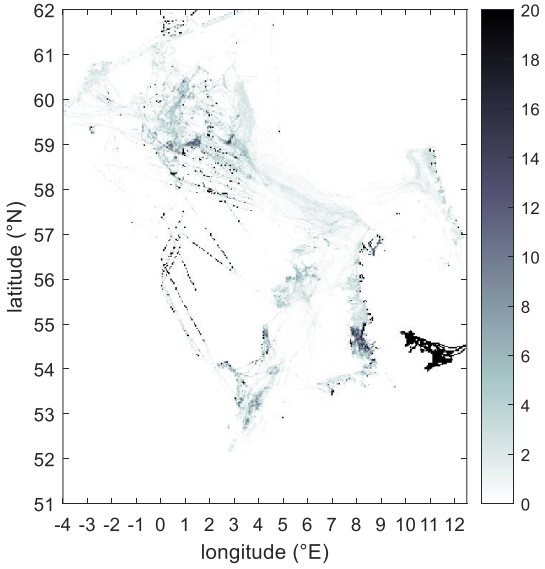

Figure C-5 increase in ship density due to addition of VMS data (delivery 3) for January 2019: $10log_{10}(\#AIS\ messages\ \ delivery\ 3\ /\#AIS\ messages\ \ delivery\ 2)$ *per grid cell.*

Annex C.3 Jomopans AIS track interpolation update

Although the AIS data appears to have been improved by the three iterations, there are still significant uncertainties. It is likely that a substantial fraction of the vessels that sailed on the North Sea in 2019 are missing in these data, but it is impossible to know how many. The density ship appears to be low in large areas in Dutch and UK waters, possibly due to incomplete AIS coverage in combination with a lack of VMS data.

It is also obvious that the vessel traffic is discontinuous along some of the shipping lanes that cross the central North Sea. This may be due to bad coverage of this area by land and satellite AIS receivers. Quiet Oceans has filled in some of the missing data by interpolation of ship tracks, but appears to have been conservative (limiting the interpolation time and distance) in the application of this interpolation. More details have been requested but have not yet been provided.

TNO has reviewed the track data and decided to redo the track interpolation with less limiting criteria: Straight line tracks were interpolated up to 100 km. Incidental outliers from ship tracks (with an apparent ship speed >40 kn) were removed. It was observed that this interpolation resulted in some unrealistic tracks, crossing land. This could likely be improved with a more customized local algorithm, but because these tracks will not contribute to the underwater noise, we decided to accept these, in favour of the improved coverage of the central North Sea. The result is illustrated for the May 2019 data set in Figure . The total amount of AIS messages (on a regular time grid of 10 min intervals) has increased by this updated interpolation, and some obvious gaps in the map have been filled in. Figure illustrates where the additional track interpolation has increased the density.

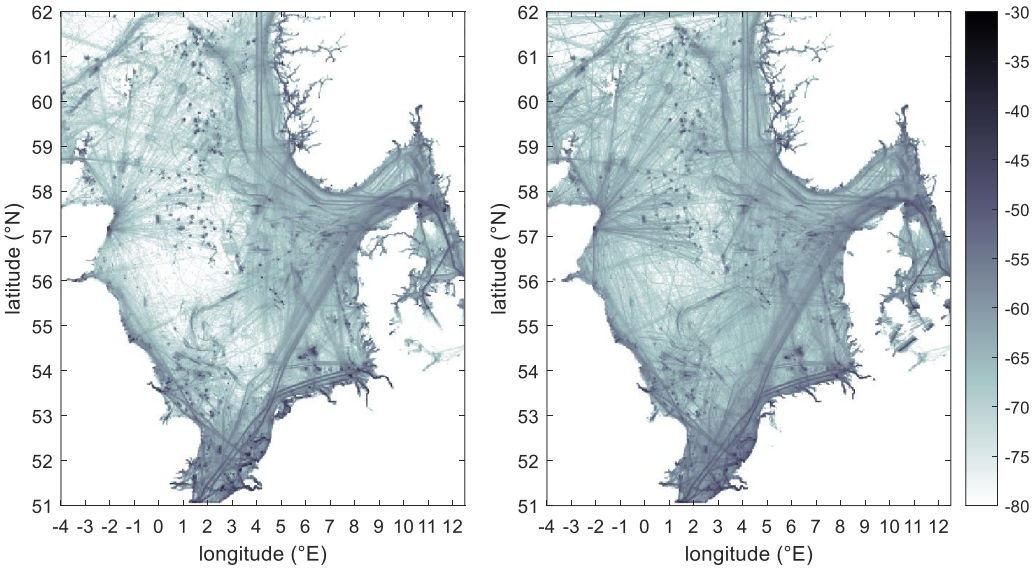

Figure C-6 Shipping density map for the month of May 2019, based on merged AIS and VMS data. Left: original from Quiet Oceans; right: with additional track interpolation by TNO

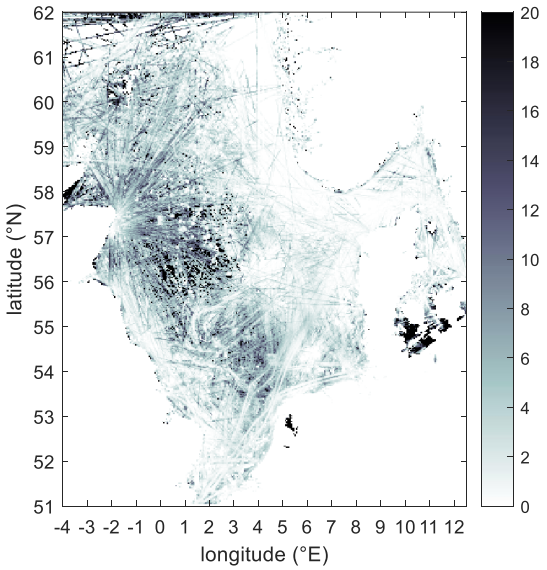

Figure C-7 Density increase, thanks to the additional track interpolation.

The following observations were made in an analysis of the May 2019 data set (before interpolation, delivery 3):

- This data set contains tracks for 29,372 ships, identified by the Maritime Mobile Service Identity (MMSI) number associated with their AIS transponder.
- The total number of AIS messages is 10,827,629.
- The total number of AIS messages with a speed over ground greater than 0.2 kn is 8,823,044 (81%).
- For 5,732 ships (20%) the presence during te month is less than 30 minutes (3 AIS messages).
- For 509 ships (2%) the ‘speed over ground’ does not exceed 0 at any time.

After interpolation:

- The total number of AIS messages is 10,975,763 (1.4% more than before interpolation)
- The total number of AIS messages with a speed over ground greater than 0.2 kn is 10,961,820 (24% more than before interpolation).
- For 7,099 ships (24%) the presence during te month is less than 30 minutes (3 AIS messages).
- For 2,080 ships (7%) the ‘speed over ground’ does not exceed 0 at any time.

Annex C.4 Other AIS parameters

The processed AIS data sets include the parameters summarized in Table C-1. The Jomopans ship source level model relies on the 'AIS Ship type ID', 'ship Length' and 'speed over ground' parameters.

Table C-1: Overview of AIS parameters provided by Quiet Oceans

Column	Description
MMSI	MMSI Number
Source	AIS=Terrestrial-AIS, ASS=Satellite-AIS
Day	DD/MM/YYYY
Hour	HH:MN:SS
longitude	longitude
latitude	latitude
speed	speed over ground
course over ground	course over ground
true heading	true heading
IMO Number	IMO Number
Name	Name
AIS Ship type	AIS Ship type
shipDraught	Draught
shipLength	AIS A+ B dimensions
shipWidth	AIS C+D dimensions
flagcode.isoCode2	Ship flag

The following observations were made in an analysis of the May 2019 data set:

- The corresponding IMO number is provided for only 7,997 ships (27%).
- Figure C-8 shows the distribution of the ships over the various AIS ship types.
- For 6,391 ships (22%) the 'AIS ship type ID' is between 0 and 9 indicating that the ship type is 'Unknown'.
- For 9,333 ships (32%) the 'ship length' parameter is reported as '0'.

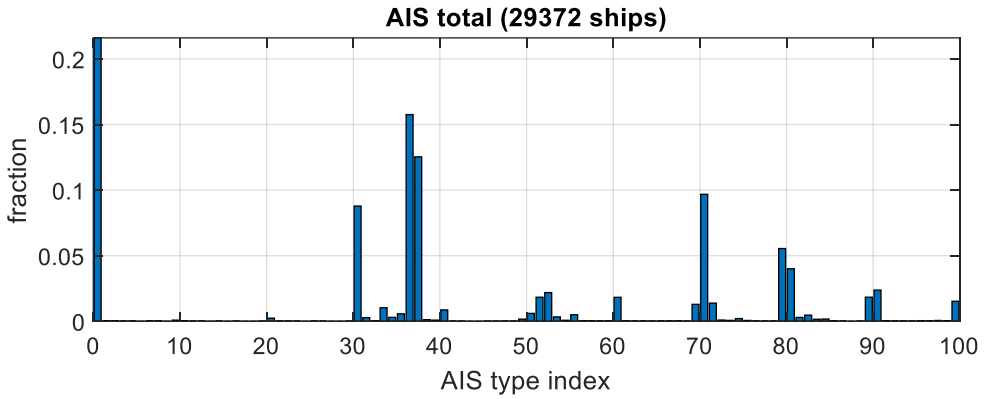

Figure C-8 Number of ships per AIS ship type ID (merged AIS/VMS data, May 2019).

After a comparison of the AIS 'speed over ground' (SOG) with the ship displacement between per AIS time steps, it was decided to use the speed derived from the ship displacement per time step rather than the AIS SOG as input for the source level model. This avoids problems with incidental errors in the SOG parameter. Especially incidental unrealistically high SOG values were shown to have an unwanted influence on the calculated monthly SPL statistics.

Annex D Sensitivity studies

Annex D.1 Required number of radials

Introduction: To reduce the computational complexity of the underwater noise modelling, spatial-temporal sound maps are typically obtained by means of interpolation of radial slices (2-dimensional simulations along straight trajectory). This method assumes that (i) out of plane propagation is negligible and that (ii) a limited number of radials suffices. In this chapter the effect of using a limited number of radials on the model precision is investigated for the JOMOPANS area.

Method: This is done by calculating the SPL map for the JOMOPANS area at a single moment in time with representative shipping and comparing the results for 16 and 36 radials. Details of the simulation are described in Table D-1.

Results: Figure D-1 shows the broadband and 250 Hz one-third octave band (base 10) (OTO) SPL for the selected snapshot using 16 and 36 radials for the calculation. Figure D-2 shows the difference between these results, indicating that using a reduced number of radials (16 instead of 36) has a small (< 1 dB) effect on the predicted SPL for the majority of JOMOPANS region. Larger differences however occur in coastal regions and at locations where there is a large depth variability and low shipping density such as the shallow Dogger Bank region in the center of the JOMOPANS area.

Recommendation: Because the JOMOPANS project aims to get good performance for the bulk of the North Sea (not focusing on local effects) the usage of 16 radials is considered to provide satisfactory performance. However, for the generation of local sound maps in coastal regions a larger number of radials may me desirable.

Table D-1: the simulations parameters used to investigate the effect of the number of radials on the model precision for the JOMOPANS region.

Source level model	RANDI3.1c2
Snapshot date and number of ships present	15-Jan-2019 11:50:00, 1838 sources from [globalAREA_From20190101_To20190201.mat]
Seabed	Uniformly modelled as medium sand (grainsize=1.5), using parameters from Table 4.18 in [Ainslie, 2010]
Water	1500 m/s,1000 kg/m^3
Surface wind	0 m/s
Simulation range	400 km (length of radial slices)
Radials	16, 36 (angle resolution 22.5 deg & 10 deg)
Wind model	Wind model (vs 1.0) results are added to the shipping noise when calculating SPL levels for the windspeed at the same time step
Tested metrics	Depth averaged, broadband and 250 Hz (efficient propagation)

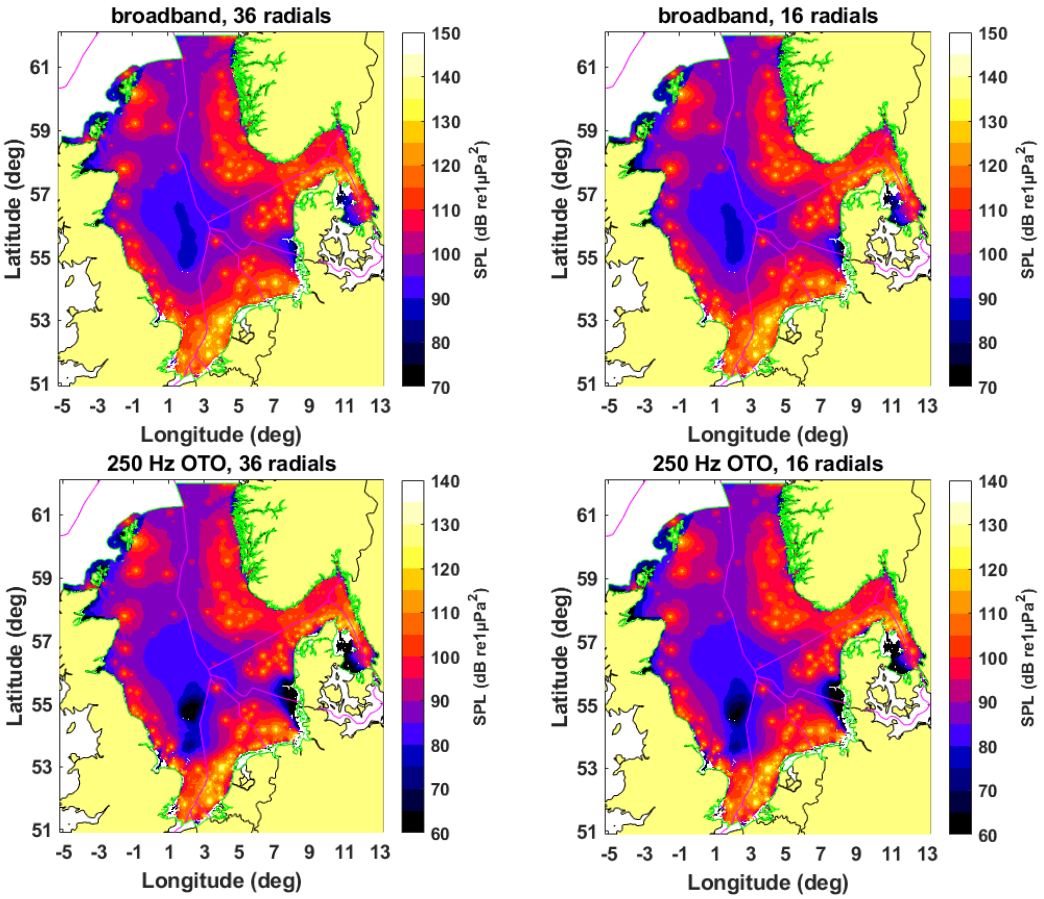

Figure D-1 Figures depicting the broadband and 250 Hz one-third octave (base 10) SPL 16 and 36 radials for the calculation

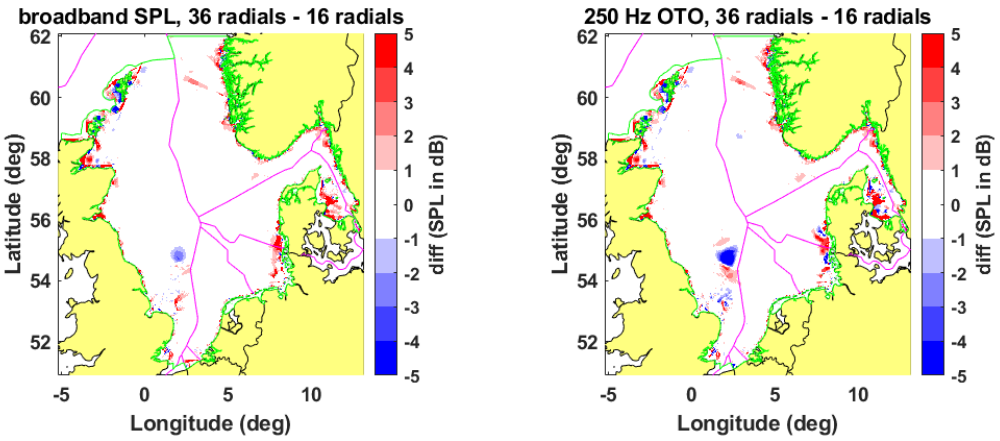

Figure D-2 Broadband and 250 Hz OTO difference between results where 36 and 16 radials were used for the calculation

Annex D.2 Required length of radials

Introduction: The maximum simulation range (i.e. the length of the radial slices) has a large effect on the calculation time. In areas with lots of ship the SPL will be dominated by nearby traffic, but in areas with little local shipping, benign propagation conditions (low propagation loss) and low ambient noise levels, ships from large distances can have a significant contribution to the underwater noise. In this chapter the effect of the length of the radials on the model precision is investigated for the JOMOPANS area. Due to the large number of sources present at all times in the North Sea and the spatially varying propagation conditions, the required simulation range cannot be accurately modelled using a simple signal (single ship + range dependent propagation) to noise (natural ambient) ratio.

Method: To determine the required simulation range the SPL levels for the JOMOPANS area are compared for a single moment in time with representative shipping conditions. A maximum simulation range of 500 km was used as a reference solution, assuming that ships at larger distances can safely be neglected. The simulation settings are specified in Table D-2. This simulation was the first one ran and still used the Wales and Heitmeyer (2002) source level model.

Results: Figure D-3 and Figure D-4 show the broadband and 250 Hz one-third octave (base 10) band SPL. Figure D-5 and Figure D-6 show the difference with respect to the reference solution. The comparison with the error criteria (the 95th area percentile of the difference) is shown in the title of each figure.

Recommendation: A 95% area percentile difference less than 0.5 dB was set to be an acceptable deviation of the reference solution. Receivers outside the JOMOPANS area and coastal areas (Depth < 10 m) were excluded from this analysis. Table D-3 shows a suggested simulation range based on the selected criteria. The maximum required range depends strongly on frequency. For the 160 Hz to 400 Hz one-third octave (base 10) bands it is observed that a large simulation range is needed. For the lower bands a large range may also be needed for locations with low shipping density and of more benign propagation conditions than the scenario considered in the simulation.

Although not required by the criteria, for the JOMOPANS project a constant simulation range of 400 km was used for the generation of the sound maps with the TNO Aquarius model because (i) the model is fast enough due to the use of source gridding and (ii) the model software architecture would have to be edited to support a frequency dependent simulation range.

Table D-2 the simulations parameters used to investigate the effect of the simulation range on the model precision for the JOMOPANS region.

Source level model	Wales & Heitmeyer [2002]
Snapshot dates and number of ships	15-Jan-2019 11:50:00, 1838 sources from [globalAREA_From20190101_To20190201.mat
Seabed	Uniformly modelled as medium sand (grainsize=1.5), using parameters from Table 4.18 in [Ainslie, 2010]
Water	1500 m/s,1000 kg/m^3
Surface Wind	0 m/s
Maximum length of radials	25, 50, 100, 200, 300, 400, 500 km
Number of radials	32 (angle resolution 11.25 deg)
Wind model	Wind model results are added to the shipping noise when calculating SPL levels
Tested metrics	Depth averaged broadband and 250 Hz

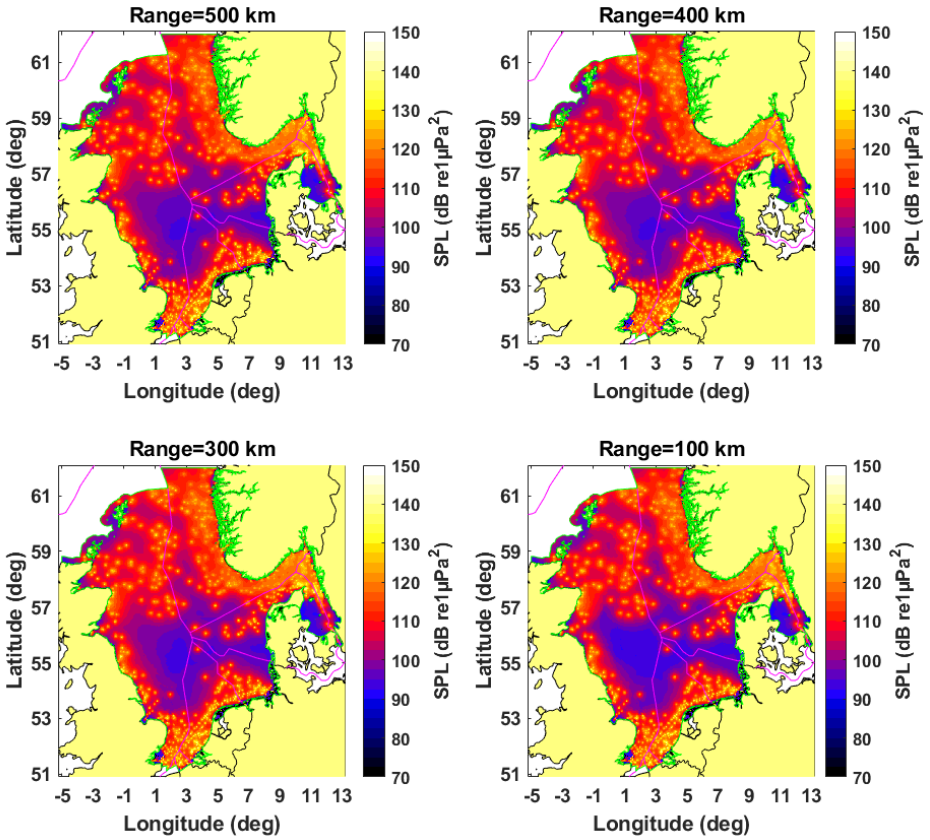

Figure D-3 Broadband SPL for different max calculation ranges

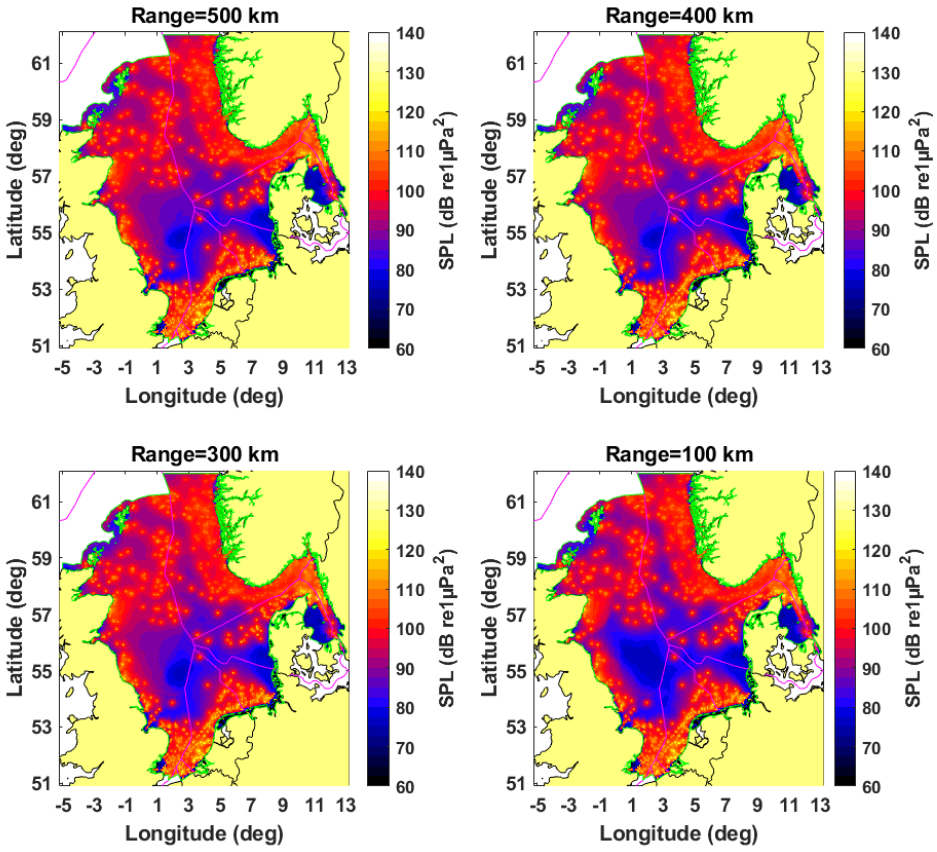

Figure D-4 250 Hz band: calculated SPL for different max calculation ranges

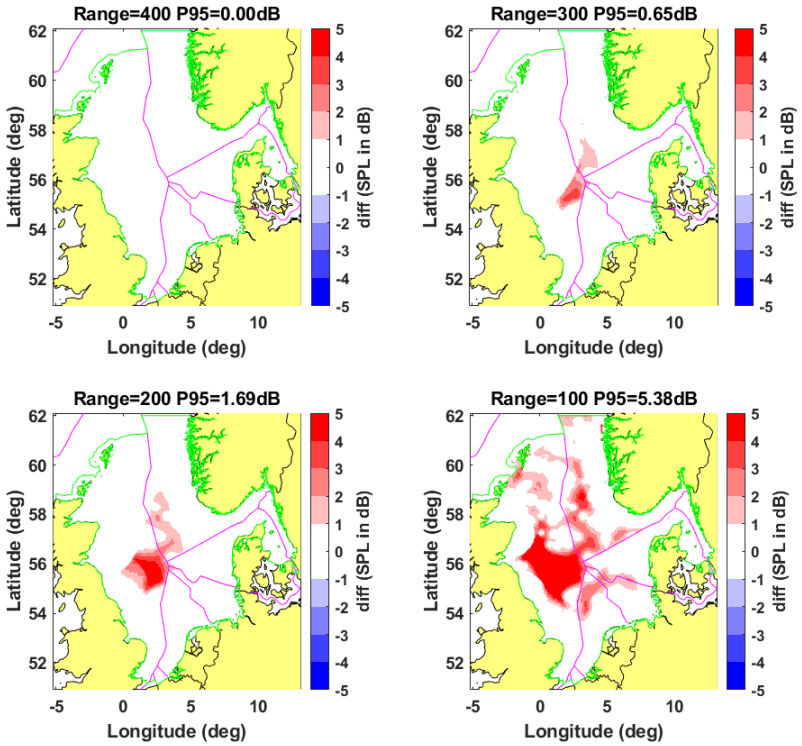

Figure D-5 250 Hz band: difference of calculated SPL for different max ranges and reference solution

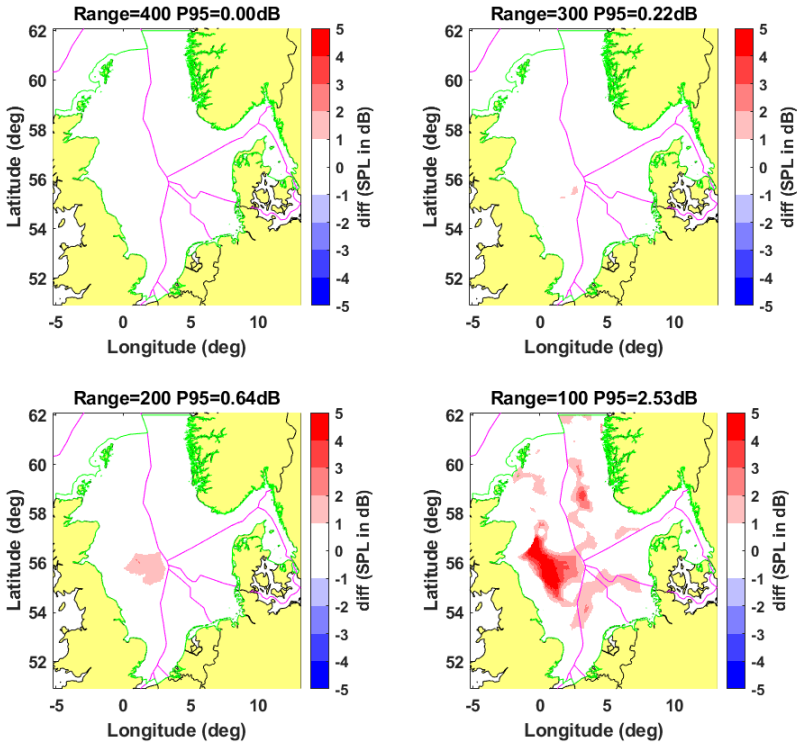

Figure D-6 broadband: difference of calculated SPL for different max ranges and reference solution

Table D-3 Proposal for acceptable and combined simulation ranges for different frequencies

Freq (Hz)	Acceptable range (km)	Combined range (km)	Freq (Hz)	Acceptable range (km)	Combined range (km)
10	100	100	500	300	300
13	100		630	300	
16	100		800	300	
20	100		1000	200	200
25	100		1.25 k	200	
31.5	200	200	1.6 k	200	
40	200		2 k	100	100
50	200		2.5 k	100	
63	200		3.150 k	50	
80	200		4 k	50	
100	200		5 k	50	
125	300	300	6.3 k	25	25
160	300		8 k	25	
200	400	400	10 k	25	
250	400		12.5 k	10	
315	400		16 k	10	
400	300	300	20 k	5	

Annex D.3 Spatial source gridding

Introduction: The computational complexity can be reduced significantly by means of source gridding, as this enables limiting the number of propagation model runs. Stored data from a single calculation of propagation loss between the source and receiver grids for the JOMOPANS area can be repeatedly used for SPL calculations at multiple time steps. In this approach, sources are relocated to the nearest source grid location. In this annex, the effect of using a spatial source grid on the model precision is investigated for the Sweden Vinga area.

Method: This is done by comparing the monthly statistics of the SPL for the Sweden Vinga area for difference source grid resolutions:

- **Reference solution:** no source gridding is applied. However, a minimum simulation range of 100 m is selected to avoid singularities (sources being at the receiver location resulting in unrealistically high sound levels.
- **Coarse grid:** the same resolution as the receiver grid, but shifted by one half of the grid resolution.
- **Fine grid:** Like the coarse grid but with additional locations added to increase resolution.

Figure shows how the receiver grid, the coarse grid and the fine grid are spatially oriented. The course grid has a resolution of 0.05 degrees longitude and 0.025 degrees latitude. The distance between two receiver grid points for the coarse grid is approximately 3 kilometers. The other simulation settings are specified in Table .

The effect of the source gridding is quantified by comparing the broadband and one-third octave (base 10) band SPL monthly statistics for the gridded scenarios against the reference solution without source gridding for the area around the Vinga measurement location.

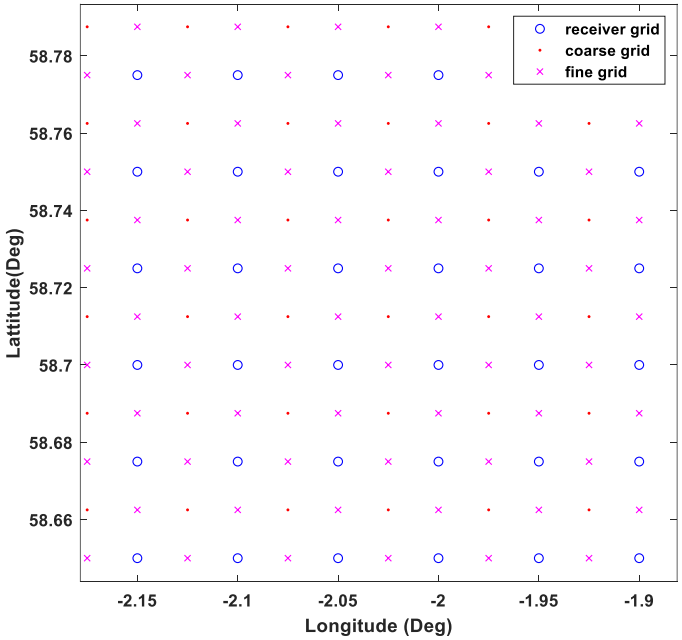

Figure D-7 Small area showing a coarse and fine source grid, along with the receiver grid

Figure D-8 and Figure D-13 show the Broadband and OTO maps of the monthly SPL statistics for calculations with the ships at their exact source position. Figures D-9 and D-10 and Figures D-14 and D-15 show the maps for calculations with the sources relocated to the ‘fine’ and ‘coarse’ grids respectively. Figures D-11 and D-12 and Figures D-16 and D-17 show the difference between the source gridding solutions and using the exact location.

From these figures it is observed that gridding sources does not lead to significant deviations except when:

- There are many sources very close to a receiver (e.g. near a port or in the vicinity of a shipping lane)
- For high percentiles
- Large bathymetric variability (e.g. in coastal areas)
- Close to the edges of a modelling area

Recommendations: The coarse grid resolution gives satisfactory performance for receivers that are not in the vicinity of a port or a shipping lane. The fine source grid significantly improves the performance in these regions. Because the computational complexity associated with the fine resolution grid was found to be acceptable, the fine source grid spacing will be used for the generation of the sound maps with the TNO Aquarius model.

Table D-4 the simulations parameters used to investigate the effect of source gridding on the model precision for the Sweden Vinga site.

Source level model	RANDI 3.1c2
Area and time period	Sweden Vinga 21-03-201803 to 20-04-2018 from MMSINavSnapShot_Sweden_Vinga_From20180321_To20180420_Step1min_DeltaHour2.mat
Seabed	Uniformly modelled as Coarse Silt (grainsize 4.5), using parameters from Table 4.18 in [Ainslie, 2010]
Water	1500 m/s,1000 kg/m^3
Surface Wind	0 m/s
Radials	16 (angle resolution 22.5 deg)
Sim range	100 km
Wind model	Wind model results are added to the shipping noise when calculating SPL levels
Tested metrics	Depth averaged broadband and 250 Hz SPL percentiles

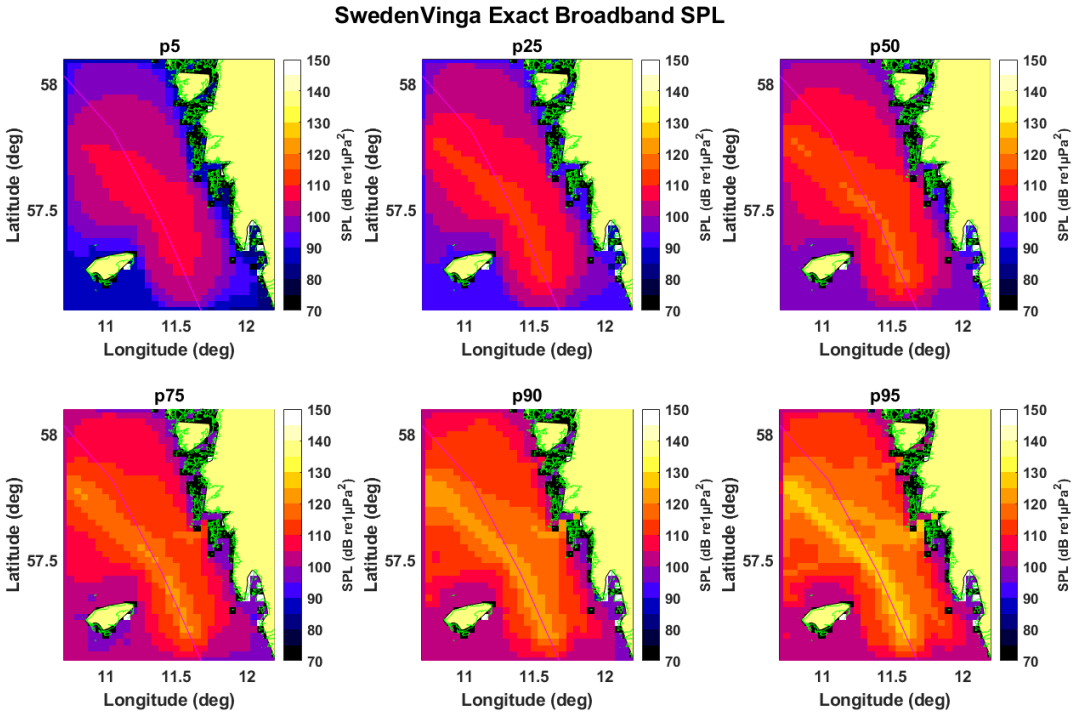

Figure D-8 Broadband SPL percentiles for exact source positions (Vinga, 2018). The magenta solid line indicates the border between Danish and Swedish waters.

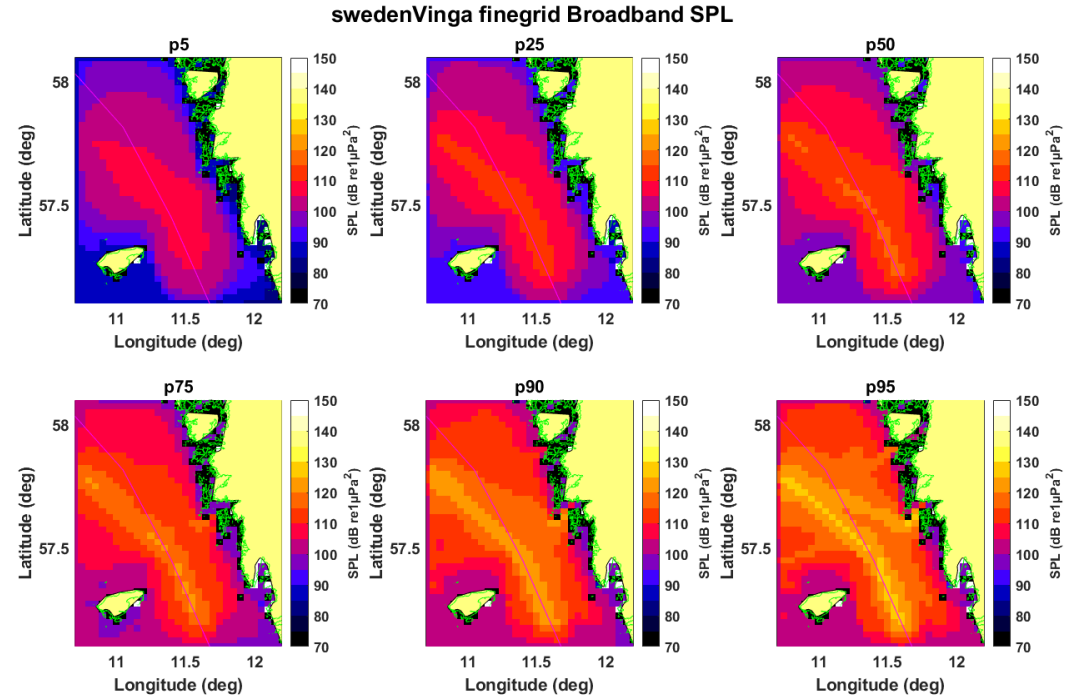

Figure D-9 Broadband SPL percentiles for fine grid source positions (Vinga, 2018)

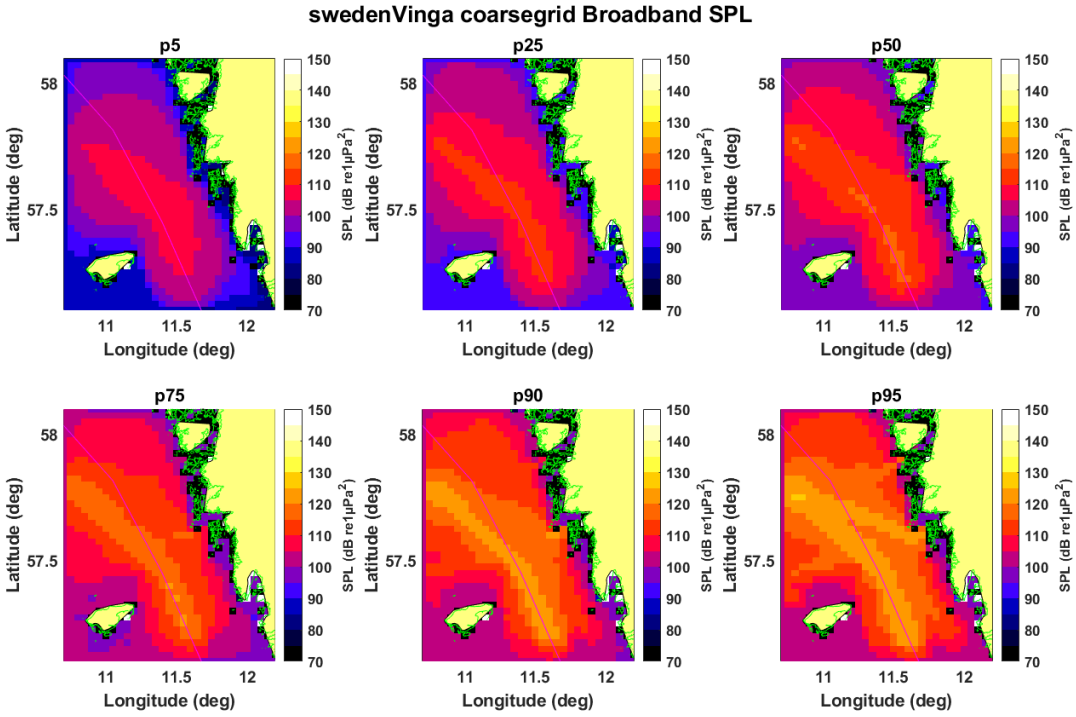

Figure D-10 Broadband SPL percentiles for course grid source positions (Vinga, 2018)

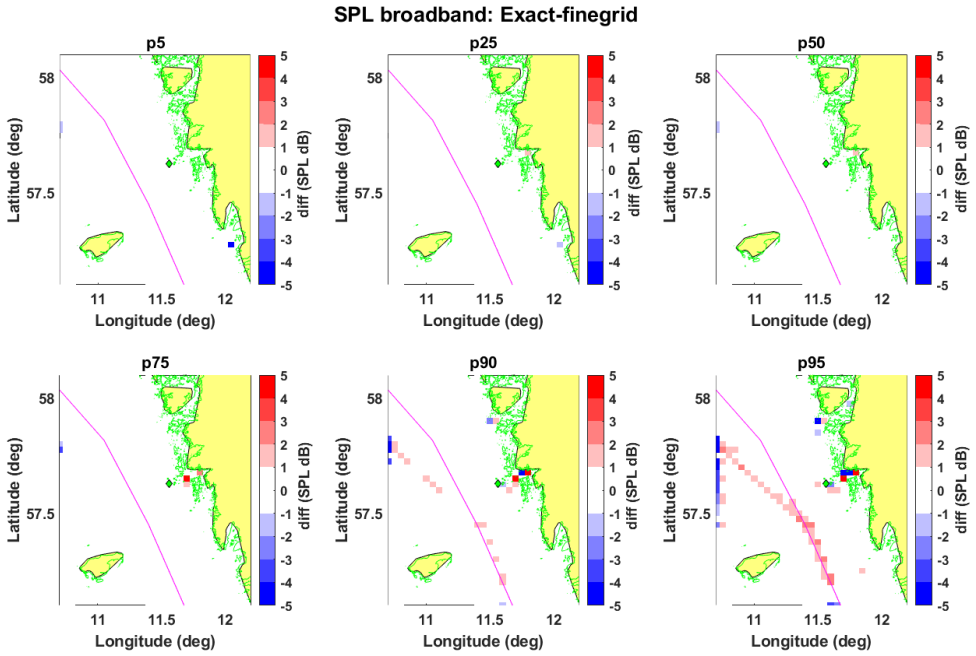

Figure D-11 difference between broadband SPL percentiles for fine source gridding compared to exact source positions (Vinga, 2018). The green diamond indicates the measurement location.

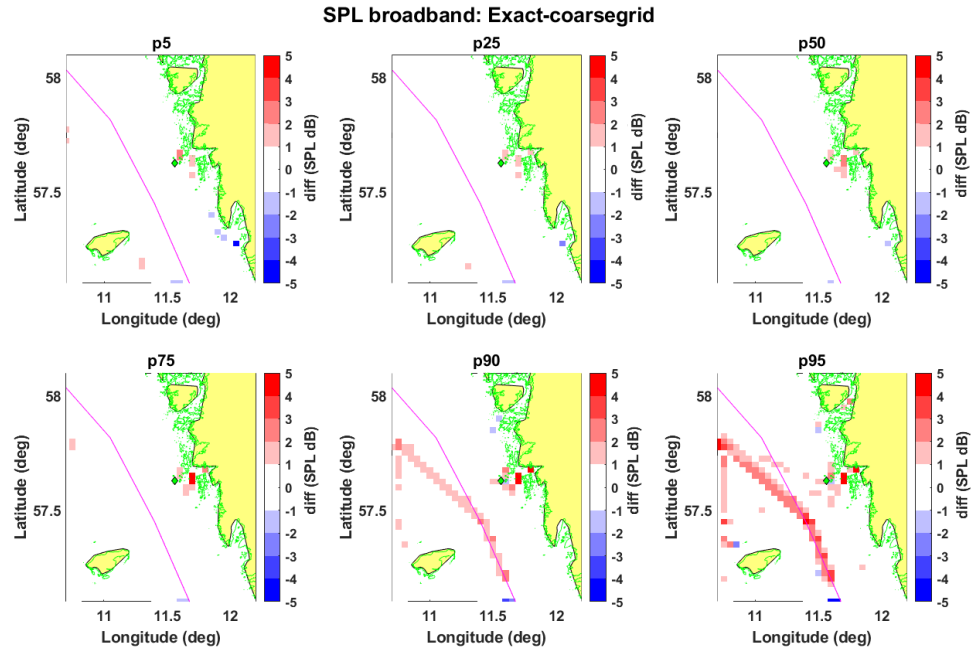

Figure D-12 difference between broadband SPL percentiles for coarse source gridding compared to exact source positions (Vinga, 2018)

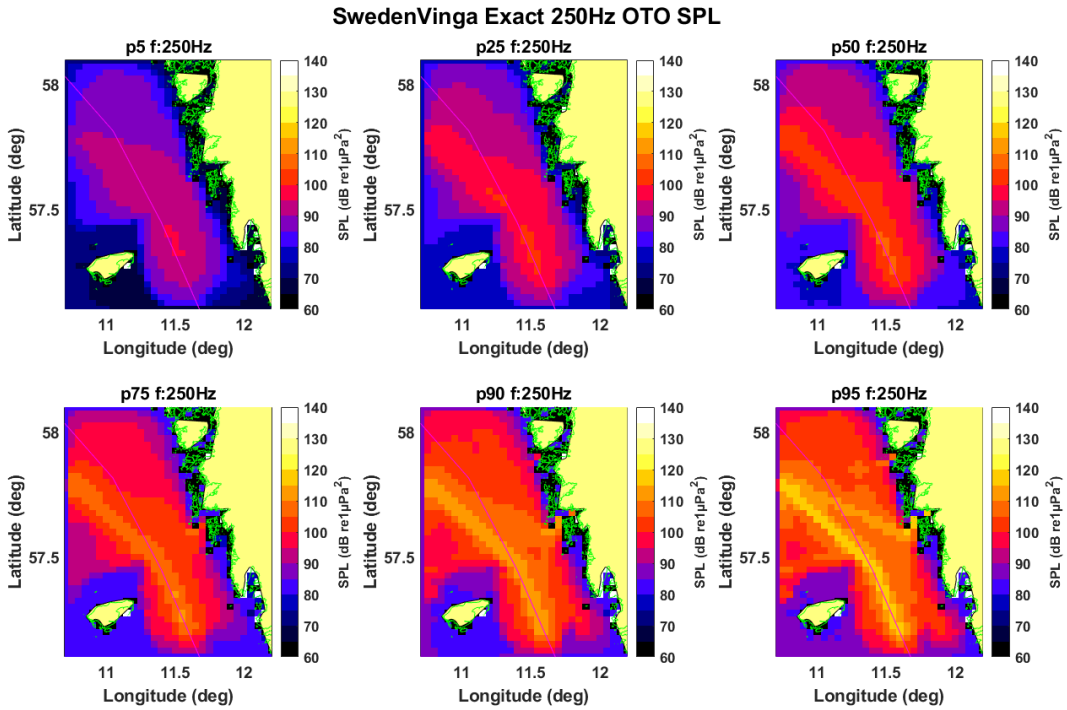

Figure D-13 *250 Hz band SPL percentiles for exact source positions (Vinga, 2018)*

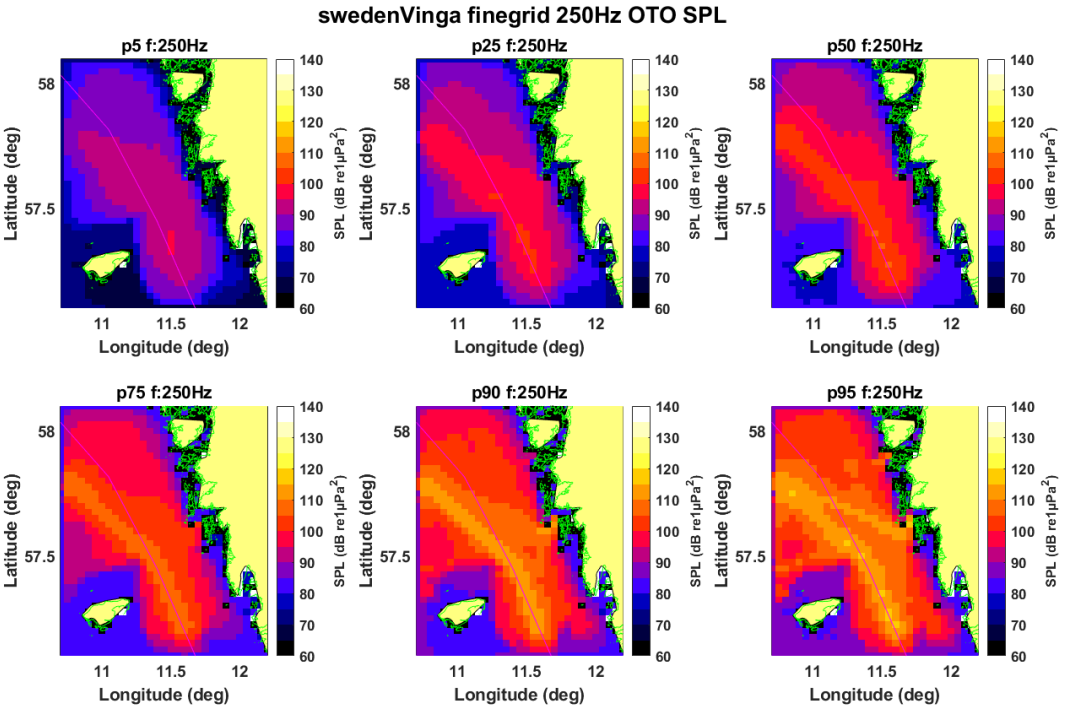

Figure D-14 *250 Hz band SPL percentiles for fine grid source positions (Vinga, 2018)*

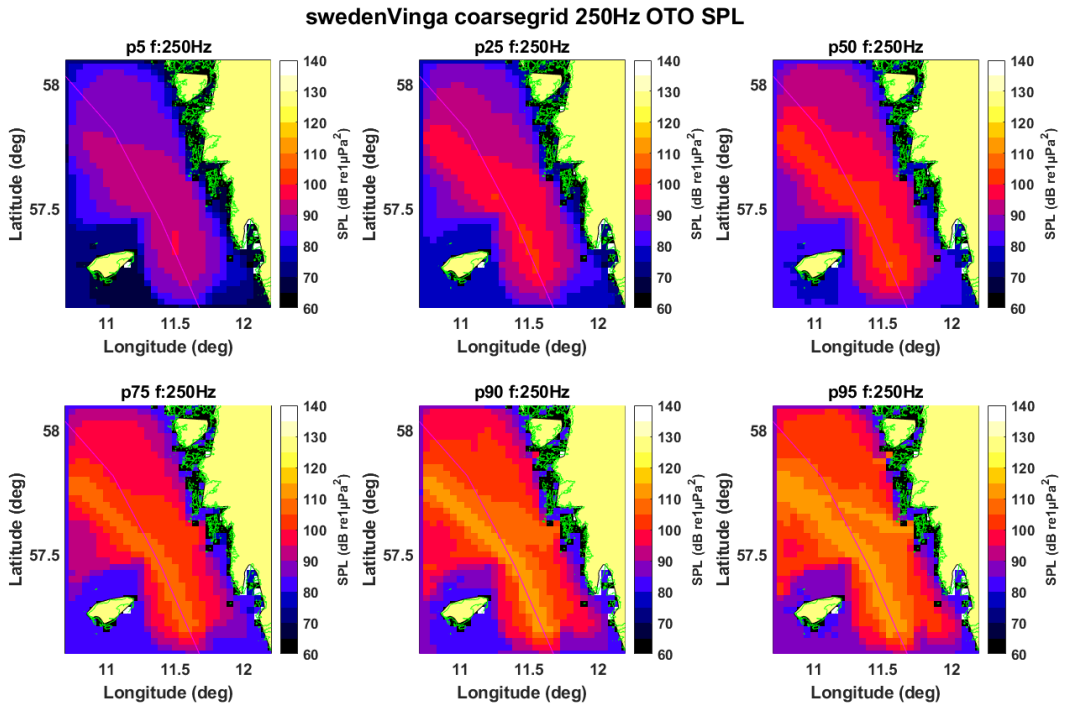

Figure D-15 250 Hz band SPL percentiles for coarse grid source positions (Vinga, 2018)

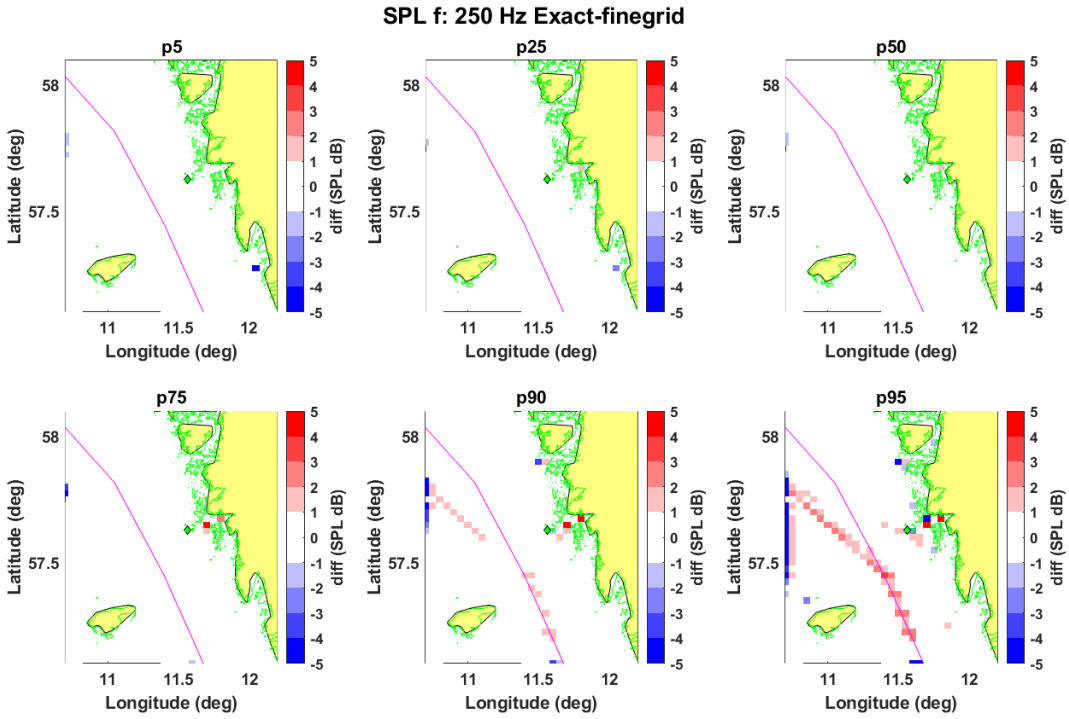

Figure D-16 difference between 250 Hz band SPL percentiles for fine source gridding compared to exact source positions (Vinga, 2018)

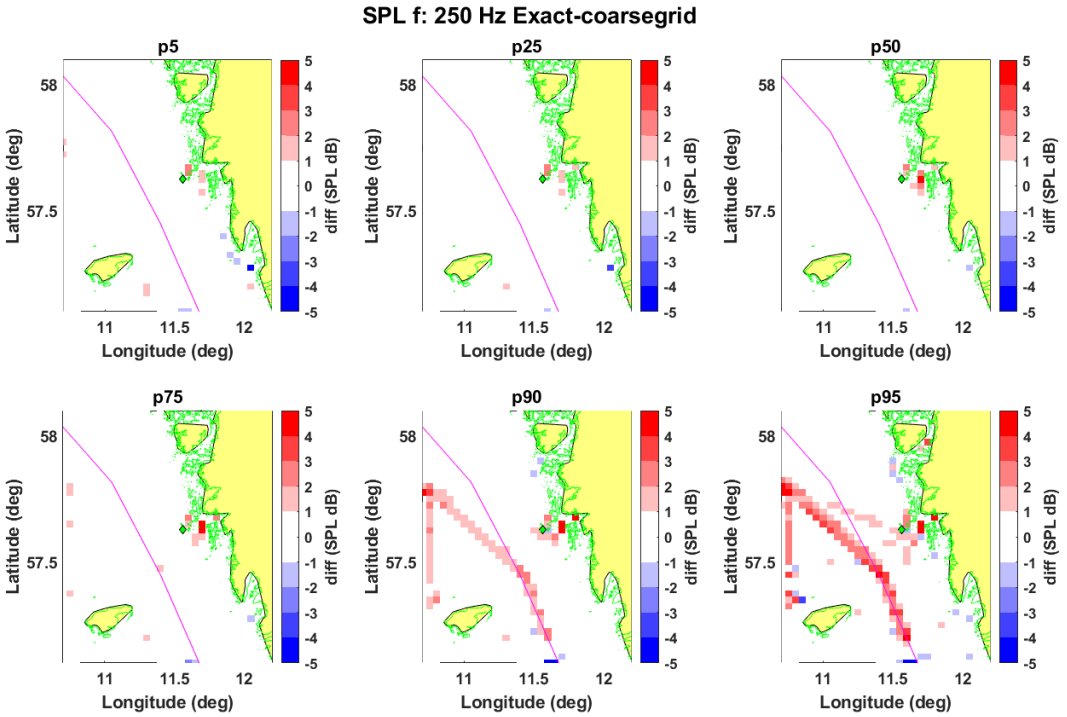

Figure D-17 difference between 250 Hz band SPL percentiles for coarse source gridding compared to exact source positions (Vinga, 2018)

Annex D.4 Time resolution

Introduction: The computational complexity can be reduced significantly by increasing the time step, reducing both the time for the post processing and the amount of data produced in the modelling process.

Method: AIS data for the JOMOPANS region was provided by Quiet Oceans with a 10-minute resolution. In this section the effect of using a coarser time step on the monthly SPL statistics is investigated. Time steps of 20, 30 and 60 minutes are considered. Details of the simulation are described in Table D-5.

Table D-5 the simulations parameters used to investigate the effect of the time resolution on the model precision for the JOMOPANS region.

Source level model	RANDI31c2
Area and time period	JOMOPANS 01-01-2019 to 01-02-2019
Seabed	Determined from Bockelmann [2018] database at location
Water	1500 m/s,1000 kg/m^3
Surface Wind	0 m/s
Sim range	400 km
Radials	16 (22.5 deg)
Wind model	Wind model 1.0 results are added to the shipping noise when calculating SPL levels for using the wind speed at the same time steps
Tested metrics	Depth averaged BB and 250 Hz (efficient propagation)

Results: Figure D-18 and Figure D-19 show the differences when using a 60-minute time step. Figure D-20 and Figure D-21 show the difference when using a 30-minute time step.

The results from the figures are summarized in Table D-6 (figures for 20 min timestep are not shown). For every frequency and time percentile the 90th area percentile of the difference over the JOMOPANS area has been calculated. Then the maximum value of the difference over all frequencies is taken.

Table D-6 Maximum deviation (in dB) over all frequencies of the 90th area percentile of the deviation when the time step is increased for 10 min to 20, 30 or 60 min.

	p5	p10	p25	p50	p75	p90	p95
60 min	0.31	0.23	0.16	0.17	0.29	0.96	1.11
30 min	0.18	0.13	0.09	0.09	0.15	0.33	0.53
20 min	0.11	0.08	0.06	0.06	0.10	0.20	0.35

Recommendation: For the JOMOPANS area using a 60-minute temporal resolution the maximum deviation is around 1 dB for the 90th area percentile of the various time percentiles of SPL. Locally however the error is observed to be larger than 2 dB for the 95% temporal percentile for the monthly statistics. TNO proposes to run the model with 30-minute time steps for the generation of the sound maps for the JOMOPANS area with the TNO Aquarius model.

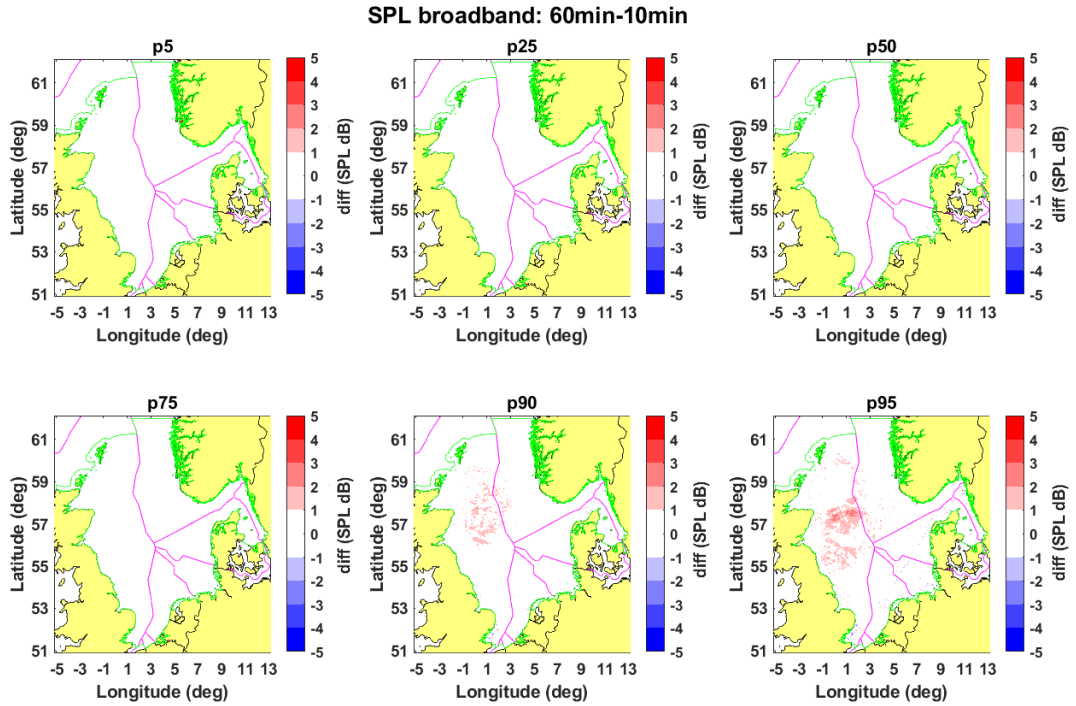

Figure D-18 *Deviation for broadband when using 60 minutes time step instead of 10 minutes*

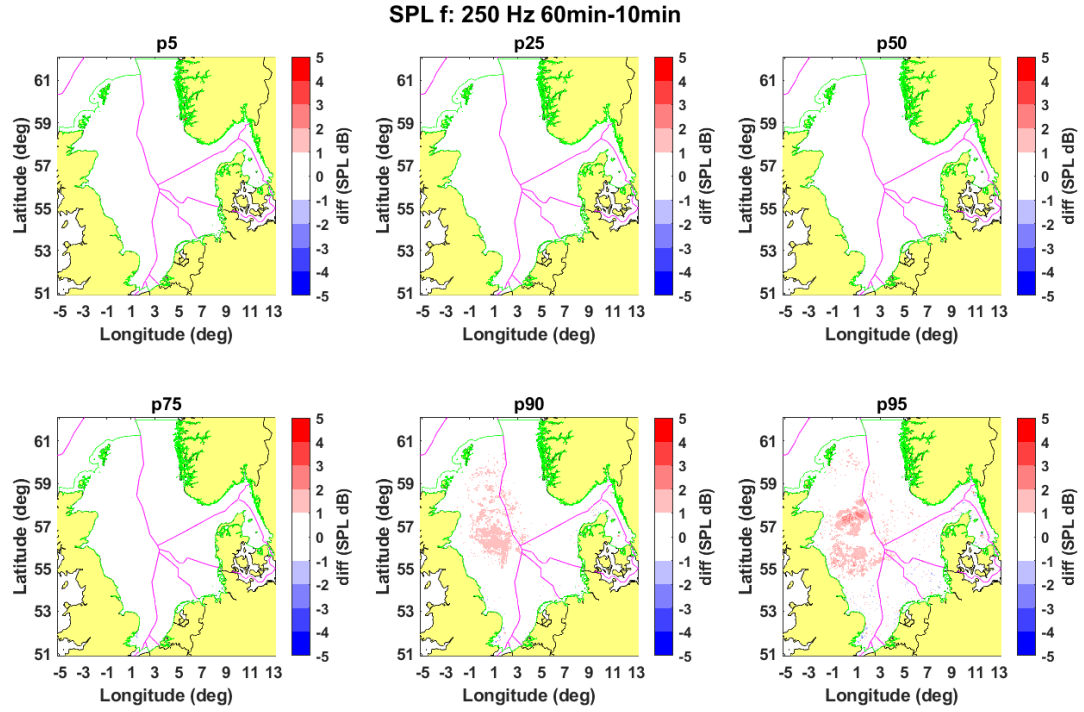

Figure D-19 *Deviation for 250 Hz OTO when using 60 minutes time step instead of 10 minutes*

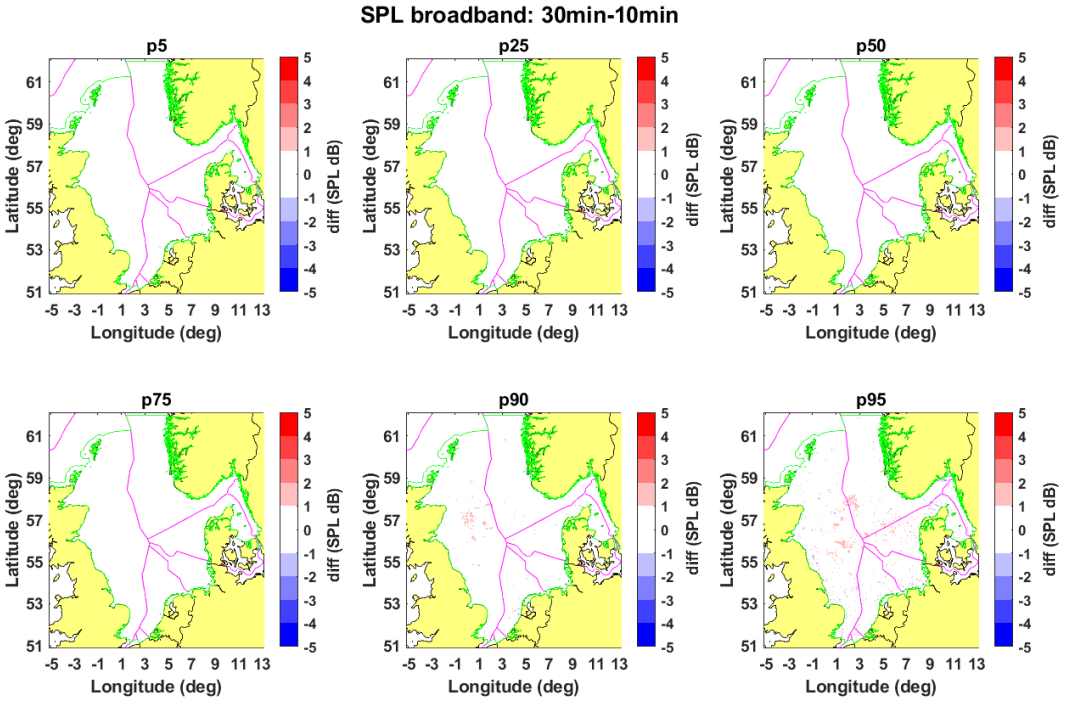

Figure D-20 *Deviation for broadband when using 30 minutes time step instead of 10 minutes*

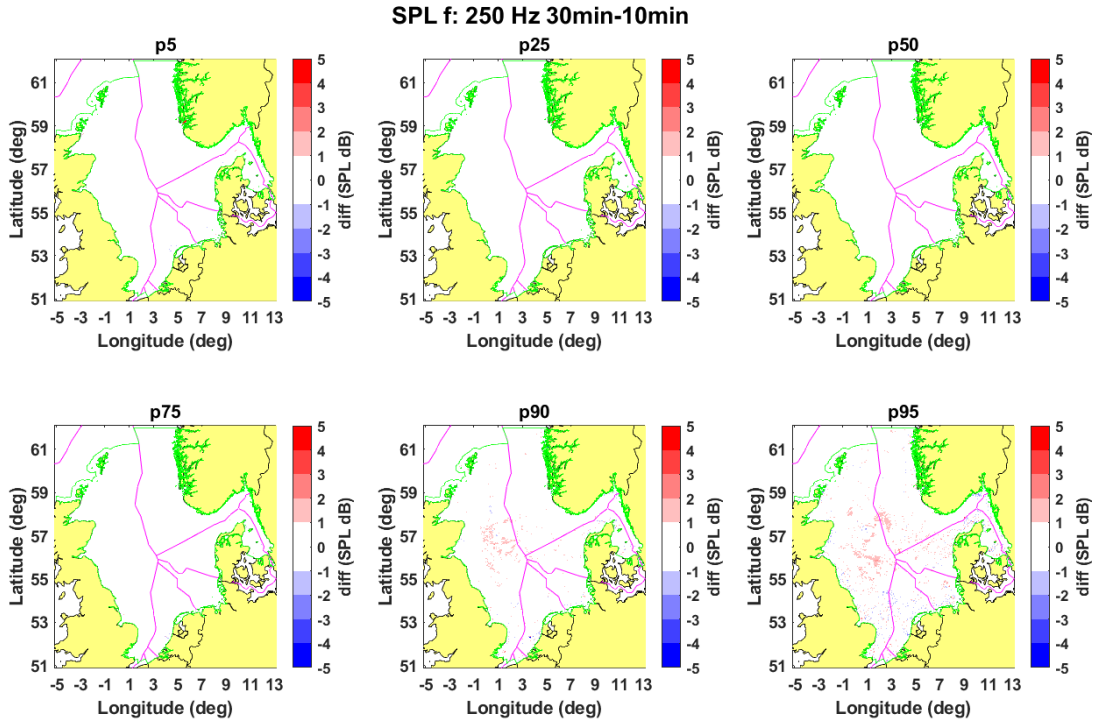

Figure D-21 *Deviation for 250 Hz OTO when using 30 minutes time step instead of 10 minutes*

Annex D.5 Source level statistics

Introduction: One of the uncertainties for sound map modelling involves the source level of individual ships. In this section a sensitivity study is described to quantify the effect of the source uncertainty on the uncertainty associated with the JOMOPANS acoustical indicator.

Method: To quantify this uncertainty, Monte Carlo simulations were carried out for the Swedish site (Vinga). For each ship, 100 source level realizations where modelled with a standard deviation of 7 dB. For these 100 realizations, the mean and standard deviation of the monthly percentiles were computed. Further details of the simulation are described in Table D-6.

Table D-6 the simulations parameters used to investigate the effect of source level uncertainty on the model uncertainty for the Sweden Vinga site.

Source level model	RANDI31c2
Area and time period	Sweden Vinga 21-03-201803 to 20-04-2018
Seabed	Uniformly modelled as Coarse Silt (grainsize 4.5), using parameters from Table 4.18 in [Ainslie, 2010]
Water	1500 m/s,1000 kg/m^3
Surface Wind	0 m/s
Radials	16 (angle resolution 22.5 deg)
Sim range	100 km
Wind model	Wind model results are added to the shipping noise when calculating SPL levels
Tested metrics	Depth averaged BB and 250 Hz (efficient propagation) time percentiles

Results: Figure E-1 to E-4 show maps of the mean and the standard deviation of the 100 realizations of the monthly percentiles for the 250 Hz one-third octave band and broadband SPL. This illustrates that the monthly statistics reduces the assumed 7 dB standard deviation of the source levels to a standard deviation of less than 1 dB in the monthly median SPL, and less than 3 dB in the highest (95%) percentile.

Figures E-5 shows probability density spectra of calculated SPL percentiles at the Vinga measurement site, and Figure E-6 shows the standard deviation of the calculated SPL percentiles. This confirms that the assumed 7 dB standard deviation of the source level spectra reduces to a standard deviation of less than 1 dB in the monthly SPL percentiles.

Recommendation: The observed uncertainty in the predicted monthly SPL percentiles due to the SL uncertainty is limited. The large extra computational effort associated with the Monte Carlo modelling approach for evaluating this uncertainty can be avoided. Note however that this only holds for monthly statistics and that the source level uncertainty is significant when comparing time series of model and measurements.

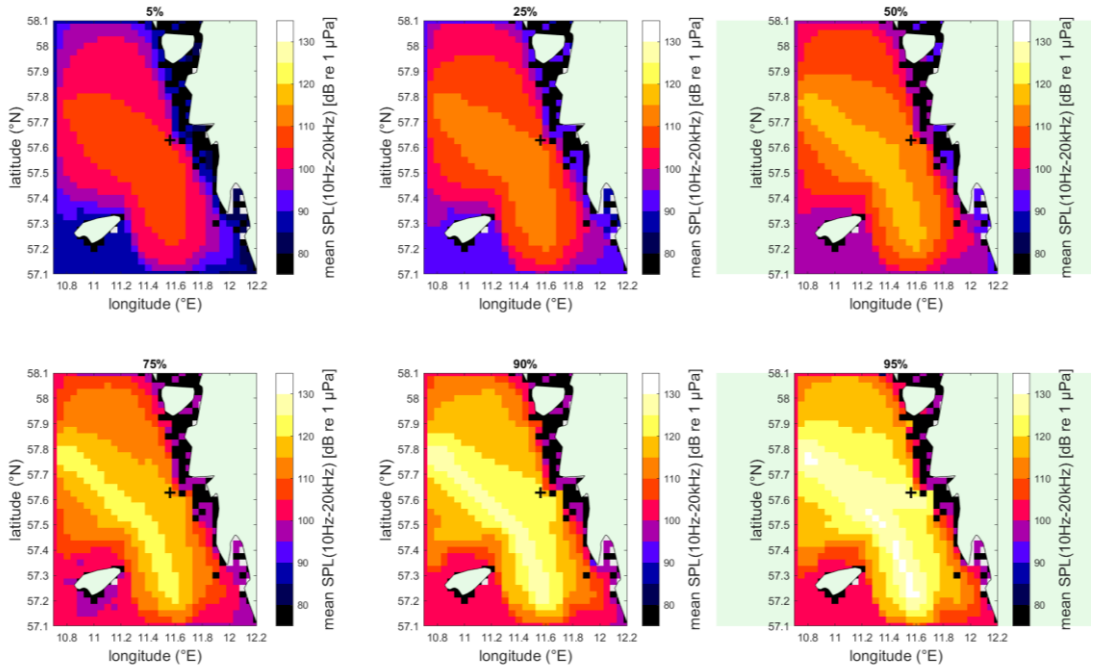

Figure E-1 maps of the mean values obtained from the 100 calculations (SL variations) of the monthly broadband SPL percentiles for the Vinga site. The '+' marker indicates the location of the Vinga measurement station.

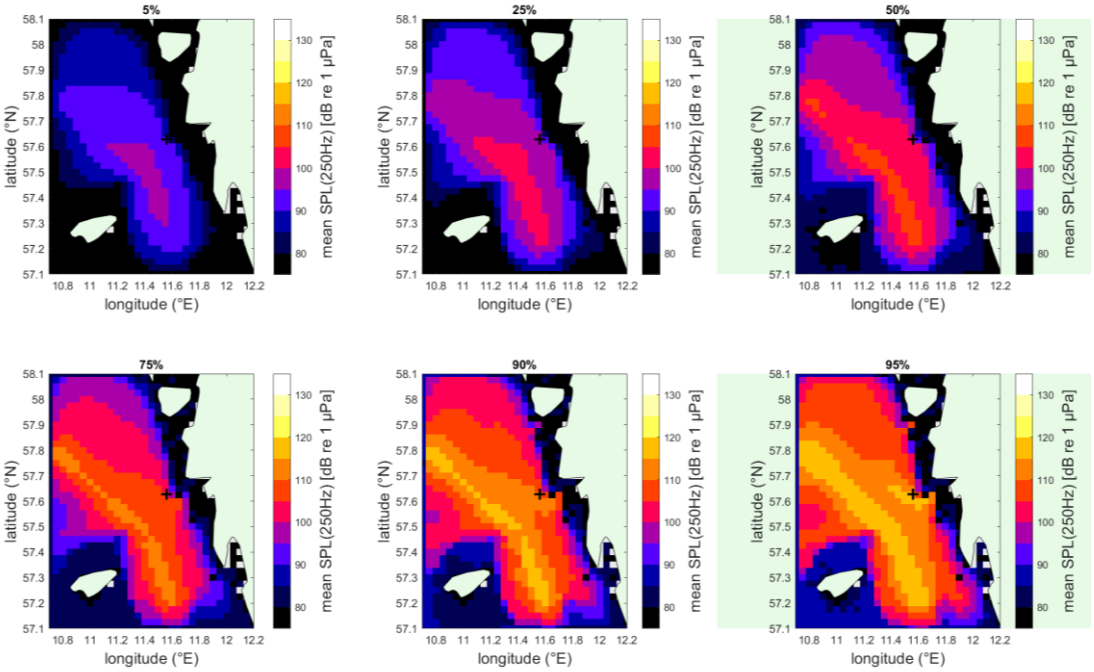

Figure E-2 maps of the mean values obtained from the 100 calculations (SL variations) of the monthly 250 Hz one-third octave band SPL percentiles for the Vinga site. The '+' marker indicates the location of the Vinga measurement station.

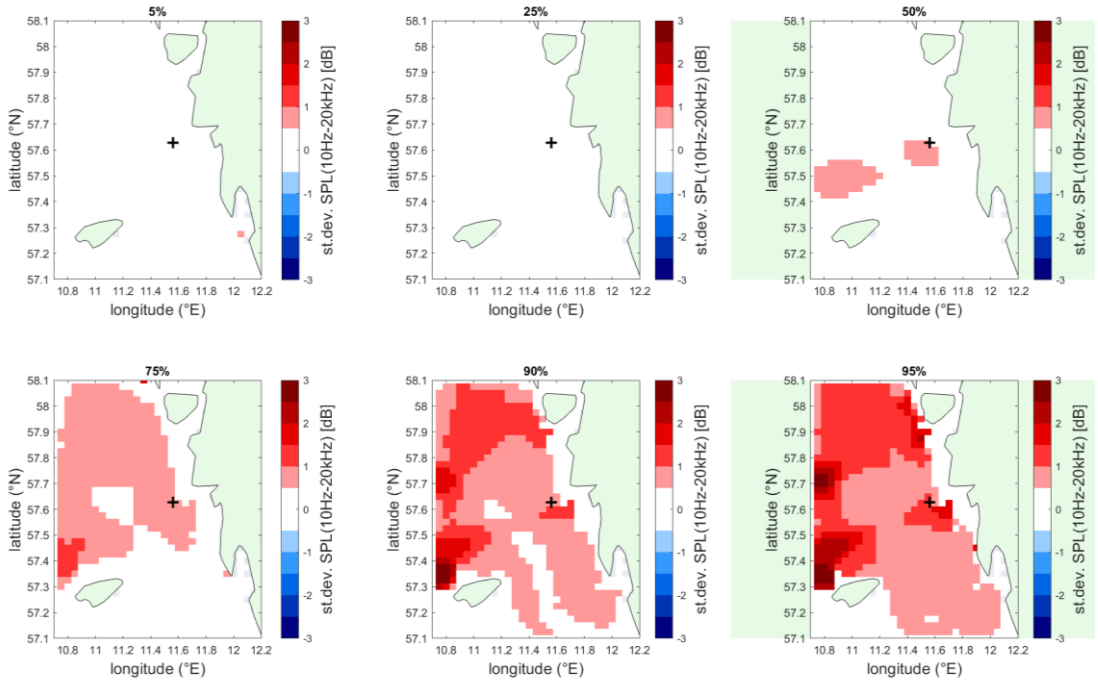

Figure E-3 maps of the standard deviation (in dB) obtained from the 100 calculations (SL variations) of the monthly broadband SPL percentiles for the Vinga site. The '+' marker indicates the location of the Vinga measurement station.

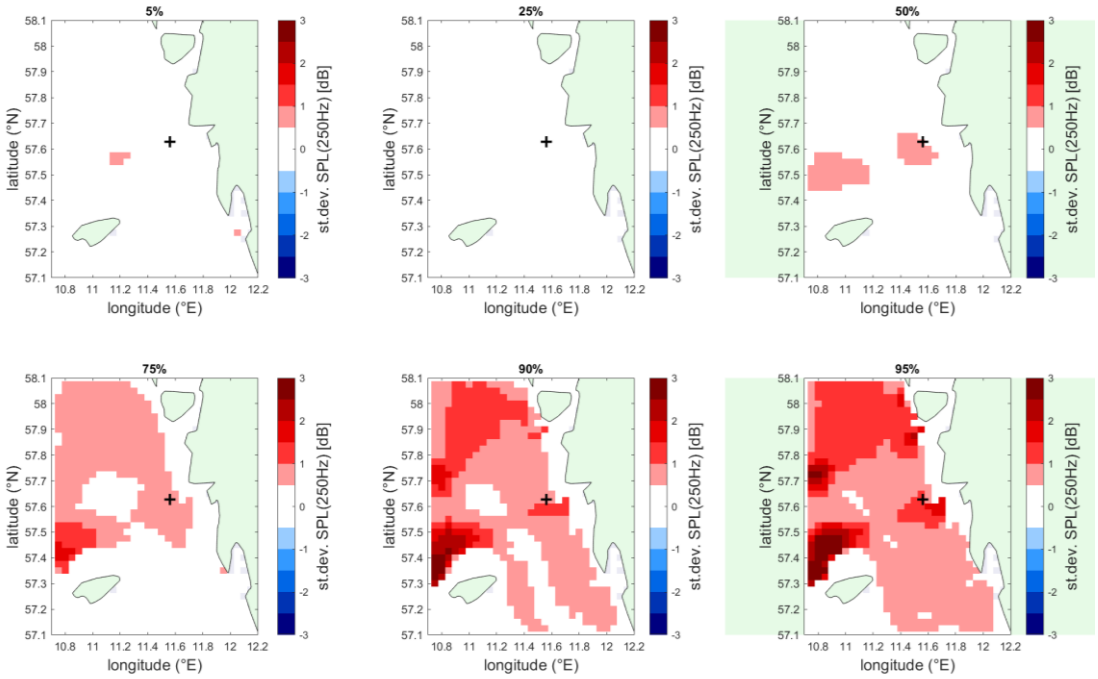

Figure E-4 maps of the standard deviation (in dB) obtained from the 100 calculations (SL variations) of the monthly 250 Hz one-third octave band SPL percentiles for the Vinga site. The '+' marker indicates the location of the Vinga measurement station.

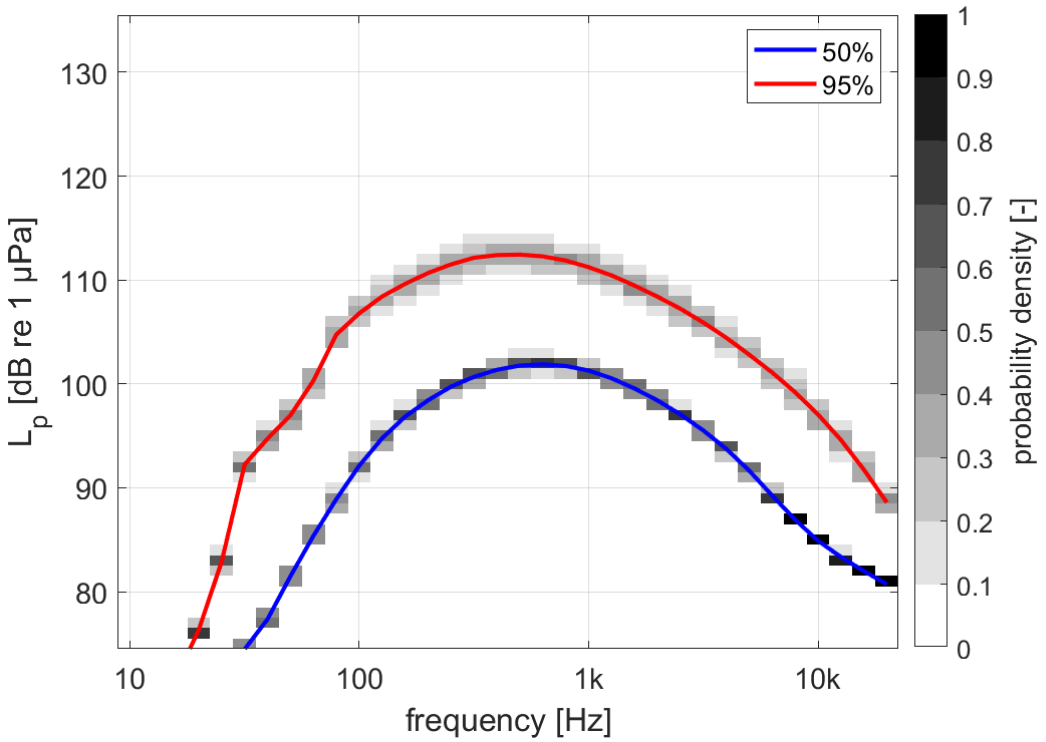

Figure E-5 Spectral probability density of the median (50%) and 95% monthly percentiles of the SPL at the Vinga measurement location, obtained from the 100 calculations (SL variations).

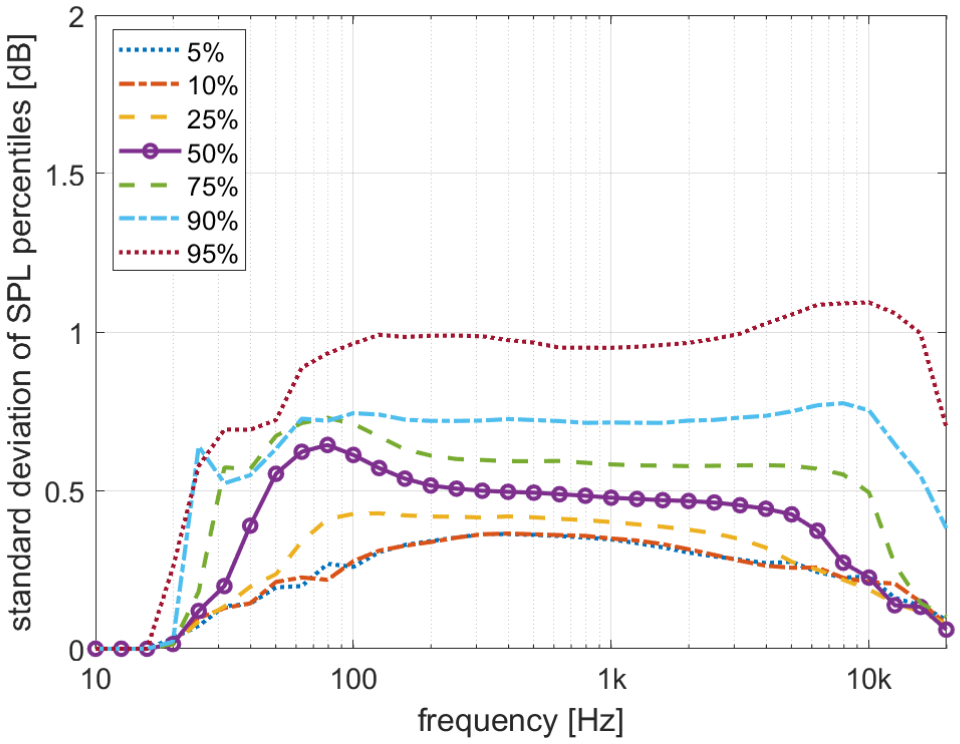

Figure E-5 Standard deviation of the monthly percentiles of the SPL spectra at the Vinga measurement location, obtained from the 100 calculations (SL variations).

Annex E Reference solutions for benchmark cases

This annex provides tabulated values of reference solutions (calculated SPL in one-third octave (base-10) bands, in decibels) for the two test cases (section 4.1.1) for verifying the implementation of shallow-water propagation loss models.

	Test Case 1 (range-independent)				Test Case 2 (range-dependent)			
	XFEM solution (FOI)				average solution of PE codes			
Frequency (Hz)	**1 km**	**5 km**	**10 km**	**50 km**	**1 km**	**5 km**	**10 km**	**50 km**
10.0	81.1	41.9	15.1	-105.4	109.3	98.9	49.0	-92.7
12.6	97.8	49.8	19.2	-110.2	112.0	102.4	56.5	-132.1
15.8	113.2	84.5	57.7	-111.2	113.3	104.3	56.0	-163.2
20.0	120.6	105.9	93.1	7.4	115.0	105.8	62.4	-200.9
25.1	123.6	111.1	101.3	40.0	119.5	108.3	69.3	-232.3
31.6	124.2	113.0	104.8	56.4	121.6	111.9	94.1	-54.1
39.8	121.5	111.4	104.3	64.8	121.5	110.2	96.6	-5.6
50.1	123.0	109.3	103.2	70.7	120.0	109.8	95.3	15.8
63.1	121.9	109.7	102.5	74.9	119.7	109.6	94.9	30.7
79.4	120.6	108.7	101.6	77.9	119.3	108.6	94.3	42.1
100.0	120.4	108.0	101.0	79.7	118.4	107.9	92.3	48.5
125.9	119.3	107.3	100.3	80.6	117.4	107.0	92.9	58.2
158.5	118.7	106.4	99.6	80.7	116.4	106.1	93.0	62.4
199.5	117.2	105.4	98.9	80.5	115.0	105.1	88.9	56.2
251.2	115.3	104.3	98.0	80.1	112.8	103.7	89.4	66.9
316.2	113.3	103.1	97.1	79.9	110.5	101.9	90.4	69.6
398.1	111.1	101.6	96.1	79.7	108.4	99.9	90.0	64.9
501.2	110.0	100.1	95.0	79.4	107.6	98.5	90.1	72.2
631.0	108.8	99.0	93.9	79.1	106.2	97.4	89.9	71.7
794.3	107.5	97.8	92.9	78.4	104.9	96.0	90.1	71.4
1000.0	106.6	96.8	91.7	77.5	103.5	95.1	89.2	71.3
1258.9	105.7	95.7	90.6	76.2	102.8	94.0	88.0	69.0
1584.9	104.8	94.7	89.5	74.5	102.0	93.2	87.6	69.7
1995.3	103.8	93.9	88.5	72.5	102.2	92.0	86.2	68.5
2511.9	103.2	92.9	87.3	70.2	100.4	90.6	86.0	67.1
3162.3	103.2	92.1	86.2	67.4	99.7	88.8	83.8	64.2
3981.1	101.1	91.7	84.9	63.8	99.3	89.5	81.7	58.9
5011.9	100.8	89.1	83.1	58.8	97.4	86.8	79.9	49.7
6309.6	99.7	88.2	81.3	51.6	96.4	85.5	78.8	45.4
7943.3	98.3	85.9	77.7	40.4	95.1	84.7	77.4	37.1
10000.0	97.8	84.7	75.9	23.8	94.7	81.7	72.6	17.6
12589.3	96.1	82.7	68.2	-2.0	92.8	78.2	65.5	-7.4
15848.9	92.5	76.9	59.4	-40.7	90.3	73.2	56.6	-44.9
19952.6	93.2	69.5	47.5	-99.7	87.5	65.9	45.0	-103.9